Thermo-Mechanical Aging of Shape Memory Polymers

by

Kannan Dasharathi

A dissertation submitted in partial fulfillment
of the requirements for the degree of
Doctor of Philosophy
(Aerospace Engineering)
in The University of Michigan
2015

Doctoral Committee:

Professor John A. Shaw, Chair
Professor Diann E. Brei
Senior Researcher Nilesh D. Mankame, General Motors Corporation
Professor Anthony M. Waas
Professor Alan S. Wineman

ACKNOWLEDGEMENTS

This dissertation would not have been possible without the help, support and guidance of a lot of people. I would like to express my sincere gratitude to my advisor Prof. John Shaw whose guidance and influence has helped me grow in more ways than I can count. It has been an honor working with Prof. Alan Wineman, interactions with whom have been an invaluable learning experience. I also gratefully acknowledge Dr. Nilesh Mankame and Prof. Diann Brei, whose support and guidance has been instrumental in the synthesis and manufacturing of shape memory polymer. Many thanks to General Motors for providing funding for this research. I would also like to thank my colleagues Ryan Watkins, Daniel Biggs, Ruiqi Chen, Tizoc Cruz-Gonzalez, Corin Bowen, Liang Liu and my seniors Benjamin Reedlunn and Christopher Churchill for bringing in new perspectives and many helpful discussions. Finally, I am in debt to my loving wife Vandana and my family for their immense sacrifices and emotional support.

TABLE OF CONTENTS

LIST OF FIGURES

Figure

LIST OF TABLES

Table

LIST OF ABBREVIATIONS

SMPs Shape Memory Polymers

SMC Shape Memory Cycle

CR Chemo-Rheological

DMA Dynamic Mechanical Analyzer

LVDT Linear Variable Differential Transformer

DIC Digital Image Correlation

TTSP Time-Temperature Superposition Principle

FTSP Frequency-Temperature Superposition Principle

WLF Williams-Landel-Ferry

CTE Coefficient of Thermal Expansion

KAHR Kovacs-Aklonis-Hutchinson-Ramos

SLS Standard Linear Solid

LIST OF APPENDICES

Appendix

ABSTRACT

Thermo-Mechanical Aging of Shape Memory Polymers

by

Kannan Dasharathi

Chair: John A. Shaw

Thermo-responsive shape memory polymers (SMPs) rely on the dramatic change in the relaxation times across the rubber-glass transition temperature (T_g) to exhibit shape memory behavior. Successful development of SMP based devices require a comprehensive understanding of the sensitivity of material response to time varying external stimuli. Chemo-rheological (CR) aging of SMPs occur at high temperature and high loads resulting in permanent changes to the macromolecular network structure due to scission and recrosslinking. SMPs also undergo physical aging, which is different from CR aging, as a result of structural relaxation (gradual sliding and untangling of the macromolecular chains) at temperatures below the T_g. While physical aging also changes the material properties, its time-frame is much longer than the CR aging process.

Due to the thermo-mechanical nature of the shape memory behavior, knowledge of the influence of CR aging is critical to establishing a design envelope and determine the life time of SMP based devices. Existing studies focus on the thermo-mechanical response of SMPs in a narrow temperature zone surrounding the T_g, also limited to the viscoelastic and structural relaxation behavior.

To fulfill this need, the thermo-mechanical response of an epoxy SMP is studied over a wide range of temperatures extending well into the CR zone. Several experimental parameters such as deformation temperature, applied load, hold time, cooling rate, recovery temperature and recovery time are identified as potential variables that influence the material response. A systematic parametric study is performed to investigate the effect of these variables. Appropriate performance metrics are defined to compare the material response for various loading conditions and discern the effects of CR aging.

A critical CR aging temperature is identified and an accelerated aging study is conducted to investigate the kinetics of CR aging and its influence on the thermo-mechanical properties. Based on multi-network theory, a constitutive model for the shape memory behavior incorporating the kinetics of CR aging is developed and calibrated. The predictions of this model are evaluated by comparing with the experimental shape memory cycle data for specific test cases.

CHAPTER I

Introduction

SMPs, as the name indicates, refers to a class of materials that are able to 'remember' and revert to a 'permanent' pre-programmed shape. The shape memory effect in polymers was first discovered in 1941 [1]. Since then, several SMPs have been engineered for applications in consumer, electronics, heath care and industrial business sectors [1–5]. Figure 1.1 shows some of the applications of SMPs.

A typical Shape Memory Cycle (SMC) involves two stages: (1) Deformation and storage of a temporary shape by application of force and an external stimulus such as temperature, light, electric field, magnetic field etc. (2) Recovery of the 'permanent' or the 'molded' shape by application of the external stimulus under constraint-free conditions. Based on the type of the external stimulus, SMPs are classified as thermo-responsive, photo-active, electro-active, magneto-responsive and chemo-responsive materials. This work focusses on thermo-responsive SMPs.

Based on the material response to rising temperature, thermo-responsive polymers are classified into *thermoplastics* and *thermosets*. *Thermoplastics* soften and eventually liquify when heated and harden when cooled. On a macromolecular level, thermoplastic polymer chains are connected through weak secondary bonds and entanglements and therefore do not possess a 'permanent' shape. As a result, thermoplastic polymers do not exhibit shape memory behavior. Common examples of thermoplastic polymers

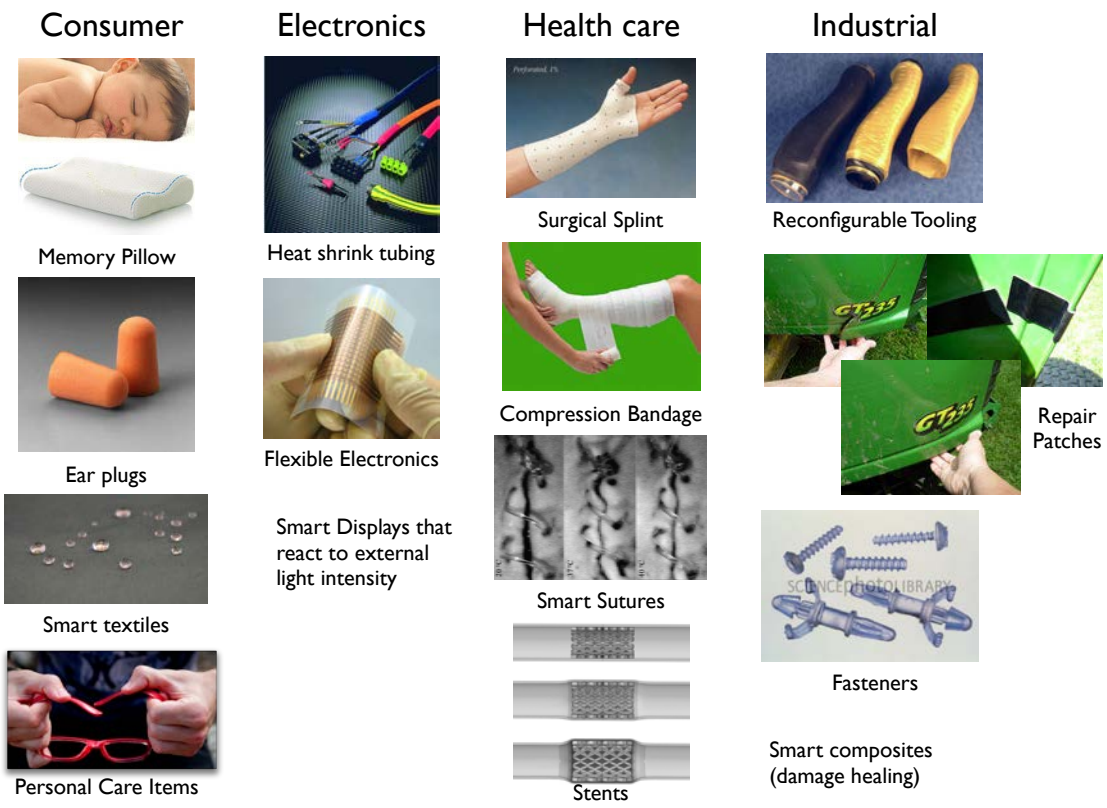

Figure 1.1: Existing and potential applications of SMPs in major business sectors

include polyethylene, polystyrene and polyvinyl chloride. *Thermosets* on the other hand do not liquify, but, soften to a lesser degree up on heating and harden when cooled. Thermosets possess a three-dimensional crosslinked network structure with covalent bonds anchoring the polymer chains giving it a permanent shape. Therefore, all thermoset polymers exhibit shape memory behavior. Common examples include vulcanized rubber, epoxies and some phenolics and polyester resins [1, 2, 5, 6].

Thermo-responsive polymers exhibit three fundamental regimes of viscoelastic behavior. Below the rubber-glass transition temperature (T_g) a polymer is glassy, stiff and relatively brittle. In the transition zone ($\approx T_g \pm 10$ °C), the viscoelastic and other physical properties change rapidly. Above the T_g a polymer is compliant and rubbery. Thermoplastics have a very short rubbery plateau which quickly transitions into a rubbery-flow and viscous-flow regions as the polymer liquifies. Understand-

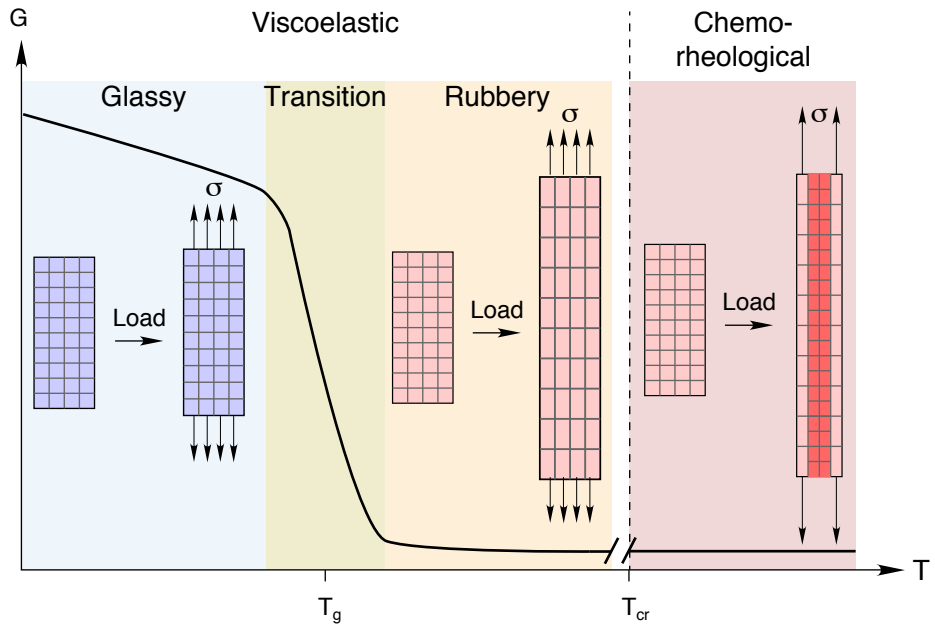

Figure 1.2: Schematic of the viscoelastic and chemo-rheological zones in a typical thermoset polymer

ably, thermosets do not exhibit the rubbery-flow and viscous-flow regions, instead, they possess a long rubbery plateau. The thermal response of both thermoplastics and thermosets are reversible and can be repeated only if the temperatures are in the viscoelastic regimes. Figure 1.2 shows a schematic of the viscoelastic regimes for a typical thermoset polymer (a.k.a SMP).

A fourth regime exists at further elevated temperature, above a so-called chemo-rheological temperature (T_{cr}), where *Chemo-Rheological (CR)* aging occurs (see Fig. 1.2) due to changes in the macromolecular network from scission (breaking of chemical bonds) and crosslinking (formation of new chemical bonds in a new reference configuration) [6, 7]. CR aging gets its name from *Chemorheology* which is the study of the change in deformation and flow characteristics due to chemical reactions. Temperature, applied loads, humidity, solvents and radiation can all cause chemical reactions which change the deformation and flow characteristics of a polymer [8]. CR aging at a high temperature under load is also referred to as *thermo-mechanical* aging and

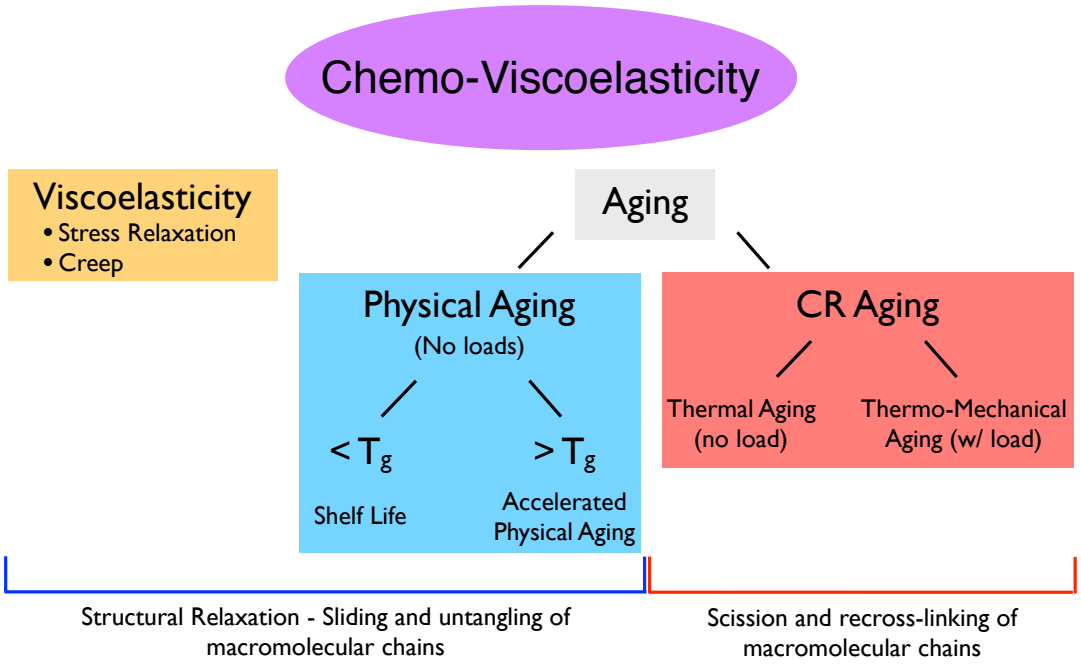

Figure 1.3: A classification of the relaxation behavior based on the macromolecular mechanism

CR aging due to temperature alone (a subset of thermo-mechanical aging) is also referred to as *thermal* aging in literature. In this work, the term CR aging refers to thermo-mechanical/thermal aging. A distinction between thermal aging and thermo-mechanical aging is made only when relevant to the discussion.

CR aging is distinct from *physical* aging, which refers to the gradual change in the material properties of a polymer around T_g under no loads due to very slow molecular rearrangement from sliding of the macromolecular chains, also known as *structural relaxation* [9–11]. A classification of relaxation behavior according to the macromolecular mechanism is shown in Fig. 1.3. CR aging causes irreversible changes to the macromolecular network structure and its particular effects vary depending on the chemistry of the polymer system and the magnitude and duration of temperature and stress, but often manifest as irrecoverable strain and stiffening or softening of the polymer.

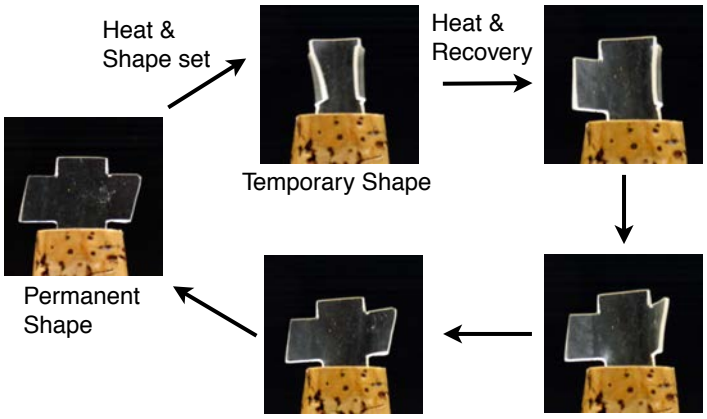

Figure 1.4: A demonstration of the SMP recovery process

1.1 Background and Motivation

Thermo-responsive SMPs exploit the dramatic change in the relaxation times across the T_g to exhibit the shape memory effect [2]. A typical SMC involves heating the SMP above its glass transition temperature T_g, mechanically deforming (shape-setting) it at an elevated *deformation temperature* T_d, then cooling below T_g under mechanical constraint, followed by unloading to 'cold-store' the temporary shape. Shape recovery is obtained by subsequent load-free heating above T_g to a *recovery temperature* T_r to regain the reference configuration of the SMP. A demonstration of the SMP recovery process is shown in Fig. 1.4.

In industrial applications of SMPs, such as reconfigurable tooling, the temperature of the entire tooling block must be above the T_g for reshaping or recovery. To ensure this, certain regions of the SMP would have to be at a much higher temperature than T_g, possibly even greater than T_{cr}, due to poor heat transfer and thermal conductivity of polymers. This causes CR aging of SMP and in turn affects the performance and limits its useful life. This fundamental work is intended to provide a new framework for characterizing and modeling the CR aging in SMPs. It is hoped that this work will lead the way to better predict the life of SMPs in engineering applications.

Cured epoxies have excellent chemical resistance, exhibit good adhesion characteristics and have good handling properties making them a popular SMP choice for many applications. In recent years, many epoxy resin based thermo-responsive SMPs have been developed [12–22]. However, epoxies are brittle and undergo CR aging at temperatures as low as 100 °C like many polymers including natural rubber [7]. Moisture is also known to adversely affect epoxies, lowering its tensile strength and reducing time to fracture under constant load [8, 23–26]. While there are several potential applications of epoxy SMPs, the limitations are the lack of understanding of the material response to various loading conditions and the availability of models to predict the cycle life of a SMP [27].

1.2 Scope and Objectives

This research is an investigation into the influence of thermo-mechanical aging on the fundamental material response of a particular epoxy-based SMP. This is a macro-mechanical study, not a chemical study. The overall goal of this work is to provide a framework for characterizing and modeling the thermo-mechanical aging in SMPs, with hopes that it will lead to the identification of optimum operating conditions and enable life cycle prediction of SMPs in engineering applications. While modeling framework presented here is applicable to any SMP, for illustration purposes, specific forms of relaxation function are calibrated for the epoxy-based SMP used in this study.

The scope and objectives of this thesis are:

- Characterize the thermo-viscoelastic material properties of virgin SMP.
- Establish suitable performance metrics to compare the thermo-mechanical response for various loading conditions.

- Investigate the influence of experimental parameters such as temperature, load and dwell times on the response of the SMP.
- Identify a critical CR temperature for the onset of CR aging.
- Investigate the kinetics of CR aging.
- Study the influence of CR aging on the viscoelastic material properties and the thermo-mechanical response of the SMP.
- Develop and calibrate a constitutive model for the shape memory behavior incorporating the kinetics of CR aging.
- Evaluate the predictive capability of this constitutive model by comparing with the shape memory response for specific test cases.

1.3 Outline of Thesis

The reminder of thesis is organized into four chapters. In Chapter II, the details of the SMP synthesis, specimen preparation and experimental test setup are provided. In Chapter III the results from a baseline thermo-mechanical characterization of viscoelastic moduli, critical transformation temperature and the thermal expansion responses are reported. In Chapter IV the results of a parametric study of the influence of experimental variables such as deformation temperature, applied load, hold time, recovery time and cooling rate are reported. A suitable set of evaluation metrics is chosen and the effect of experimental variables on the material performance is quantified. A critical CR aging temperature is identified for accelerated aging studies. In Chapter V, two viscoelastic models are first calibrated and their predicted response is evaluated against the experimental data. Structural relaxation and physical aging effects are not modeled. A chemo-viscoelastic modeling framework is then developed. From the experimental data, a kinetic model for CR aging is calibrated. The effect

of CR aging on the viscoelastic behavior of the SMP is experimentally investigated and suitable assumptions are made to pick and calibrate a chemo-viscoelastic relaxation function. Lastly, the predictive capability of the chemo-viscoelastic model is evaluated against the experimental SMC data.

CHAPTER II

Material and Experimental Details

Since their commercial debut in 1947, several formulations of epoxy have been developed. The versatility of epoxy resins stem from its unique chemistry which facilitates the use of a variety of curing agents, resulting in a wide range of attainable properties such as enhanced toughness, chemical resistance, mechanical properties ranging from highly compliant to high strength and hardness, high adhesive strength, good heat resistance and electrical resistance. As a result of this versatility epoxies are used in several market segments, prominently in coatings, electronics, construction, composites, adhesives, tooling, etc [8]. A detailed review of the chemistry of epoxy based polymers is beyond the scope of this thesis. Readers are referred to some of the excellent treatises on this matter [8, 28, 29].

There are several formulations of epoxy based SMPs [12–22]. In this work, a recently-formulated epoxy SMP, designated as NGDE-1 [14] is used. The details of this formulation, SMP synthesis and sample fabrication process are discussed in Section 2.1. A description of the experimental setup is provided in Section 2.2.

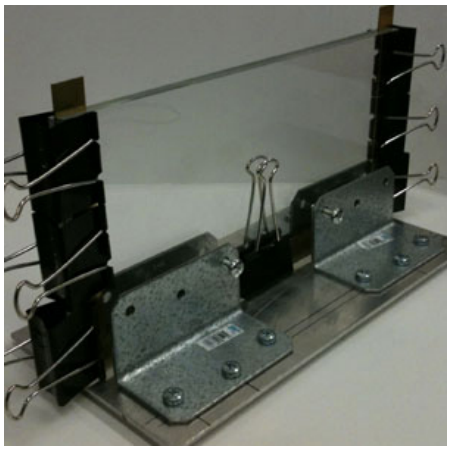

Figure 2.1: Photograph of the glass mold used to manufacture the SMP sheet

2.1 Synthesis of an Epoxy SMP

An epoxy resin of diglycidyl ether of bisphenol A (EPON™ 826 from Momentive Speciality Chemicals Inc.), Neopentyl Glycol Diglycidyl Ether (Jeffamine™ D230 from TCI America) and Poly-oxyporpylene-diamine (from Huntsman International LLC) were purchased and used as-received. The composition of the SMP designated NGDE-1 [14] is 0.015 mol of EPON™826 (mol. wt.= 350 g, mass density = 1.17 g/cm^3), 0.01 mol of Jeffamine™ D230 (mol. wt.= 230 g, mass density = 0.95 g/cm^3), and 0.005 mol of NGDE (mol. wt.= 216.3 g, mass density = 1.08 g/cm^3). Borosilicate glass plates were used to prepare a mold of size 285.75 × 184.15 × 0.81 mm^3. A photograph of the glass mold is shown in Fig. 2.1. The appropriate quantity (36 g) of EPON™ 826 was weighed into a pyrex container and melted in an oven preheated to 70 °C. The calculated mass (7.1 g) of NGDE1 and Jeffamine™ D230 (15.2 g) were added to the melted EPON™ 826 and then mixed to a uniform consistency. This mixture was then degassed in a vacuum oven by pulling a vacuum for 20 mins and poured into the glass mold. Using the recommended curing cycle [14], it was then cured at 100 °C for 1.5 h and post-cured at 130 °C for 1 h. After the cure, the mold was cooled to room temperature, and the SMP was removed. Water-jet machining

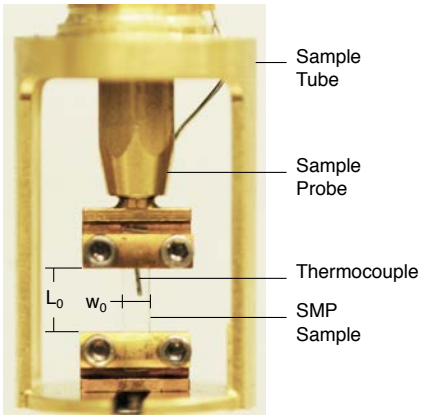

Figure 2.2: Experimental setup within the DMA

was used to cut rectangular samples (21 mm × 2 mm × 0.88 mm) for subsequent thermo-mechanical testing.

2.2 Details of the Experimental Setup

A Perkin Elmer Dynamic Mechanical Analyzer (DMA) was used with its extension measurement fixture for uniaxial testing of the synthesized NGDE-1 epoxy SMP specimens. Figure 2.2 shows the experimental setup within the DMA. The specimen was held between the fixed bottom grip and movable top grip attached to the sample probe. The loads were measured using the DMA's 6500 mN load cell, and a Linear Variable Differential Transformer (LVDT) measures the probe displacement. A thermocouple was positioned in air about 5 mm behind the specimen and was used to sense and control the temperature in the DMA's thermal chamber surrounding the sample tube. Dry air purge gas was used to maintain a consistent testing environment.

When the glass mold with SMP is cooled to room temperature, thermal gradients and differences in the thermal expansion coefficients cause residual stresses in the SMP. To relieve this residual stress, prior to testing, all samples were subjected to an additional 'stress-relief heat treatment' involving a heat-cool cycle to a maximum temperature

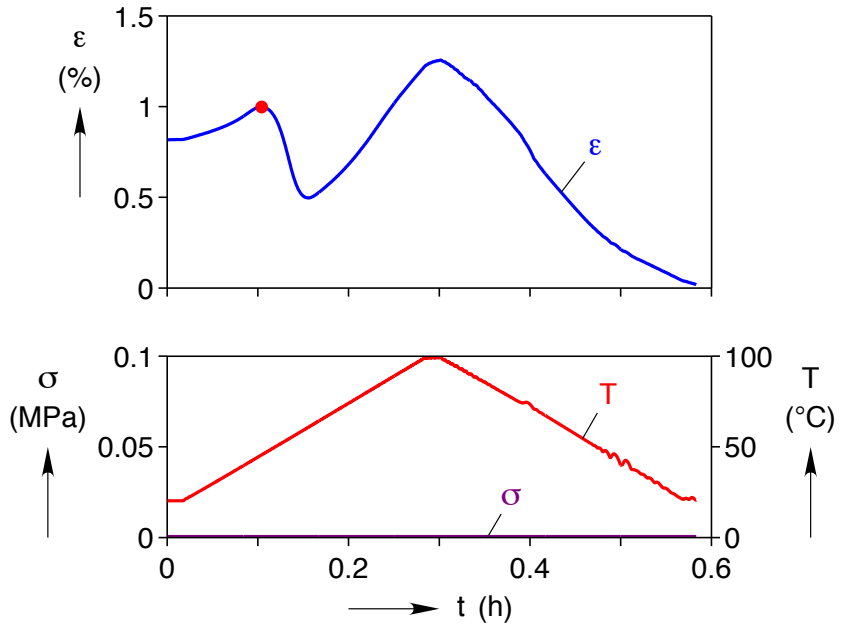

Figure 2.3: Representative stress (σ), temperature (T) and strain (ε) history during a post-cure heat-cool cycle

of 100 °C and dwell time of 1 min. During this stress-relief heat treatment, a small tensile load (1 mN) was applied to keep the specimen taut and a temperature rate of ±5°C/min is used.

Figure 2.3 shows a representative stress (σ), temperature (T) and strain (ε) history during the stress-relief heat treatment. As the temperature is increased the strain increases due to thermal expansion. At a temperature greater than the T_g for this material, the strain decreases by about 0.5% as the residual stresses in the macromolecular chains are relieved. After this 'recovery', the strain continues to increase due to thermal expansion as the SMP is heated to a maximum temperature of 100 °C. The sample is then cooled to 20 °C to establish a reference zero strain state.

The specimen strain in the DMA is measured between the grips. Clamping causes higher localized stresses near the grip region which can affect the thermomechanical response and lead to early failure. To mitigate the grip effects, the aspect ratio of the gripped specimen, which is the gauge length between the grips-to-width ratio,

was picked to be approximately 7:1. Grip effects were quantified by measuring the strain field of a SMP specimen in a tensile test conducted using the DMA extension setup. A non-periodic speckle pattern was applied on the specimen and 2-D Digital Image Correlation (DIC) technique [30] was used to measure the in-plane strains. Since the DMA thermal chamber does not allow for any imaging, this experiment was conducted in ambient air. At room-temperature (20 °C) the SMP is in the glassy-state and undergoes negligible deformation ($< 0.1\%$ strain). Therefore, this experiment was conducted at a higher temperature of 70 °C where, the SMP was sufficiently compliant. The temperature of the specimen was increased uniformly using a heat gun and the load is applied after equilibrating the temperature at 70 °C.

Figure 2.4 shows the DIC strain maps in the loading direction (ε^m_{yy}) and the in-plane lateral direction (ε^m_{xx}). In Fig. 2.5 the DMA grip strain measurements and a DIC extensometer strain measurements (averaged over the entire strain field) are compared. The stress and temperature history are also shown. It can be seen from the strain maps in Fig. 2.4a that the grip effect is minimal until 2% strain in the loading direction (ε^m_{yy}) and it is roughly the size of the specimen width at strains above 8%. Implying that the strain measurements have less grip effect at small strains. Figure 2.6 shows a compariosn of the DIC extensometer strains in the loading direction (ε^m_{yy}) and the in-plane lateral direction (ε^m_{xx}). A linear elastic Poisson's ratio, defined as $\nu = -\varepsilon^{\mathrm{m}}_{xx}/\varepsilon^{\mathrm{m}}_{yy}$, is also plotted for comparison. This linear elastic poisson's ratio appears to be about 0.4.

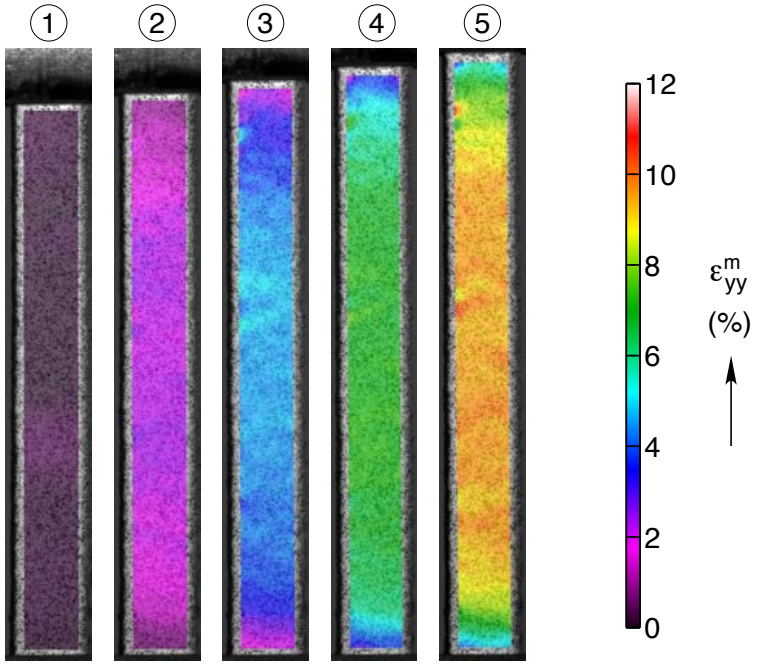

(a)

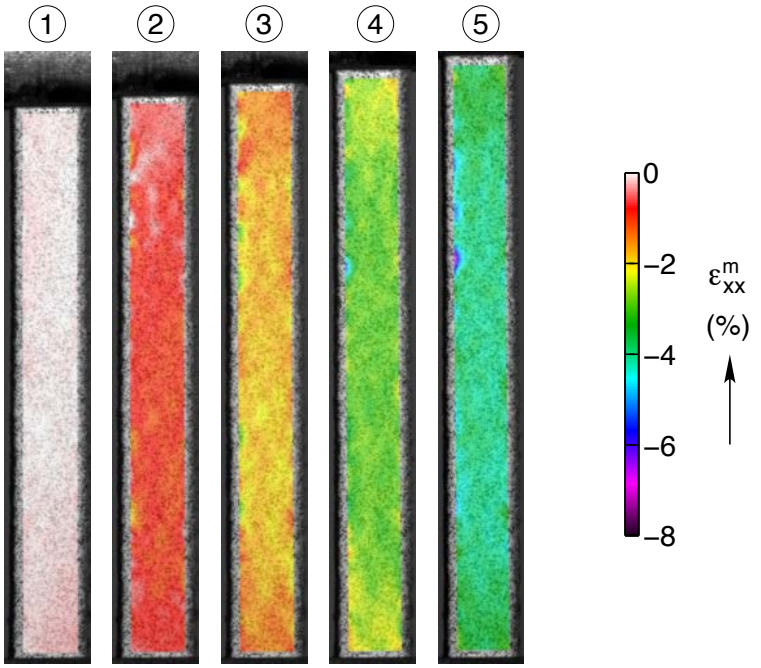

(b)

Figure 2.4: DIC mechanical strain maps in the (a) loading direction (ε^m_{yy}) (b) lateral direction (ε^m_{xx})

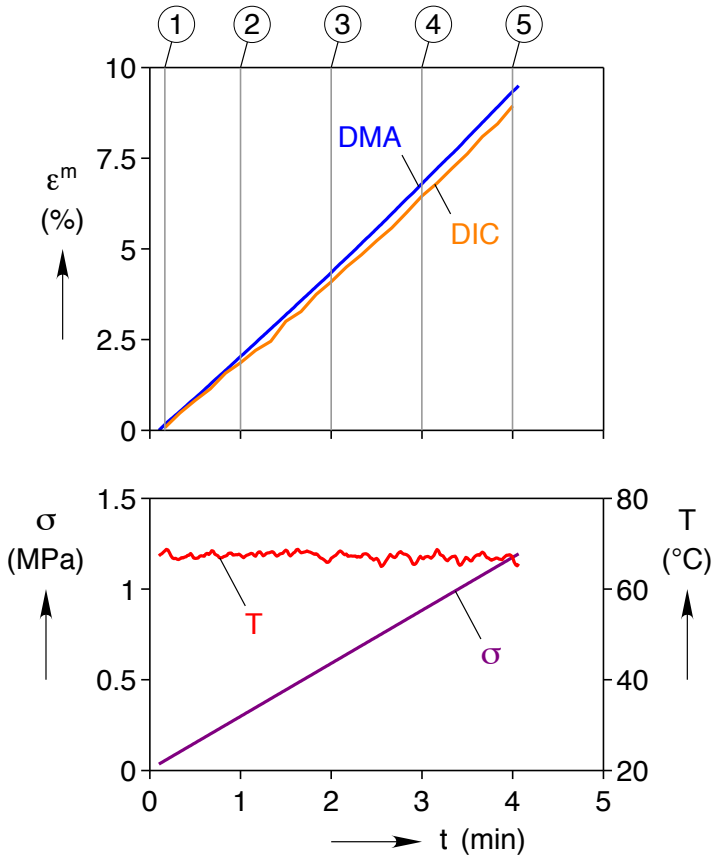

Figure 2.5: Comparison of the DIC and DMA mechanical strain measurement in the loading direction (ε^m_{yy}) (top panel), corresponding stress (σ) and temperature (T) history (lower panel)

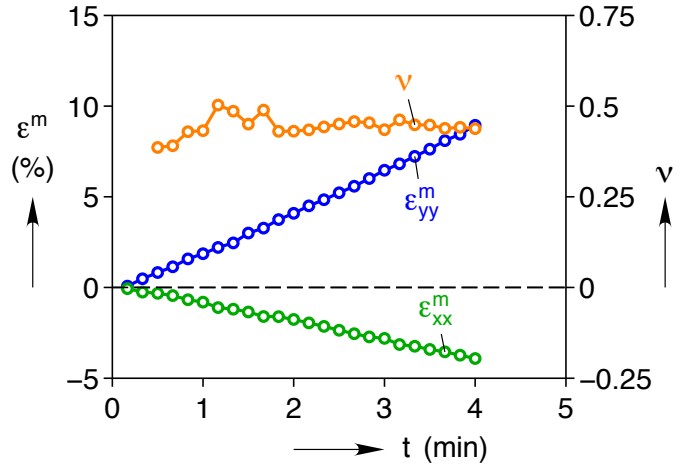

Figure 2.6: Comparison of the DIC mechanical strain measurement in the loading direction (ε^m_{yy}), lateral direction (ε^m_{xx}) and Poisson's ratio (ν)

CHAPTER III

Baseline Thermo-Mechanical Characterization

Thermo-mechanical properties of the SMP was characterized in the absence of CR aging to establish a baseline. The measurement of viscoelastic moduli and rubber-glass transition temperature T_{g} is discussed in Section 3.1. The coefficients of thermal expansion and the nature of thermo-viscoelastic behavior is discussed in Section 3.2.

3.1 Viscoelastic Moduli and Transition Temperature

Under a step strain input, the stress in a viscoelastic solid decreases with time monotonically (and asymptotically) from an initial value to a non-zero value as $t \to \infty$ [31, 32]. This response is given by a stress relaxation function $G(t)$. The stress relaxation function represents a sequence of micro-rheological events such as sliding, untangling and reorientation of the macromolecular chains. Experimental evidence indicates that for certain polymeric materials, an increase in temperature merely speeds up this sequence of micro-rheological events while a decrease in temperature slows down the process. In other words, increase or decrease in temperature is akin to speeding up or slowing down time on an intrinsic or material clock. This time-temperature equivalence supports a theoretical proposition known as *Time-Temperature Superposition Principle (TTSP)*. The materials that satisfy TTSP are

known as 'rheologically simple materials'. The main consequence of TTSP is that the stress relaxation function at any temperature ($G(t,T)$) can be expressed by two material properties, a relaxation function at a reference temperature ($G(t,T_{\text{ref}})$) and a temperature shift function ($a_{\text{T}}(T,T_{\text{ref}})$). The relaxation function represents the sequence of micro-rheological events at the reference temperature (T_{ref}) and the shift function represents the relaxation time at a temperature relative to the reference temperature.

There are several experimental techniques to measure the relaxation function and the temperature shift function [31, 33]. In this work, it is measured by subjecting a SMP sample to dynamic uniaxial tensile load. This technique gives the stress relaxation function in the frequency domain, represented by the *complex modulus* ($G^*(\omega) = G'(\omega) + iG''(\omega)$, where $i = \sqrt{-1}$ and ω is the circular frequency). Complex modulus consists of the *storage modulus* ($G'(\omega)$, real part) and *loss modulus* ($G''(\omega)$, imaginary part). In a sinusoidal deformation, the storage modulus is defined as the stress in phase with strain divided by the strain and the loss modulus is defined as the stress 90° out of phase with strain divided by strain. Storage modulus is a measure of elastic stiffness and the loss modulus is a measure of viscosity. The ratio $G''/G' = \tan\delta$, also known as loss tangent, is a measure of the ratio of energy lost to energy stored in a cyclic deformation.

To measure the viscoelastic moduli, the SMP sample was subject to a mean force of 260 mN (144 kPa) with a sinusoidal dynamic amplitude of 200 mN (110 kPa) over a 0.1 to 10 Hz frequency range under isothermal conditions. This was repeated for temperatures across the range $20 - 102$ °C in 3 °C increments, spanning the viscoelastic regimes (non-CR regimes) of the SMP. Figure 3.1a shows the variation of storage modulus (G') with frequency at several temperatures, and Fig. 3.1b shows the corresponding variation in loss modulus (G'').

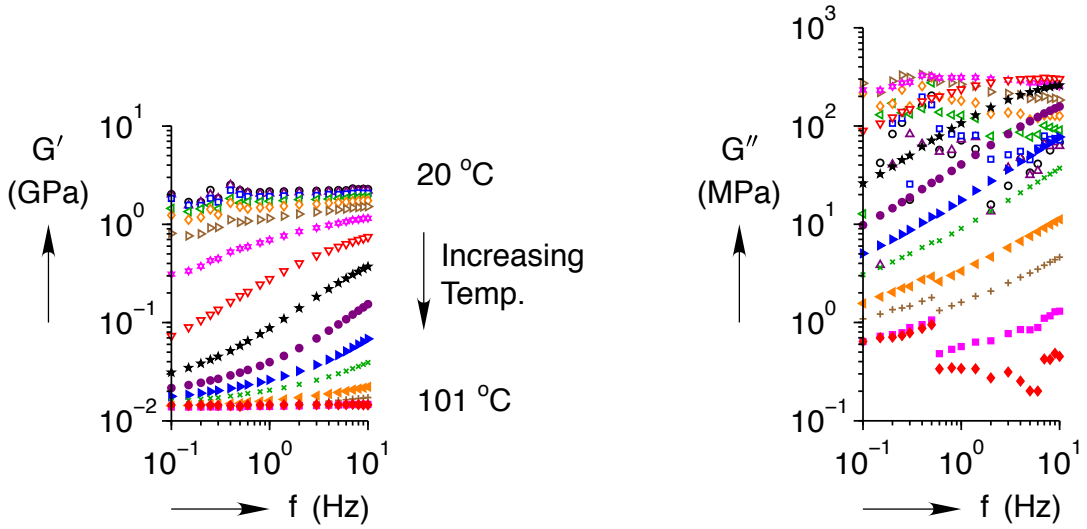

(a) (b)

Figure 3.1: (a) Storage modulus vs frequency (b) Loss modulus vs frequency - isothermal curves from $20 - 102$ °C

Due to time-temperature equivalence, it is possible to identify critical transformation temperatures by plotting storage, loss moduli and $\tan\delta$ as a function of temperature. Figure 3.2 shows this variation of viscoelastic storage and loss moduli (G', G'') and $\tan\delta$ with temperature at a frequency of 1 Hz. The storage modulus (G') changes from 2.2 GPa in the glassy state to about 15 MPa in the rubbery state, i.e. over two

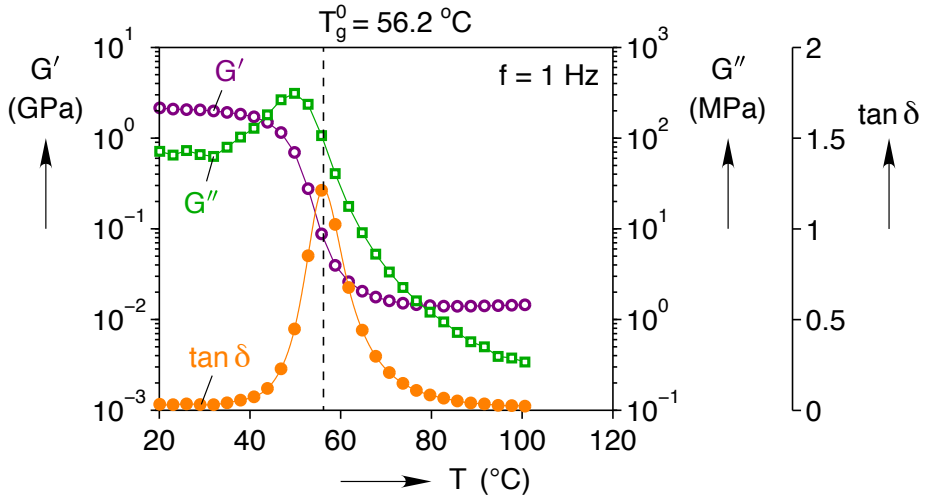

Figure 3.2: Measured viscoelastic storage and loss moduli (G', G''), $\tan\delta$ and the glass transition temperature (T_g^0)

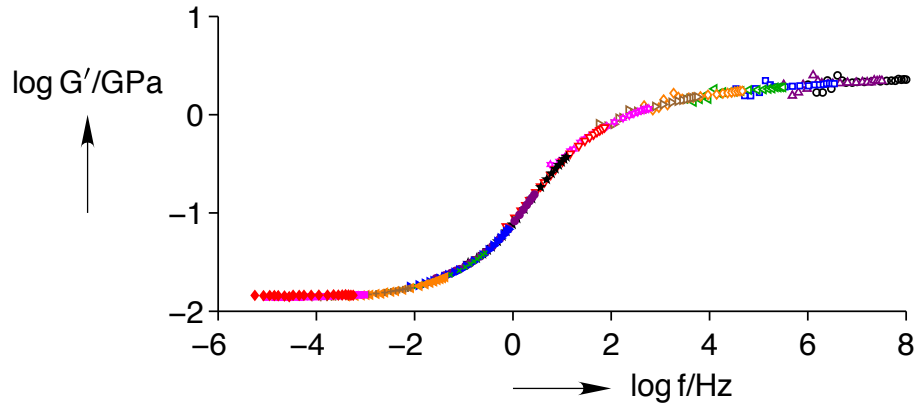

(a)

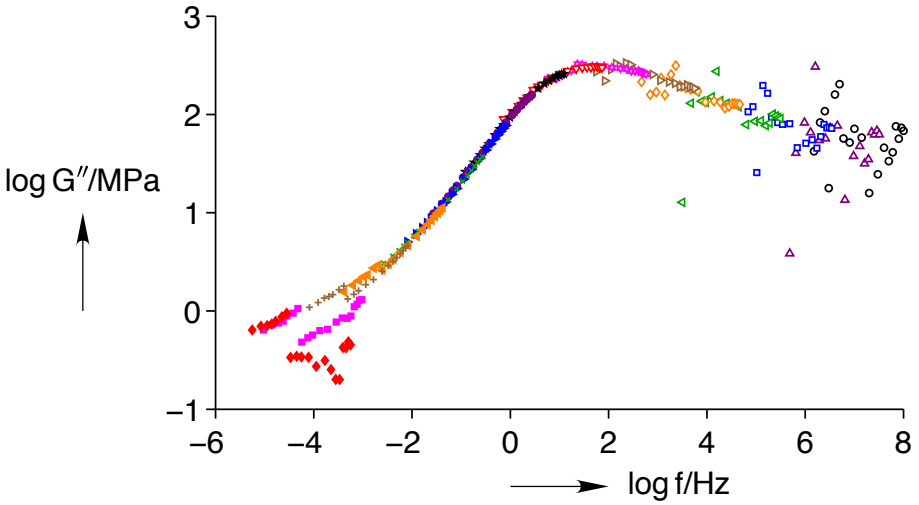

(b)

Figure 3.3: (a) Storage modulus-frequency (b) Loss modulus-frequency curves at the reference temperature T_g^0

orders of magnitude change across the T_g. The $\tan\delta$ peak, conventionally chosen as the glass transition temperature, is $T_g^0 = 56.2$ °C for the virgin epoxy SMP.

Using *Frequency-Temperature Superposition Principle (FTSP)* (i.e. TTSP in the frequency domain), storage modulus and loss modulus-frequency curves were constructed at the T_g^0 and is shown in Fig. 3.3. The corresponding temperature shift function (a_T) with T_g^0 as the reference temperature is shown in Fig 3.4.

The temperature shift function a_T is fitted using the Williams-Landel-Ferry (WLF)

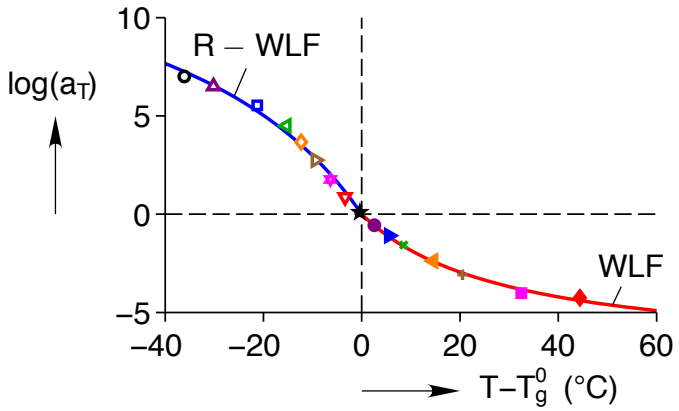

Figure 3.4: Temperature shift function with $T_g^0 = 56.2$ °C as the reference temperature

C_1	C_2 (°C)	C_3	C_4 (°C)
7.34	29.76	16.11	44.10

Table 3.1: WLF constants used to fit the temperature shift function a_T

equation above the T_g^0 and the *reverse* WLF equation below the T_g^0. The expressions for WLF and reverse WLF equations are given by

$$\log a_T = \begin{cases} \dfrac{-C_1(T - T_g^0)}{C_2 + (T - T_g^0)} & : T > T_g^0 \\ \dfrac{-C_3(T - T_g^0)}{C_4 - (T - T_g^0)} & : T < T_g^0 \end{cases} \tag{3.1}$$

where, C_1, C_2, C_3 and C_4 are material properties and are given in Table 3.1.

3.2 Thermal Expansion Behavior

The rubber-glass transition phenomena exhibits the characteristics of a second order transition. While the change in length is a continuous function of temperature, its derivative, the Coefficient of Thermal Expansion (CTE) is discontinuous at the glass transition temperature. CTE below the T_g is designated as the glassy CTE (α_g) and above T_g, it is the rubbery CTE (α_r).

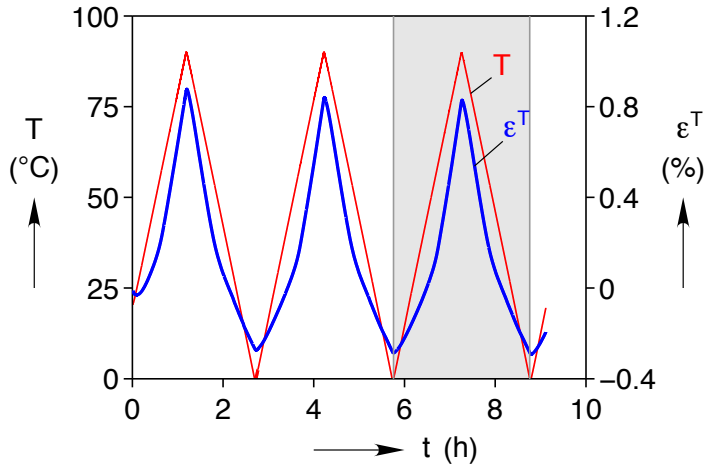

(a)

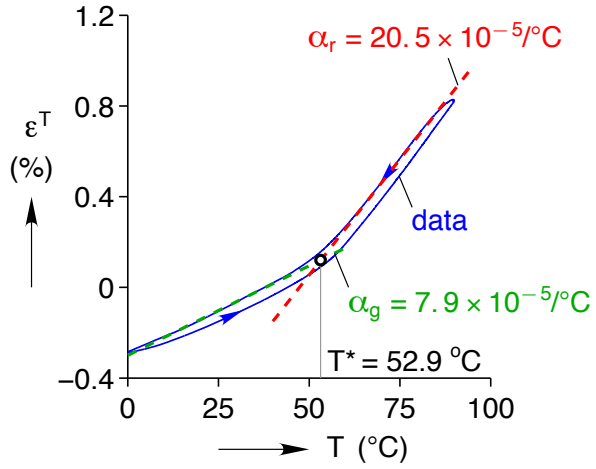

(b)

Figure 3.5: (a) Thermal cycling at ±1 °C/min and the corresponding strain response (b) Coefficients of thermal expansion (α_r, α_g) and the cross-over temperature (T^*)

Temperature scans under a small constant force (1 mN) at a slow heating and cooling rate (1 °C/min) were used to obtain the equilibrium CTE. Figure 3.5a shows the temperature scan data and the corresponding thermal strain history. The last cycle (3^{rd}) data in $\varepsilon^T - T$ space is shown in Fig. 3.5b. The CTE, obtained from fitting only the cooling path of the thermal strain data, in the rubbery state is $\alpha_r = 20.5 \times 10^{-5}$ /°C and in the glassy state $\alpha_g = 7.9 \times 10^{-5}$ /°C. The fitted crossover temperature is $T^* = 52.9$ °C. The CTE are measured from the cooling path of the thermal strain

because a contracting specimen (cooling path) is always closer to equilibrium than the expanding one (heating path). This is because heating increases the kinetic energy of the macromolecules causing them to deviate from their equilibrium state. Isothermal conditions and cooling process leads to 'self-accommodation' of the macromolecular chains due to structural relaxation and results in the recovery of the equilibrium state. This difference in the macromolecular process is partly responsible for the hysteresis observed in thermal strain response shown in Fig. 3.5b. Therefore, clearly structural relaxation effects and the accompanying physical aging are inherent to shape memory behavior.

Figure 3.6 shows the ± 3 °C/min thermal cycling response. The ratcheting of thermal strain is due to structural relaxation resulting from self accommodation of the macromolecular chains. Observe that the hysteresis at ± 3 °C/min in Fig. 3.6b is larger than the hysteresis at ± 1 °C/min shown in Fig. 3.5b. This hysteresis is the result of a combination of structural relaxation and thermal lag effects. Due to the low thermal conductivity epoxy SMPs, the specimen temperature lags the ambient temperature giving rise to increased hysteresis at faster heating/cooling rates. While slower heating/cooling rates reduces the thermal lag, it does not completely eliminate the hysteresis.

It is well established that temperature plays a very important role in the CR aging of polymers [6, 7]. In CR aging studies, the polymer must be unaged at the start of an experiment so that the state of the material can be used as a reference to measure the effects of aging. While slower heating/cooling rates decrease the thermal lag effect, the increase in the time spent at temperatures greater than T_{cr} may cause substantial CR aging even before the start of an experiment. Therefore, in this work, to minimize the CR aging of the material during temperature ramps, faster heating/cooling rates (± 5 °C/min) are used. Figure 3.7 shows the thermal cycling response at ± 5 °C/min.

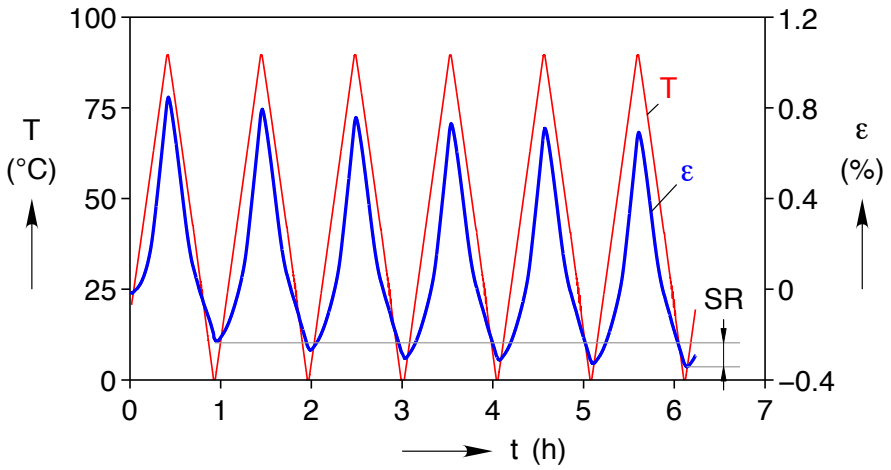

(a)

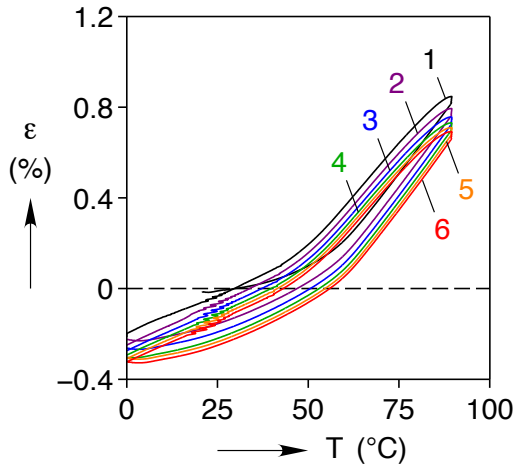

(b)

Figure 3.6: (a) Thermal cycling at ±3 °C/min and the corresponding strain response showing the strain ratcheting due to structural relaxation (b) Temperature vs thermal strains showing the hysteresis due to thermal lag

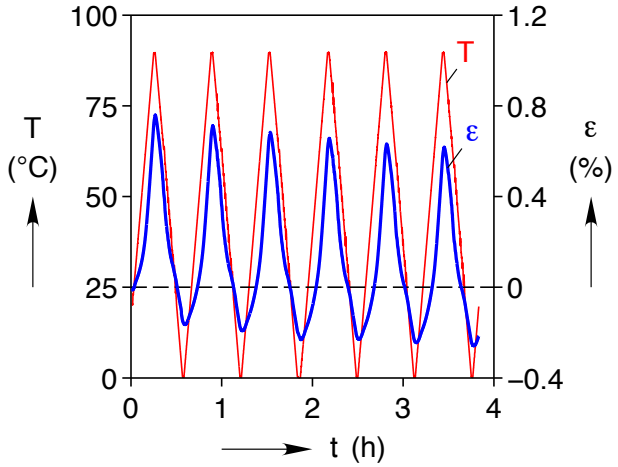

(a)

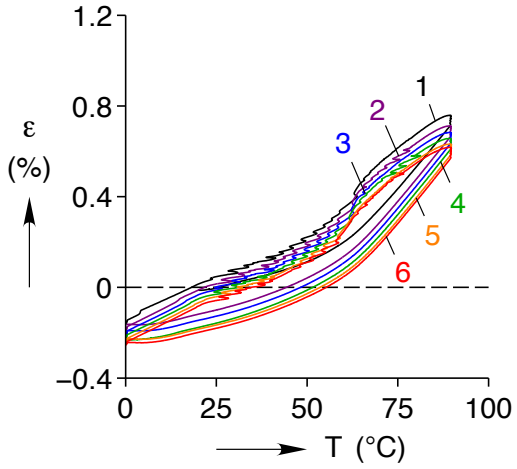

(b)

Figure 3.7: (a) Thermal cycling at ±5 °C/min and the corresponding strain response showing the strain ratcheting due to structural relaxation (b) Temperature vs thermal strains showing the hysteresis due to thermal lag

CHAPTER IV

A Parametric Study of Experimental Variables

Figure 4.1 shows a representative SMC in terms of the engineering stress σ, total engineering strain ε, and temperature T. The time histories are shown in Fig. 4.1a, where stress and temperature were controlled and measured (lower panel) while the strain response was measured (upper panel). The thermal strain (ε^{T}) history shown in Fig. 4.1a (upper panel) is measured on a separate virgin specimen using identical temperature history but under zero load. Using small strain kinematics, the total strain $\varepsilon = \varepsilon^{\mathrm{m}} + \varepsilon^{\mathrm{T}}$ is decomposed into mechanical strain ε^{m} and thermal strain ε^{T} to individually observe the mechanical and thermal expansion responses. The corresponding isometric 3-D plot is provided in Figure 4.1b. The reference configuration is taken at the initial (room) temperature T_0 at zero load to define the zero strain state at ⓪.

The SMC proceeds like this - initially, the SMP specimen is heated load-free to a deformation temperature $T_{\mathrm{d}} = 100$ °C. This results in a thermal strain $\varepsilon_1^{\mathrm{T}}$ at the start of SMC ①. Load is applied, resulting in a stress $\sigma = 0.23$ MPa and the sample is mechanically strained to 1.8% at ②. The sample is held isothermally at constant stress for a duration t_{d}. While still maintaining this applied load, the sample is cooled between ③ and ④ at a constant rate $\dot{T}$ to the initial temperature T_0. During cooling, while ε and ε^{T} decrease, ε^{m} increases slightly due to entropic softening and then

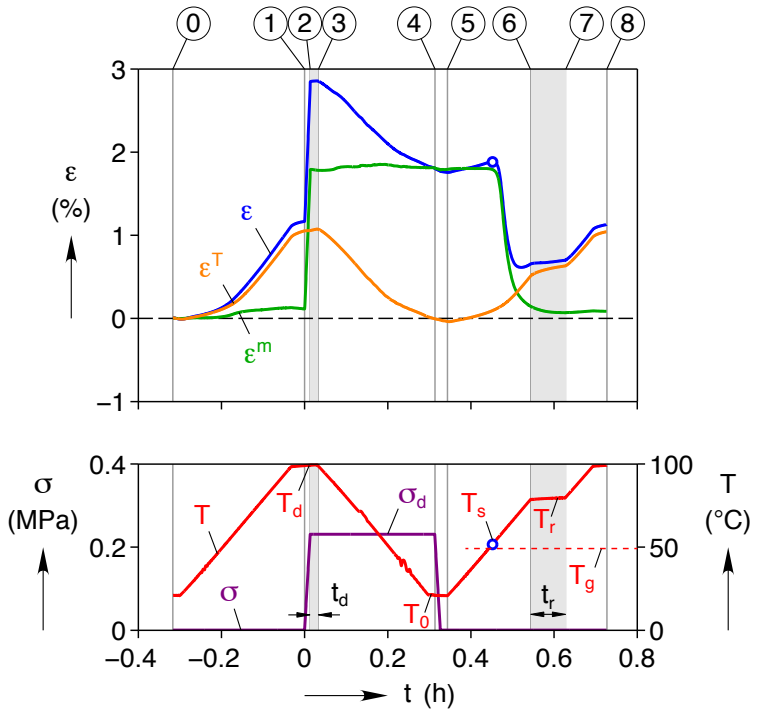

(a)

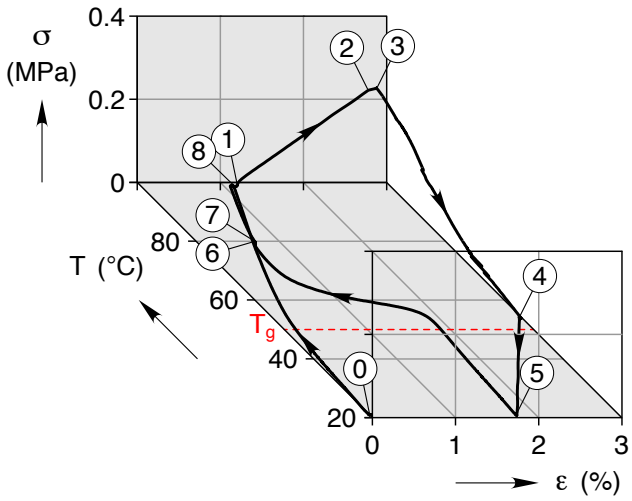

(b)

Figure 4.1: Example SMC data: (a) histories of engineering stress (σ), temperature (T), total strain (ε), thermal strain (ε^{T}) and mechanical strain (ε^{m}) (b) isometric view in $\sigma - \varepsilon - T$ space.

reaches a plateau at temperatures below T_g. The load is then removed at ④, and the SMP has a cold-stored temporary strain. Load-free heating starts at ⑤ to a recovery temperature T_r at ⑥, where it is held for a duration t_r to allow strain recovery. During this heating segment, the start of recovery is taken to be the local maximum of the total strain history (open circle), which defines the start temperature T_s. Then, at ⑦ it is heated (or in later cases, cooled) load-free back to the deformation temperature T_d to start a new SMC at ⑧.

From the SMC procedure the following experimental variables are identified - T_d, σ_d, t_d, $\dot{T}$, T_r and t_r. The exact influence of each of these experimental variables is investigated in this chapter. Based on the understanding of shape memory behavior, it is clear that the T_d and T_r must be greater than T_g for shape-setting and recovery. However, if either of these temperatures exceed the critical CR aging temperature T_{cr} (which is identified later in this chapter) the SMP undergoes CR aging. The magnitude of applied stress σ_d and the hold time during deformation t_d determines the amount of cold-stored strain, thus affecting the thermodynamic driving force for recovery. The hold time during recovery t_r must be long enough to allow viscoelastic recovery of the deformation. The cooling rate $\dot{T}$ can also influence the thermodynamic driving force for recovery since it affects the structural relaxation behavior, as observed during the measurement of CTE (see Section 3.2). Clearly, the choice of these variables not only influences the performance of the SMP, but may alter its thermo-mechanical properties. As such, investigating the effects of these variables is necessary to identify the operation space of the SMP and to establish design guidelines for functionally useful devices.

Several studies exist addressing the effect of experimental variables on the thermo-mechanical behavior of various SMPs [13,16–18,34–39]. Here brief summaries of a few recent studies on the thermo-mechanical behavior of epoxy-based SMPs is provided.

- Castro et. al. [18] investigated the effect of shape fixing (deformation) temperature and recovery temperature on residual strain, recovery ratio (a measure of the ability to recover the permament shape) and recovery time. Using an epoxy-based SMP ('one-part' Veriflex-E™ of Cornerstone Research Group (CRG), $T_g = 75$ °C), they tested specimens in compression up to -20 % strain and a maximum temperature of 100 °C. They found the recovery rate to be strongly dependent on the shape fixing temperature and recovery temperature. They observed highest recovery speeds when shape fixing was performed at a temperature T_d slightly greater than T_g and recovery temperature was larger yet ($T_r > T_d$).

- Feldkamp and Rousseau [17] investigated the influence of deformation temperature on the failure and recovery characteristics of several epoxy SMPs. They found that by changing the fixing temperature to the onset of rubber-glass transition temperature (a. k. a. crossover temperature T^*), typically less than T_g, the failure strains improved five-fold. In shape memory experiments with shape fixing at the crossover temperature and recovery above T_g, they observed recovery ratios in excess of 90 % along with a slight irrecoverable strain.

- McClung, et. al. [36] investigated the influence of deformation rate and hold time on the accumulation of residual strain and 'viscous relaxation' (in the context of viscoelastic fluids, which we believe can be interpreted as CR aging due to scission/crosslinking), using an epoxy-based SMP ('two-part' Veriflex-E™ of CRG, $T_g = 105$ °C). Their experimental procedure involved, in the same cycle, combined 'soak times' at high temperature up to 130 °C before loading the sample (thermal aging) and after loading to 60 % strain (thermo-mechanical aging). They observed an increase in irrecoverable strain with the shape fixing time.

- Rousseau and Xie [16] investigated the effects of stress, recovery heating rate, and shape fixing time on the performance of several epoxy SMPs. They observed the fixity ratio (a measure of the ability to fix the cold-stored shape) to be quite poor below the thermo-elastic inversion strain of $6-7$ % due to large thermal strains (>2 % for a $\Delta T = 100$ °C). Recovery speed was observed to increase with the magnitude of cold-stored strains. The effect of shape fixing time was negligible for the range of fixing temperatures they considered ($T_{\mathrm{f}} \approx T_{\mathrm{g}} + 30$ °C). Heating rates in excess of 10 °C/min was observed to cause a delayed recovery, which we suspect was due to the low thermal conductivity of the SMPs and consequent non-uniform temperature evolution.

The novel contributions of this work come from characterizing the thermo-mechanical behavior of a relatively new epoxy-based SMP and exploring a broader range of experimental variables, encompassing even the chemo-rheological range. In Section 4.1, a discussion of prevalent performance metrics is provided, and due to the thermo-mechanical behavior of epoxy SMP and the range of experimental variables, some of these metrics are re-defined for meaningful interpretation. Section 4.2 then reports the results of a parametric study to assess the influence of deformation temperature, deformation hold time, applied stress, cooling rate, recovery temperature and recovery hold time on these performance metrics. Finally, a brief summary and concluding remarks are given in Section 4.3

4.1 Performance Parameters

A variety of evaluation parameters have been used to quantify the shape memory performance and compare the behavior for different choices of experimental variables [5, 13, 16–18, 34–39]. In this section, some of these evaluation parameters are reviewed and suitable modifications are made to obtain meaningful interpretations.

4.1.1 Shape fixity ratio

The shape fixity ratio (R_f) measures the ability of the SMP material to fix an imposed strain during a SMC. This is commonly expressed as

$$R_\mathrm{f} = \frac{\varepsilon_5 - \varepsilon_1}{\varepsilon_\mathrm{max} - \varepsilon_1}, \tag{4.1}$$

where ε_1 is the strain at the start of the SMC, ε_5 is the cold-stored strain and ε_max is the maximum strain imposed during shape setting. Note that ε is the *total* strain measured during the SMC. In heavily cross-linked polymers such as epoxies the thermal strains and mechanical strains often have similar magnitudes at large deformation temperatures ($T_\mathrm{d} \gg T_\mathrm{g}$), leading to aphysical R_f values. To avoid an incorrect interpretation arising from disparate thermal strains, the shape fixity ratio is re-defined in terms of *mechanical* strains (see again Fig. 4.1a) as

$$R_\mathrm{f} = \frac{\varepsilon_5^\mathrm{m} - \varepsilon_1^\mathrm{m}}{\varepsilon_\mathrm{max}^\mathrm{m} - \varepsilon_1^\mathrm{m}}. \tag{4.2}$$

4.1.2 Shape recovery ratio

The shape recovery ratio (R_r) measures the ability of the SMP material to recover the original shape after a temporary strain is cold-stored during a SMC. In the recovery process, SMP is heated load-free and held first at a recovery temperature T_r and then heated (or cooled) to the deformation temperature T_d for starting a subsequent SMC (see again Fig. 4.1a). As such, recovery ratio can be defined at two temperatures. Similar to shape fixity ratio, recovery ratios are re-defined in terms of *mechanical* strains to avoid potential erroneous values.

Shape recovery ratio at the recovery temperature (R_r^r) is given by

$$R_r^r = \frac{\varepsilon_5^m - \varepsilon_7^m}{\varepsilon_5^m - \varepsilon_1^m} \tag{4.3}$$

and shape recovery ratio at the deformation temperature (R_r^d) is given by

$$R_r^d = \frac{\varepsilon_5^m - \varepsilon_8^m}{\varepsilon_5^m - \varepsilon_1^m} \tag{4.4}$$

It is important to note that due to the thermo-mechanical nature of the SMCs, it is not possible to directly measure the *mechanical* strain. Instead, it is calculated by subtracting the thermal strain data from total strain, which are measured experimentally on separate virgin specimens using identical temperature histories. Incidentally, this also allows subtraction of structural relaxation and thermal lag effects accompanying the temperature changes, see Section 3.2. However, it introduces specimen variability into the calculation of shape fixity and recovery ratios. To minimize this variability, care is taken to homogenize the properties during SMP fabrication and all the specimens were picked from a same molded SMP sheet. Based on thermal strain measurements in DMA for 16 specimens taken to several elevated temperatures (60 to 175 °C), the strain uncertainty due to specimen variability was less than 0.06% strain.

4.1.3 Recovery start temperature

The shape recovery process in a SMC starts at ⑤, see Fig. 4.1a, when the temperature is increased load-free. Initially (between ⑤ and ⑥), as the temperature is raised the strain increases due to the coefficient of thermal expansion. But at a certain temperature (corresponding to the peak in *total* strain between ⑤ and ⑥), the thermodynamic driving force for shape recovery dominates over the thermal expansion

effect, leading to shape recovery. The temperature at which this onset of recovery happens is designated as T_s.

4.1.4 Residual strain

Residual strain accumulation is an important indication of CR aging [6]. Here, residual strain ε_R is defined as the *mechanical* strain at the end of the SMC, i.e. $\varepsilon_R = \varepsilon_8^m$.

4.1.5 Failure strain

Failure strain in epoxies is known to vary with the deformation temperature [8, 17]. As such, failure strain serves as an important evaluation parameter that not only quantifies the effect of deformation temperature, but also establishes a safe strain limit for other experiments.

4.2 Results

In this section, results from the study of influence of experimental variables is reported. The effect of deformation temperature (T_d), applied stress (σ_d), hold time (t_d), recovery time (t_r), cooling rate ($\dot{T}$) and recovery temperature (T_r) are evaluated by comparing the performance metrics.

4.2.1 Deformation temperature

The influence of deformation temperature on the failure of SMP was studied to determine a safe envelope for SMC tests. Stretch to failure tests were performed at several deformation temperatures spanning the viscoelastic transition, rubbery and

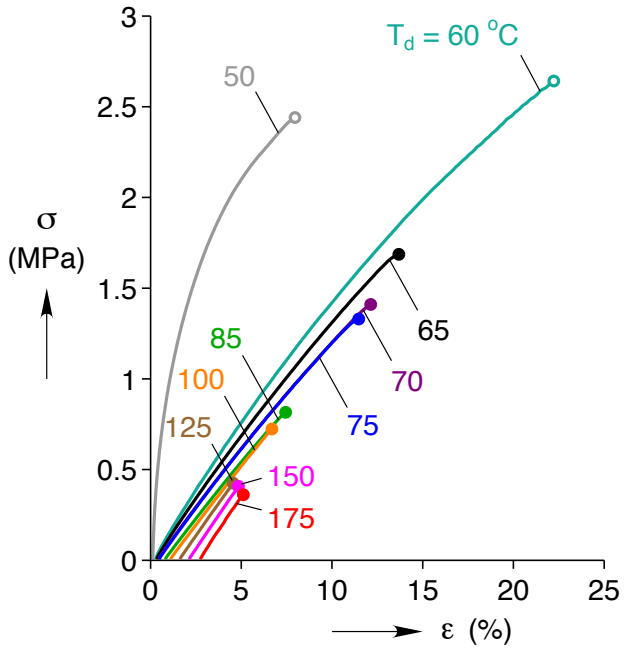

(a)

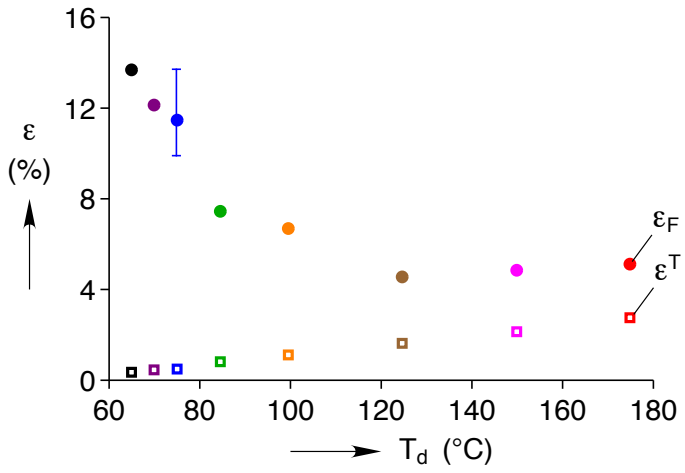

(b)

Figure 4.2: (a) Engineering stress-strain ($\sigma - \varepsilon$) response at different deformation temperatures (T_d) (b) Failure strain (ε_F, filled circles) and thermal strain (ε^T, open squares) vs deformation temperature - open circles: no failure, reached DMA limit

CR zones. A loading rate of 0.5 N/min was used and the reference length is measured at $T_0 = 20$ °C when load-free. Figure 4.2a shows the engineering stress-strain response at different deformation temperatures (T_d). The SMP is much stiffer at $T_\mathrm{d} = 50$ °C ($< T_\mathrm{g}^0$) because it is partially glassy. The open circles indicate that the sample could not be stretched to failure due to DMA limits and that the experiment was stopped. Failure of samples is indicated by filled circles. In all the cases, specimen failure occurred near the grips due to a higher stress concentration. Figure 4.2b shows the strains at failure as a function of the deformation temperature. The variability, measured by testing 5 specimens, is also shown for the 75 °C case. It is observed that large deformation is possible at temperatures slightly greater than T_g and that the failure strain drops drastically with an increase in deformation temperature. Large thermal strains at high deformation temperatures ($T_\mathrm{d} >> T_\mathrm{g}$) also limits the available mechanical deformation.

4.2.2 Applied stress

To study the effect of applied load, SMC tests were performed at deformation temperatures of 60, 65, 70 and 75 °C. A virgin specimen was used for each test. The loading rate is 0.5 N/min and in successive SMCs the peak load was incremented by 0.4 N (a stress increment of 0.23 MPa). Other experimental variables $t_\mathrm{d} = 1$ min, $t_\mathrm{r} = 5$ min, $T_\mathrm{r} = 80$ °C and $\dot{T} = 5$ °C/min, were maintained constant for all the tests. Figure 4.3 shows the engineering stress (σ), temperature (T), the total strain (ε) and thermal strain (ε^T) history during the SMC test with $T_\mathrm{d} = 60$ °C. The thermo-mechanical histories at other deformation temperatures are similar, so are not shown. Using this set of data, mechanical strains are obtained and the shape fixity ratio and shape recovery ratio are calculated from Eqs. 4.2 and 4.4.

Figure 4.4a shows the shape fixity ratio R_f as a function of applied stress at different

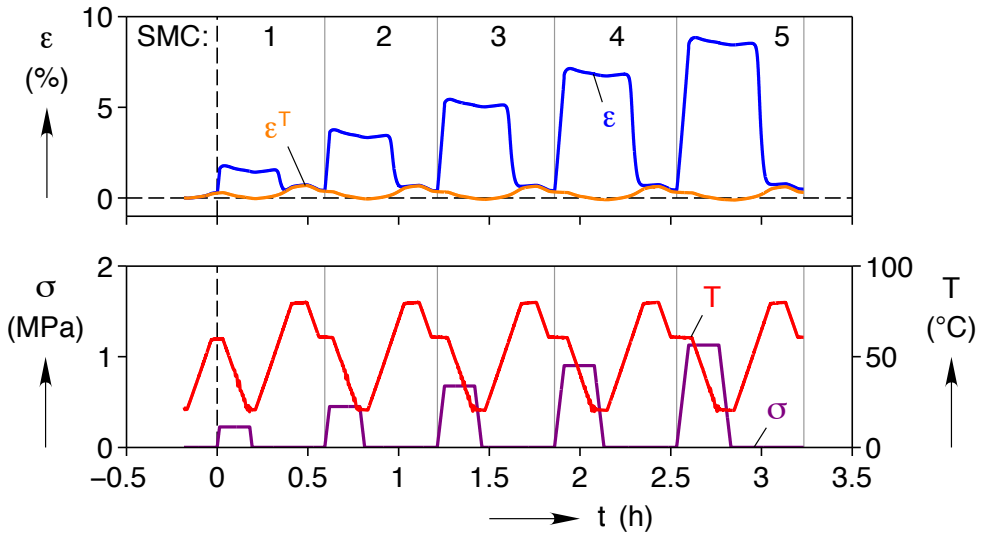

Figure 4.3: Representative engineering stress (σ), temperature (T) total strain (ε) and thermal strain (ε^{T}) history during SMC test ($T_{\mathrm{d}} = 60$ °C) to study the influence of applied load

deformation temperatures. R_{f} in excess of 94 % is observed in all cases. Perfect shape fixity ratio is not expected because some elastic (mechanical) recovery occurs while unloading the sample at temperature T_0 (between ④ and ⑤ in Fig. 4.1). At larger applied stresses fixity ratios of up to 99% are observed. The increasing trend in the R_{f} with applied stress is independent of the deformation temperature. R_{f} increases with applied stresses because of an increase in the imposed strain due to compliance of the SMP at T_{d} (rubbery state) but does not substantially change the elastically (mechanical) recovered strain at T_0 (glassy state) due to the drastic decrease in the compliance at temperatures below T_{g}.

Figure 4.4b shows the variation of recovery ratio at deformation temperature ($R_{\mathrm{r}}^{\mathrm{d}}$) as a function of applied stress. Recovery ratios of 98.5 ± 1.5 % is seen for all cases and it appears to be largely independent of applied stress and deformation temperature.

Figure 4.4c shows the variation in temperature at the start of recovery (T_{s}) as a function of applied stress at various deformation temperatures. It is observed that independent of the deformation temperature, larger applied stress triggers an earlier

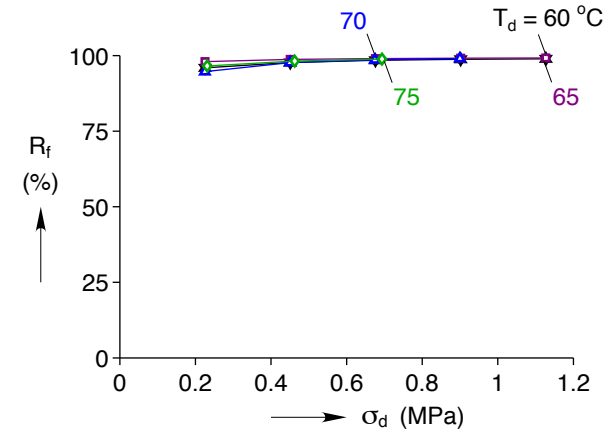

(a)

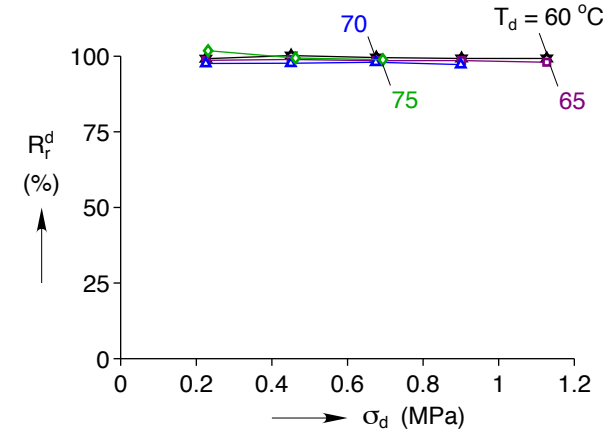

(b)

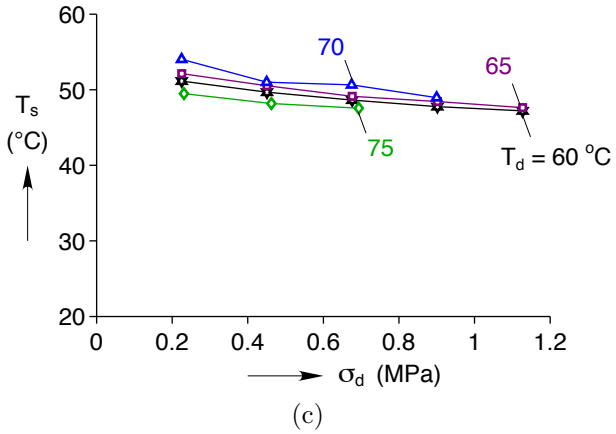

(c)

Figure 4.4: (a) Shape fixity ratio (R_f) vs applied stress (σ_0) at different deformation temperatures (T_d) (b) Shape recovery ratio at the deformation temperature ($R_r^{T_d}$) vs the applied stress (c) Temperature at the start of recovery (T_s) vs applied stress (σ_0) at different deformation temperatures (T_d)

onset of recovery by about 4.5 °C/MPa. This is because shape fixing with a larger applied load causes the macromolecular chains in the polymer to shift farther away from its minimum energy configuration. This leads to an increase in the driving force for recovery, thus lowering the start of recovery temperature.

4.2.3 Hold time and deformation temperature

The effect of hold time at various deformation temperatures was investigated from SMC tests. The data from these experiments also provide a means to identify a possible chemo-rheological temperature $T_{\rm cr}$ and compare the pre and post aging shape memory performance. SMC tests were conducted at $T_{\rm d} = 60$, 75, 100, 125, 150, 158, 166 and 175 °C. At a deformation temperature $T_{\rm d}$, the hold time ($t_{\rm d}$) is varied from cycle to cycle. In the first cycle, $t_{\rm d} = 1$ min, in the next, 15, then 30, 60, 120 and finally a repeat of the 1 min cycle. A virgin specimen was used for each test. The loading rate is 0.5 N/min and other experimental variables $\sigma_{\rm d} = 0.23$ MPa, $t_{\rm r} = 5$ min, $T_{\rm r} = 80$ °C and $\dot{T} = 5$ °C/min, were maintained constant for all the tests.

The engineering stress (σ), temperature (T) the total strain (ε) and the thermal strain ($\varepsilon^{\rm T}$) history during SMC test at the deformation temperatures of 75, 125 and 175 °C are shown in Figs 4.5a ,4.5b and 4.6a. Figure 4.6c shows the test samples after the SMC experiments at different deformation temperatures. An interesting result of these experiments is the color development in the test samples. This color development is attributed to the presence of Amines (see Section 2.1) and the formation of quinone-methide groups due to CR aging [24–26]. Within the time scale of these experiments, color development is first visible in the $T_{\rm d} = 100$ °C sample. Therefore, it is probable that $T_{\rm cr} \approx 100$ °C.

Observe that at $T_{\rm d} = 75$ and 125 °C (Fig. 4.5a and 4.5b), the structural relaxation effects are apparent by the strains ε and $\varepsilon^{\rm T}$ ratcheting downward with each cycle.

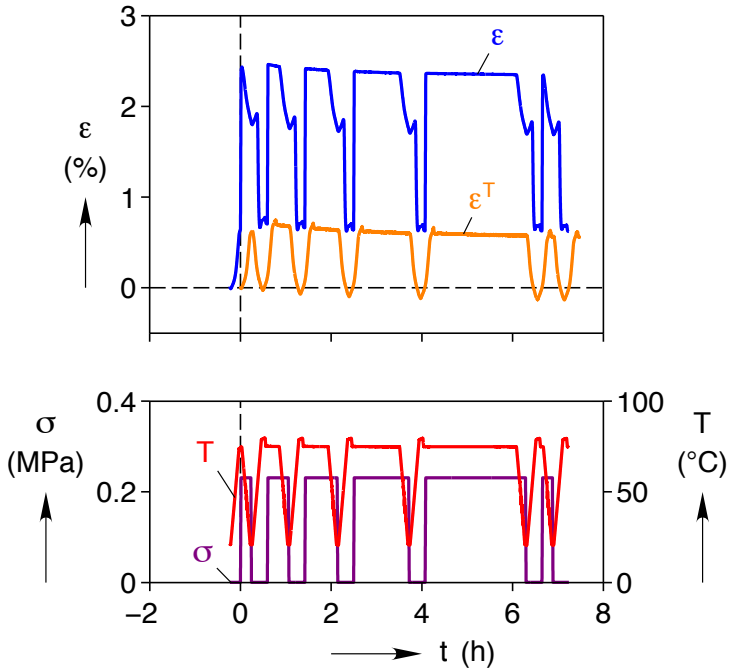

(a)

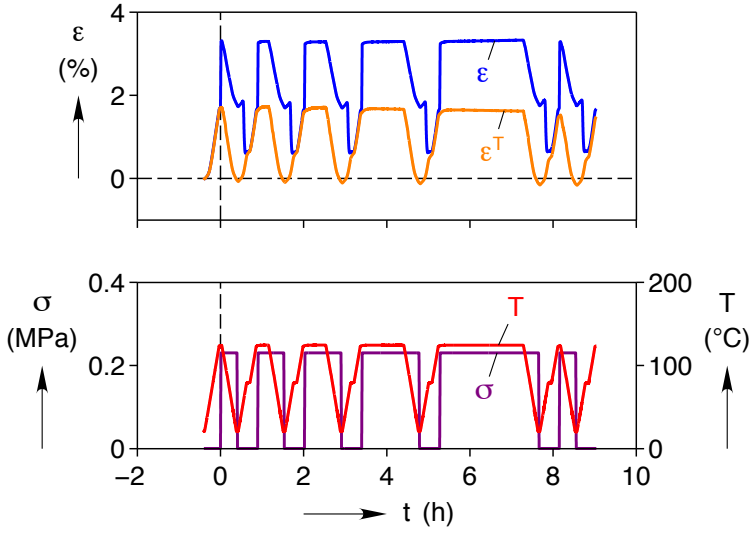

(b)

Figure 4.5: Engineering stress (σ), temperature (T) total strain (ε) and thermal strain (ε^{T}) history during SMC tests to study the influence of hold time (a) $T_{\mathrm{d}} = 75$ °C (b) $T_{\mathrm{d}} = 125$ °C

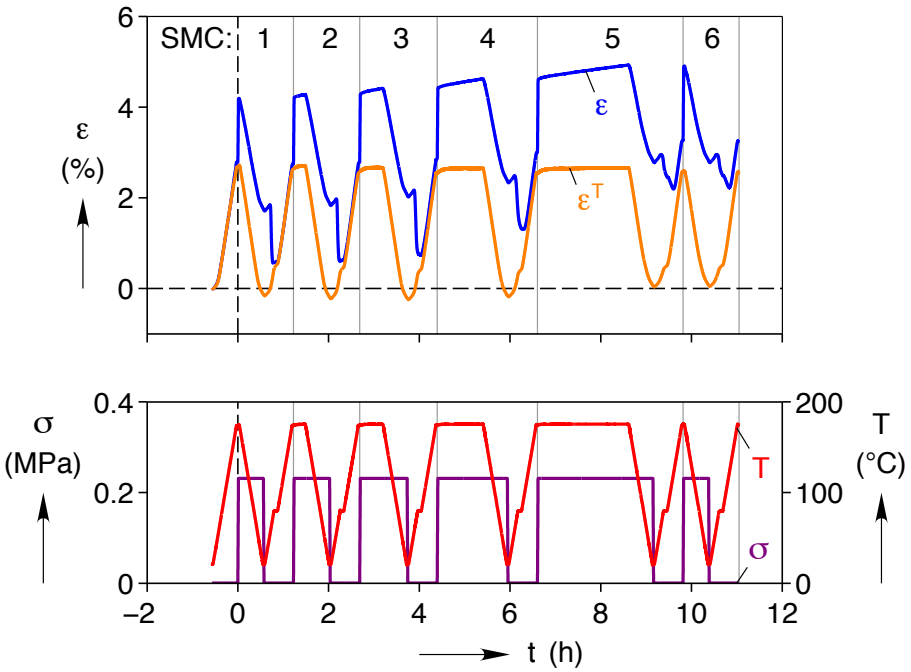

(a)

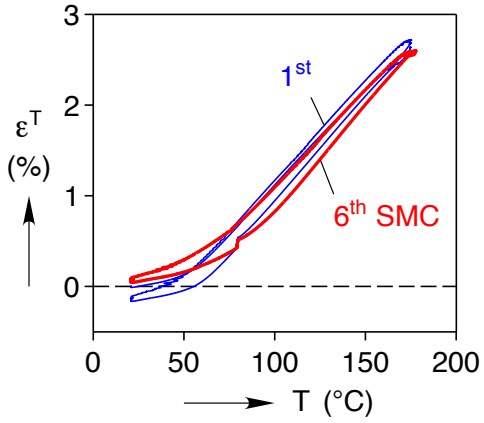

(b)

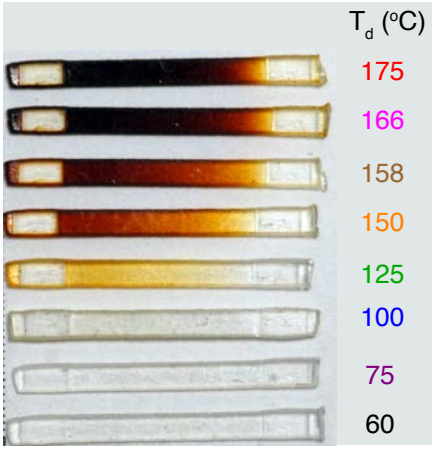

(c)

Figure 4.6: (a) Representative engineering stress (σ), temperature (T) total strain (ε) and thermal strain (ε^{T}) history during SMC test ($T_{\mathrm{d}} = 175$ °C) to study the influence of hold time (b) Comparison of the 1$^{\mathrm{st}}$ and the 6$^{\mathrm{th}}$ cycle thermal strain (ε^{T}) response as a function of temperature (c) Photographs of SMP specimens after SMCs

At $T_{\mathrm{d}} = 175$ °C, as seen in Fig. 4.6a the CR aging causes the total strain ε to increase due to scission and recrosslinking of the macromolecular chains. The creep deformation (at $T_{\mathrm{d}} > T_{\mathrm{cr}}$) due to scission and recrosslinking of the macromolecular chains is known as *chemical creep* [6]. CR aging also influences the thermal strain response as seen in Fig. 4.6b. A comparison of the 1^{st} and the 6^{th} cycle thermal strains as a function of temperature indicates that contrary to structural relaxation effects, CR aging causes the thermal strain to ratchet upwards. According to network theory [6, 7], this can be attributed to the formation of a secondary macromolecular network from recrosslinking. The reference configuration of this secondary network corresponds to the maximum thermal strain since CR aging happens at $T_{\mathrm{d}} = 175$ °C. This disparity in the reference configurations causes the thermal strain to ratchet up with CR aging.

Figure 4.7a compares the shape fixity ratio at different deformation temperatures as a function of hold time. In all cases, a fixity ratio better than 95 % is observed. Fixity ratio appears to marginally increase with holding time. This is to be expected because longer hold times at T_{d} result in larger imposed strains due to creep but it does not affect the elastic recovery associated with unloading at T_0.

Figure 4.7b shows the recovery ratio at different deformation temperatures as a function of hold time. It is observed that for $T_{\mathrm{d}} < 125$ °C, the recovery ratio is relatively constant ($\approx$ 99%) for all t_{d} and for $T_{\mathrm{d}} \geq 125$ °C, the recovery ratio drops with holding time. The extent of drop in $R_{\mathrm{r}}^{\mathrm{d}}$ depends on T_{d}. The drop in the recovery ratio can be attributed to the CR aging. Because $T_{\mathrm{d}} > T_{\mathrm{cr}}$, during shape fixing the SMP undergoes chemical creep resulting in irrecoverable creep deformation. The magnitude of this chemical creep increases with hold time and thus the recovery ratio decreases. While there is some evidence of CR aging at $T_{\mathrm{d}} = 100$ and 125 °C (see Fig. 4.6c), due to the time scale of the experiment the amount of aging is not significant to drastically

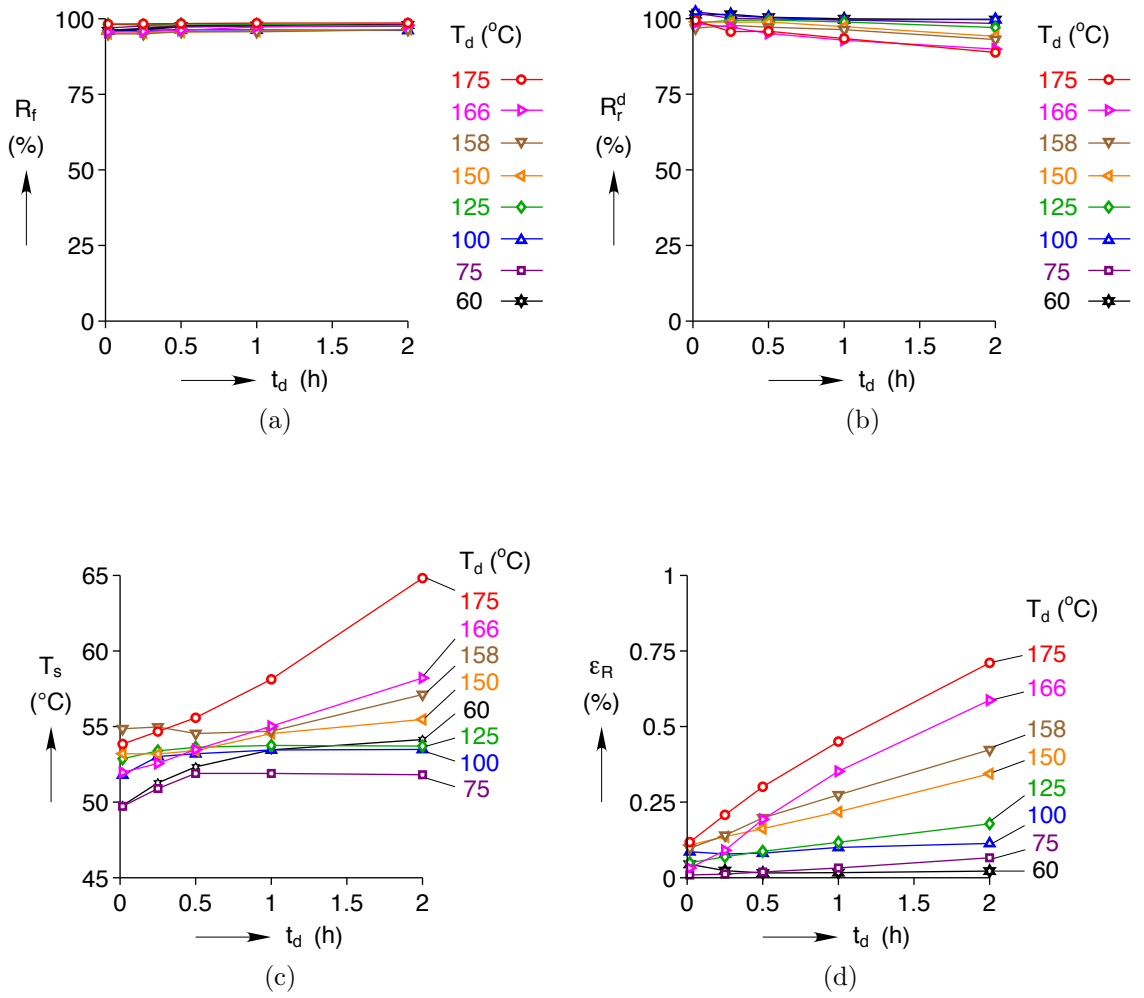

Figure 4.7: (a) Shape fixity ratio (R_f) vs hold time (t_d) at different deformation temperatures (T_d) (b) Shape recovery ratio at the deformation temperature ($R_r^{T_d}$) vs the hold time (c) Temperature at the start of recovery (T_s) vs hold time (t_d) at different deformation temperatures (T_d) (d) Residual strain (ε_R) vs hold time

affect the recovery ratio at T_d. Therefore, in summary it can be said that in the absence of CR aging the shape recovery ratio is independent of hold time. However, the recovery ratio decreases due to CR aging and the rate of decrease depends on the deformation temperature.

Figure 4.7c shows the temperature at the start of recovery T_s as a function of holding time. It is observed that in the absence of aging, the T_s increases with hold time and reaches a plateau, whereas CR aging causes the T_s to monotonically increase with hold time. In the absence of aging, contrary to the case of increased applied load, longer hold times allow for the relaxation of macromolecular chains in the polymer. This decreases the driving force for recovery, hence requiring higher start of recovery temperatures. At $T_d > T_{cr}$, there is increased CR aging with hold time. It is known that CR aging in epoxies increases the glass transition temperature [24]. This rise in T_g is the cause of increased start of recovery temperature (T_s) for $T_d > T_{cr}$.

Residual mechanical strain is plotted as a function of hold time in Fig. 4.7d. Significant accumulation of residual strain happens at deformation temperatures greater than 150 °C. This indicates that $T_d > 150$ °C are suitable for accelerated CR aging studies within a convenient timeframe but bad for applications in which SMP length is critical for operation.

4.2.4 Cooling rate

A SMC test was conducted where the cooling rate was varied from cycle to cycle as 1, 3, 5, 7 and 10 °C/min. Figure 4.8 shows the engineering stress (σ), temperature (T) and total strain (ε) history during this experiment. The loading rate was maintained 0.5 N/min and other experimental variables $\sigma_d = 0.23$ MPa, $T_d = 75$ °C, $t_d = 1$ min, $T_r = 80$ °C and $t_r = 5$ min were kept constant. The cooling rate effect was found to be negligible and perfect recovery was observed in all the cases. However, if the

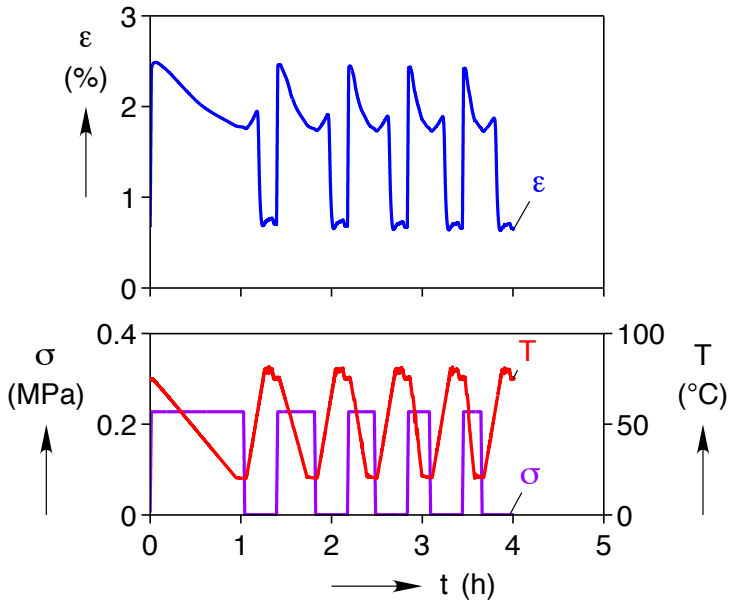

Figure 4.8: Engineering stress (σ), temperature (T) and total strain (ε) history during SMC test ($T_{\mathrm{d}} = 75$ °C) to study the influence of cooling rate

deformation temperature were to be greater than T_{cr}, then slower cooling rates would lead to CR aging of SMP.

4.2.5 Recovery time

The effect of recovery time t_{r} was not explicitly investigated in this work. Nevertheless, its effects can be inferred from the SMC test data presented in Section 4.2.3. To set an appropriate value of t_{r}, two factors have to be considered. First, thermal lag due to heating from T_0 to T_{r} and second, the choice of T_{r} relative to T_{cr}.

If the material is heated at a very fast rate (⑤-⑥ in Fig. 4.1a) then, due to low thermal conductivity of the polymer, sufficient time must be provided for the material to heat up and viscoelastically recover the deformation. Therefore the heating rate, thermal conductivity and the relaxation times for the SMP dictate the lower bound for the recovery time. If the choice of t_{r} is greater than this lower bound then it has no effect as long as $T_{\mathrm{r}} < T_{\mathrm{cr}}$. If $T_{\mathrm{r}} > T_{\mathrm{cr}}$, then, a longer t_{r} increases the amount of thermal

aging of SMP. This thermal aging might be beneficial if it leads to an increase in recovery. However, the material property changes accompanying this thermal aging are irreversible and it can affect the performance of SMP.

4.2.6 Recovery temperature

The effect of recovery temperature T_{r} is investigated using the SMC test data from Section 4.2.3. The recovery temperature was fixed at 80 °C for all the SMC experiments. Figure 4.9a shows the recovery ratio at the *recovery* temperature (calculated using Eq. 4.3) as a function of holding time. Data for $T_{\mathrm{d}} = 60$ and 75 °C are not shown because $T_{\mathrm{d}} < T_{\mathrm{r}}$ and there was perfect recovery for these cases as seen in Fig. 4.7b. In Fig. 4.9a it is observed that for $T_{\mathrm{d}} = 100$ °C there is perfect recovery even though $T_{\mathrm{d}} = T_{\mathrm{cr}}$. This is because the SMP did not undergo substantial CR aging at T_{cr} within the time-frame of the SMC experiment. However, at other deformation temperatures $T_{\mathrm{d}} > T_{\mathrm{cr}}$, the recovery ratio drops drastically as the material undergoes CR aging.

A comparison of recovery ratios calculated at the recovery temperature $R_{\mathrm{r}}^{\mathrm{r}}$ and deformation temperature $R_{\mathrm{r}}^{\mathrm{d}}$ is shown in Fig. 4.9b for the two cases of very little aging ($T_{\mathrm{d}} = T_{\mathrm{cr}}$) and severe aging ($T_{\mathrm{d}} >> T_{\mathrm{cr}}$). It is observed that the recovery ratio of the aged SMP improves when heated to a higher temperature as in the case of $T_{\mathrm{d}} = 175$ °C. However, one must be aware of the fact that recovery temperatures greater than T_{cr} causes thermal aging of the SMP. The accompanying material property changes would be irreversible. The effect of thermal aging on the material properties of SMP is investigated in Chapter V.

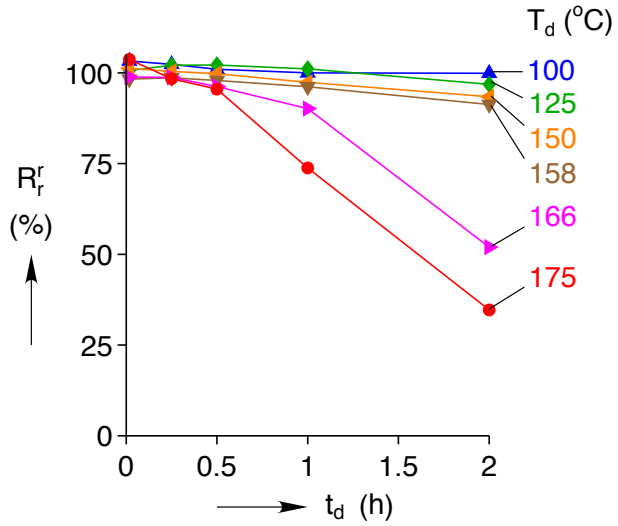

(a)

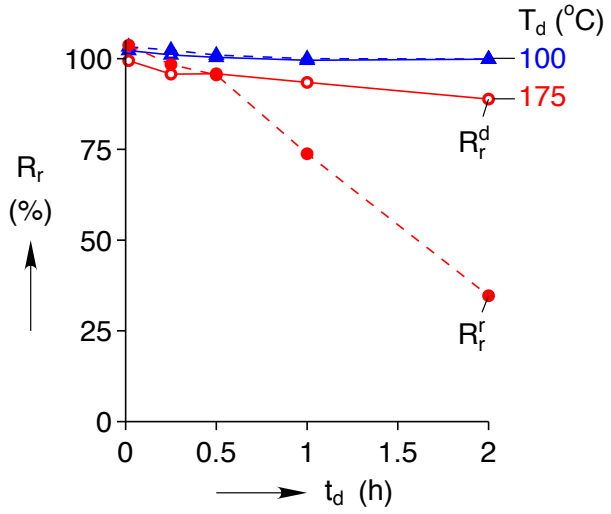

(b)

Figure 4.9: (a) Recovery ratio at recovery temperature ($R_{\mathrm{r}}^{\mathrm{T_r}}$) vs hold time ($t_{\mathrm{d}}$) for different deformation temperatures (T_{d}) (b) comparison of recovery ratios at two recovery temperatures (T_{r} and T_{d}) for the cases of $T_{\mathrm{d}} = 100$ and 175 °C

4.3 Summary

The purpose of this experimental study was to investigate the influence of experimental variables such deformation temperature (T_{d}), applied applied (σ_{d}), hold time (t_{d}), cooling rate, recovery temperature (T_{r}) and recovery time (t_{r}) on the thermomechanical behavior and the performance of the epoxy SMP. Experiments were performed under uniaxial tension in dry air environment using a new specimen for each test. In SMC experiments, thermal strain was measured on a separate virgin specimen using an identical temperature history and mechanical strain was obtained from small strain kinematic decomposition. Performance evaluation parameters such as fixity ratio R_{f}, recovery ratios at recovery temperature $R_{\mathrm{r}}^{\mathrm{r}}$ and deformation temperature $R_{\mathrm{r}}^{\mathrm{d}}$, temperature at the start of recovery T_{s}, residual strain ε_{R} and failure strain ε_{F} were defined to compare the shape memory responses and interpret the influence of experimental variables.

Stretch to failure tests were performed at several deformation temperatures in the range of ($T_{\mathrm{g}}-10, T_{\mathrm{g}}+120$ °C) to establish a safe strain envelope for SMC experiments. At deformation temperatures very close to the T_{g} large deformation was possible leading to strains in excess of 20%. At higher deformation temperatures ($T_{\mathrm{g}}+44$ °C) the failure strains dropped drastically to below 6%.

Effect of applied load on the shape memory behavior was studied at deformation temperatures in the range of ($T_{\mathrm{g}} < T_{\mathrm{d}} < T_{\mathrm{g}} + 20$). In SMC tests, the applied stress σ_{d} was varied from 0.2-1.2 MPa. A fixity ratio in excess of 94% and a recovery ratio of 98.5±1.5% was observed in all cases. While fixity ratio increased up to 99% with applied stress, the recovery ratio remained invariant. Increased applied stresses also resulted in an earlier start of recovery.

Effect of hold time and deformation temperature was investigated using SMC tests to

identify the critical CR temperature T_{cr} and also obtain the effect of aging on shape memory performance. SMC tests were performed at several deformation temperatures in the range of (T_g, T_g+120 °C) and at each T_d hold times were varied from 1-120 min from cycle to cycle (6 SMCs). After the tests, several SMP specimens (starting with the one corresponding to T_d = 100 °C) showed color development which is a sign of CR aging. Based on color development it was established that $T_{cr} \approx 100$ °C. For all the cases, shape fixity ratio in excess of 95% was observed and it increased marginally with holding times. The recovery ratio on the other hand, was about 99% for $T_d \leq T_{cr}$ at all hold times and decreased for $T_d > T_{cr}$ because of increased CR aging. The start of recovery temperature (T_s) and residual strains (ε_R) also increased with CR aging. In the absence of CR aging, recovery time and cooling rate did not affect the performance of SMP and a recovery temperature above the T_g and T_s was sufficient to achieve complete recovery. For aged samples higher recovery temperatures led to *better* recovery.

CHAPTER V

A Chemo-Visco Model for SMPs

In this chapter, a constitutive model is developed for shape memory behavior incorporating the kinetics of CR aging. The existing constitutive models of shape memory behavior [22, 40–55] only incorporate the structural relaxation phenomena and its accompanying effects. Some of these existing models is reviewed here.

- Tobushi et al. [40, 41] developed a 1-D thermo-mechanical constitutive model by modifying the standard linear viscoelastic solid. A slip element was added in series with the equilibrium branch to model the structural relaxation and the thermal expansion behavior. The variation of the mechanical properties due to glass transition was modeled as a single exponential function of temperature.

- Liu et al. [44] proposed a small strain 3D constitutive model based on the framework reported by Dinani et al [43] to simulate strain and stress recovery for various boundary conditions. In this model, the configurational changes in the SMP across the glass transition was modeled using a glassy 'frozen phase' and a rubbery 'active phase'. The volume fraction of these phases and the cold-stored strain were chosen as internal state variables. Internal energy was considered to be the dominating factor in the deformation of the frozen phase and entropic changes were associated with the deformation of the active phase. The effect of cooling/heating rate on the volume fraction of phases (structural

relaxation effects) was not modeled. Hooke's law was used to model the elastic response of the frozen phase and the Neo-Hookean model was used for the active phase.

- Chen and Lagoudas [48,49] and Volk et al. [52,53] model the SMP by considering a glassy frozen phase and a rubbery active phase. Their approach is based on the work of Liu et al. [44] with some differences. The volume fraction of the frozen phase (internal variable) was modeled as a function of temperature only. In the transition zone, the SMP was modeled like a composite by using average kinematic quantities. A Neo-Hookean constitutive equation was used to represent the elastic behavior of both the glassy and rubbery phases.

- Nguyen et al. [46, 51] proposed a thermo-viscoelastic model incorporating the time and temperature dependent effects of structural and stress relaxation. The material's approach to equilibrium due to structural relaxation was represented by the Kovacs-Aklonis-Hutchinson-Ramos (KAHR) model and the thermodynamic theory of glass transition was used to model the structural relaxation time. The nonlinear viscoelasticity framework of Reese and Govindgee [56] was used to model the stress relaxation (mechanical) response. The glassy response of the material was represented by a Neo-Hookean model and the rubbery response was modeled using the eight-chain model of Aruda-Boyce [57] with Langevin chain statistics to capture finite extensibility effects.

- Westbrook et al [54] and Yu et al. [22] developed a 'multi-branch' model that is similar to a generalized 1D viscoelastic model consisting of N-Maxwell elements in parallel with a spring. In this multi-branch branch model, $N_1 < N$ Maxwell elements are used to model the relaxation mechanisms in the glassy phase (structural relaxation) and $N_2 = N - N_1$ Maxwell elements are used to model the relaxation mechanisms of the rubbery phases (stress relaxation). The

structural relaxation is modeled by considering a 33 parameter KAHR model. The same viscous flow rules are considered for both the glassy and rubber non-equilibrium branches. For the glassy non-equilibrium branch, the shear modulus is taken to be independent of temperature and the Maxwell elements in rubbery non-equilibrium branch have the same Neo-Hookean shear modulus. The constitutive behavior of the equilibrium branch is represented by the eight-chain Arruda-Boyce model.

The novel contribution of this work is the development of a constitutive model for shape memory behavior of SMP incorporating the kinetics of CR aging. Multi-Network theory is used to describe the macromolecular structure of the SMP [6, 7]. According to this theory, CR aging causes degradation of the original (1^{st}) macromolecular network resulting in the formation of new (secondary) interpenetrating macromolecular networks having new properties and possibly a different stress-free configuration. In this 'chemo-visco' constitutive model, the viscoelastic response is modeled using Maxwell model elements in parallel with a spring. During CR aging, structural relaxation effects and contributions of physical aging are negligible, therefore they are not modeled. Thermal history response is modeled using the equilibrium linear coefficients of thermal expansion.

A viscoelastic constitutive equation for time varying temperature histories [32] can be used to model the baseline (unaged) thermo-mechanical behavior of SMPs. This viscoelastic constitutive framework is reviewed in Section 5.1 to illustrate the concepts. Two models for the relaxation function, a 12-term Prony series and a Standard Linear Solid (SLS) are calibrated. The thermo-mechanical response of these models are compared with the SMC experiments.

Then, a constitutive framework for CR-viscoelastic behavior of SMPs is developed in three parts (a) SMP undergoing CR aging during stress relaxation at a constant

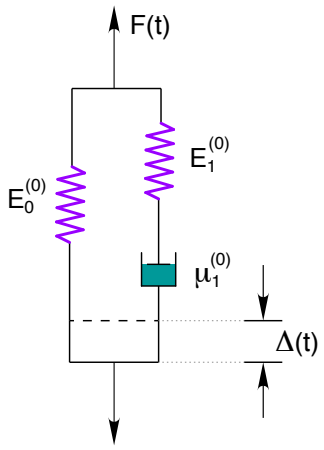

Figure 5.1: Mechanical analog model of the undegraded SMP

temperature (b) SMP undergoing CR aging during creep at a constant temperature (c) SMP undergoing CR aging under arbitrary strain and stress histories at a constant temperature. Results from an experimental investigation into the kinetics of CR aging and its influence on the viscoelastic behavior of SMP are presented. Based on this empirical study, a suitable form of relaxation function is assumed and material properties are calibrated. This model is then generalized to the case of viscoelastic relaxation and CR aging under time varying temperature and arbitrary stress or strain histories. To evaluate the predictive capability, the thermo-mechanical response of this chemo-visco model is compared with the SMC experiments.

5.1 Baseline Viscoelastic Model

This is a review of the viscoelastic constitutive framework [32] for the thermo-mechanical behavior of an unaged SMP. It is presented to illustrate the concepts which will be later used in the development of the chemo-visco model in Sections 5.4 and 5.6. The presentation of ideas is carried out using a SLS model representation. In this derivation, unless mentioned otherwise, temperature is taken to be constant in time. Figure 5.1 shows the mechanical analog model of the 1^{st} network (undegraded) of

a SMP. From the fundamental treatment of viscoelasticity [32], the force-elongation ($F(t)$-$\Delta(t)$) relation for this 1$^{\text{st}}$ network is given by

$$\left(\frac{D}{E_1^{(0)}}+\frac{1}{\mu_1^{(0)}}\right)F(t)=\left[D\left(1+\frac{E_0^{(0)}}{E_1^{(0)}}\right)+\frac{E_0^{(0)}}{\mu_1^{(0)}}\right]\Delta(t) \tag{5.1}$$

where, D is the differential operator d/dt. This gives a constitutive relation of form

$$p_0^{(0)}\sigma+p_1^{(0)}\dot{\sigma}=q_0^{(0)}\varepsilon^{\mathrm{m}}+q_1^{(0)}\dot{\varepsilon}^{\mathrm{m}} \tag{5.2}$$

where, $p_0^{(0)}=\dfrac{1}{\mu_1^{(0)}}$, $p_1^{(0)}=\dfrac{1}{E_1^{(0)}}$, $q_0^{(0)}=\dfrac{E_0^{(0)}}{\mu_1^{(0)}}$, $q_1^{(0)}=1+\dfrac{E_0^{(0)}}{E_1^{(0)}}$, σ is the stress and ε^{m} is the mechanical strain.

5.1.1 Initial Condition

In the development of fundamental models of viscoelasticity, jump discontinuities in stress and strain histories must be considered to describe creep and stress relaxation tests. Equation 5.2 is only valid at times when there are no jump discontinuities. So, difficulties arise when a step stress or strain is applied at $t = 0$. The procedure to derive the initial conditions is presented here using a creep test analogy[1]. Experimentally it is not possible to apply a true step-stress history. The actual stress history is continuous and varies very fast during loading. Therefore a step-stress history can be regarded as the limit of this smooth rapidly varying, continuous stress history (see, Figure 5.2).

Let $\sigma(t)$ be an arbitrary stress history with $\sigma(0-)=0$ and $\sigma(0+)\neq 0$. Let $\sigma_n(t)$ be a sequence of smooth rapidly varying stress histories such that $\sigma_n(0-)=\sigma_n(0+)=0$ and $\sigma_n(t)=\sigma(t)$ for $t\geq\delta_n$. Where, δ_n is a small duration of time when the stress

[1]Understandably, we would get the same initial condition if we used a stress relaxation test analogy.

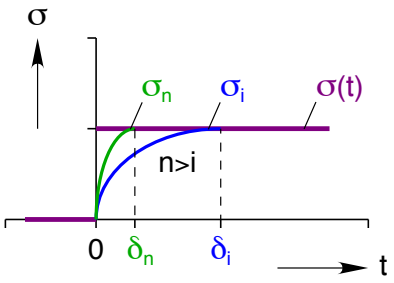

Figure 5.2: A sequence of continuous stress histories (σ_n) approaching the step-stress history

history σ_n is continuous but varying rapidly. Let the sequence of times δ_n be such that as $n \to \infty$, $\delta_n \to 0+$.

If $\varepsilon_n^{\mathrm{m}}(t)$ is the mechanical strain response to $\sigma_n(t)$, then from Eq. 5.2

$$q_0^{(0)}\varepsilon_n^{\mathrm{m}} + q_1^{(0)}\dot{\varepsilon}_n^{\mathrm{m}} = p_0^{(0)}\sigma_n + p_1^{(0)}\dot{\sigma}_n, \quad t > \delta_n \tag{5.3}$$

Since $\sigma_n(0-) = \sigma_n(0+) = 0$, it is possible to assume, $\varepsilon_n^{\mathrm{m}}(0-) = \varepsilon_n^{\mathrm{m}}(0+) = 0$. In other words, a continuous stress history implies a continuous strain response. Integrating Eq. 5.3 in the interval $(0-, \delta_n)$ and applying the initial condition for the continuous history,

$$\int_{0-}^{\delta_n} q_0^{(0)}\varepsilon_n^{\mathrm{m}} dt + q_1^{(0)}\varepsilon_n^{\mathrm{m}}(\delta_n) = \int_{0-}^{\delta_n} p_0^{(0)}\sigma_n dt + p_1^{(0)}\sigma_n(\delta_n) \tag{5.4}$$

In the limit $n \to \infty$, $\delta_n \to 0+$ and

$$\varepsilon_n^{\mathrm{m}}(t) \to \varepsilon^{\mathrm{m}}(t), \quad t > 0 \qquad\qquad \varepsilon_n^{\mathrm{m}}(\delta_n) \to \varepsilon^{\mathrm{m}}(0+)$$

$$\sigma_n(t) \to \sigma(t), \quad t > 0 \qquad\qquad \sigma_n(\delta_n) \to \sigma(0+)$$

Also,

$$\lim_{\delta_n \to 0+} \int_{0-}^{\delta_n} \varepsilon_n^{\mathrm{m}}(t) dt = 0 \quad \text{and} \quad \lim_{\delta_n \to 0+} \int_{0-}^{\delta_n} \sigma_n(t) dt = 0$$

to ensure $\varepsilon_n^{\mathrm{m}}(t)$ and $\sigma_n(t)$ are bounded. Therefore, in the limit we get the initial

condition to be

$$q_1^{(0)}\varepsilon^{\mathrm{m}}(0+) = p_1^{(0)}\sigma(0+) \tag{5.5}$$

5.1.2 Stress Relaxation Response

Taking Laplace transform of Eq. 5.2 and using the initial condition Eq. 5.5, we get

$$\left(p_0^{(0)} + p_1^{(0)}a\right)\overline{\sigma} = \left(q_0^{(0)} + q_1^{(0)}a\right)\overline{\varepsilon}^{\mathrm{m}} \tag{5.6}$$

Equation 5.6 relates the Laplace transform ($\overline{\sigma}(a)$) of a general stress history ($\sigma(s)$) to the Laplace transform ($\overline{\varepsilon}^{\mathrm{m}}(a)$) of a general strain history ($\varepsilon^{\mathrm{m}}(s)$). Stress relaxation response is obtained when a viscoelastic solid is subject to a step strain input. That is, $\varepsilon^{\mathrm{m}}(t) = \varepsilon_0^{\mathrm{m}}$ for $t \geq 0$ or $\overline{\varepsilon}^{\mathrm{m}}(a) = \dfrac{\varepsilon_0^{\mathrm{m}}}{a}$. From Eq. 5.6,

$$\overline{\sigma} = \frac{\varepsilon_0^{\mathrm{m}}}{a}\frac{q_0^{(0)} + q_1^{(0)}a}{p_0^{(0)} + p_1^{(0)}a} = \varepsilon_0^{\mathrm{m}}\overline{G}^{(0)}(a) \tag{5.7}$$

where, $\overline{G}^{(0)}(a) = \dfrac{1}{a}\dfrac{q_0^{(0)} + q_1^{(0)}a}{p_0^{(0)} + p_1^{(0)}a}$ is the Laplace transform of the stress relaxation function $G^{(0)}(t)$. Taking the inverse Laplace transform of Eq. 5.7

$$\sigma(t) = G^{(0)}(t)\varepsilon_0^{\mathrm{m}} \tag{5.8}$$

where, $G^{(0)}(t)$ has a form $G^{(0)}(t) = G_\infty^{(0)} + G_1^{(0)}\exp\left(-\dfrac{t}{\tau_{\mathrm{R1}}^{(0)}}\right)$ for some constants $G_\infty^{(0)}$, $G_1^{(0)}$ and $\tau_{R1}^{(0)}$.

5.1.3 Creep Response

For a creep test, $\sigma(t) = \sigma_0$ for $t \geq 0$. From Eq. 5.6 the strain response is given by

$$\overline{\varepsilon}^{\mathrm{m}}(a) = \frac{\sigma_0}{a} \frac{p_0^{(0)} + p_1^{(0)} a}{q_0^{(0)} + q_1^{(0)} a} = \overline{J}^{(0)}(a)\sigma_0 \tag{5.9}$$

where, $\overline{J}^{(0)}(a) = \dfrac{1}{a} \dfrac{p_0^{(0)} + p_1^{(0)} a}{q_0^{(0)} + q_1^{(0)} a}$ is the Laplace transform of the creep compliance function $J^{(0)}(t)$. Taking the inverse Laplace transform of Eq. 5.9

$$\varepsilon^{\mathrm{m}}(t) = J^{(0)}(t)\sigma_0 \tag{5.10}$$

where, $J^{(0)}(t)$ has a form $J^{(0)}(t) = J_\infty^{(0)} + J_1^{(0)} \exp\left(-\dfrac{t}{\tau_{\mathrm{C1}}^{(0)}}\right)$ for some constants $J_\infty^{(0)}$, $J_1^{(0)}$ and $\tau_{C1}^{(0)}$.

5.1.4 Isothermal Response to Arbitrary Stress and Strain Histories

From Eq. 5.6,

$$\overline{\varepsilon}^{\mathrm{m}}(a) = \frac{p_0^{(0)} + p_1^{(0)} a}{q_0^{(0)} + q_1^{(0)} a} \overline{\sigma}(a) = a\overline{J}^{(0)}(a)\overline{\sigma}(a) \tag{5.11}$$

This can be further written as

$$\overline{\varepsilon}^{\mathrm{m}}(a) = \sigma(0+)\overline{J}^{(0)}(a) + \overline{J}^{(0)}(a)\left[a\overline{\sigma}(a) - \sigma(0+)\right] \tag{5.12}$$

Taking the inverse Laplace transform, the mechanical strain response to arbitrary stress history is obtained to be

$$\varepsilon^{\mathrm{m}}(t) = \sigma(0+)J^{(0)}(t) + \int_0^t J^{(0)}(t-s)\dot{\sigma}(s)ds \tag{5.13}$$

Likewise, the stress response of the SMP to arbitrary mechanical strain history is given by

$$\sigma(t) = \varepsilon^{\mathrm{m}}(0+)G^{(0)}(t) + \int_0^t G^{(0)}(t-s)\dot{\varepsilon}^{\mathrm{m}}(s)ds \tag{5.14}$$

5.1.5 Extension to Time-Varying Temperature Histories

So far, in the derivation of the constitutive equations the temperature was assumed to be constant in time. In this section, the case of time-varying temperature histories is considered. Based on TTSP, it is possible to relate the macromolecular reconfiguration during a small time interval of time to the average temperature during this interval. The idea is presented using the stress relaxation response analogy.

At the beginning of stress relaxation, during a time interval $0 \leq s \leq t_1$, let $\hat{T}_1$ be the average temperature. From TTSP, the increment in $G^{(0)}$ at temperature $\hat{T}_1$ during the time interval $(t_1 - 0)$ is the same as the increment in $G^{(0)}$ at a reference temperature T_{g}^0 during the time interval $\dfrac{t_1 - 0}{a_{\mathrm{T}}(\hat{T}_1, T_{\mathrm{g}}^0)}$, where a_{T} is the temperature shift function. Thus,

$$G^{(0)}\left[t_1, \overset{t_1}{\underset{s=0}{\mathrm{T(s)}}}\right] = G^{(0)}\left[\frac{t_1 - 0}{a_{\mathrm{T}}(\hat{T}_1, T_g^0)}, T_g^0\right] \tag{5.15}$$

where, $\overset{t_1}{\underset{s=0}{\mathrm{T(s)}}}$ represents the temperature history $T(s)$, $s \in [0, t_1]$. During the time interval $t_1 \leq s \leq t_2$ with an average temperature $\hat{T}_2$, the increment in $G^{(0)}$ is

$$G^{(0)}\left[t_2, \overset{t_2}{\underset{s=0}{\mathrm{T(s)}}}\right] = G^{(0)}\left[\frac{t_1 - 0}{a_{\mathrm{T}}(\hat{T}_1, T_g^0)} + \frac{t_2 - t_1}{a_{\mathrm{T}}(\hat{T}_2, T_g^0)}, T_g^0\right] \tag{5.16}$$

Continuing in this manner,

$$G^{(0)}\left[t_n, \overset{t_n}{\underset{s=0}{\mathrm{T(s)}}}\right] = G^{(0)}\left[\sum_{k=1}^{n} \frac{t_k - t_{k-1}}{a_{\mathrm{T}}(\hat{T}_k, T_g^0)}, T_g^0\right] \tag{5.17}$$

where $\hat{T}_k$ is the average temperature during the interval $t_{k-1} \leq s \leq t_k$. As the time

intervals get smaller, in the limit, the relaxation function becomes

$$G^{(0)}\left[t, \mathrm{T}\underset{s=0}{\overset{t}{(\mathrm{s})}}\right] = G^{(0)}\left[\int_0^t \frac{ds}{a_{\mathrm{T}}(T(s), T_g^0)}, T_g^0\right] \tag{5.18}$$

where, the integral $\xi(t) = \displaystyle\int_0^t \frac{ds}{a_{\mathrm{T}}(T(s), T_g^0)}$ is called the reduced time or intrinsic time.

The mechanical strain history is treated as a superposition of step strain increments. Assuming that scaling and superposition are still valid when the temperature varies with time, the stress response at time t is given by the superposition of responses to step strain increments. For the strain increment $\varepsilon^{\mathrm{m}}(t_k) - \varepsilon^{\mathrm{m}}(t_{k-1})$ applied at time t_k, the stress response at time t is

$$\begin{aligned}\left[\varepsilon^{\mathrm{m}}(t_k) - \varepsilon^{\mathrm{m}}(t_{k-1})\right] G^{(0)}\left[t, \mathrm{T}\underset{s=t_k}{\overset{t}{(\mathrm{s})}}\right] &= \left[\varepsilon^{\mathrm{m}}(t_k) - \varepsilon^{\mathrm{m}}(t_{k-1})\right] G^{(0)}\left[\int_{t_k}^t \frac{ds}{a_{\mathrm{T}}(T(s), T_g^0)}, T_g^0\right] \\ &= \left[\varepsilon^{\mathrm{m}}(t_k) - \varepsilon^{\mathrm{m}}(t_{k-1})\right] G^{(0)}\left[\xi(t) - \xi(t_k), T_g^0\right]\end{aligned}$$

From superposition of strain increments, the total stress response at time t is given by

$$\begin{aligned}\sigma(t) =& \varepsilon^{\mathrm{m}}(0) G^{(0)}\left[\int_0^t \frac{ds}{a_{\mathrm{T}}(T(s), T_g^0)}, T_g^0\right] \\ &+ \sum_{k=1}^{N}\left[\varepsilon^{\mathrm{m}}(t_k) - \varepsilon^{\mathrm{m}}(t_{k-1})\right] G^{(0)}\left[\int_{t_k}^t \frac{ds}{a_{\mathrm{T}}(T(s), T_g^0)}, T_g^0\right]\end{aligned} \tag{5.19}$$

In the limit, this leads to

$$\sigma(t) = \varepsilon^{\mathrm{m}}(0) G^{(0)}\left[\xi(t), T_g^0\right] + \int_0^t G^{(0)}\left[\xi(t) - \xi(s), T_g^0\right] d\varepsilon^{\mathrm{m}}(s) \tag{5.20}$$

Equation 5.20 is the constitutive equation for the stress response to arbitrary strain history and time varying temperature history.

Similarly, the constitutive equation for the strain response to arbitrary stress history and time varying temperature history is given by

$$\varepsilon^{\mathrm{m}}(t) = \sigma(0)J^{(0)}\left[\xi(t), T_g^0\right] + \int_0^t J^{(0)}\left[\xi(t) - \xi(s), T_g^0\right] d\sigma(s) \tag{5.21}$$

It is important to note that Eqs. 5.8, 5.10, 5.13, 5.14, 5.20 and 5.21 are general forms and can be used with any choice of relaxation and creep compliance functions.

5.2 Calibration of the Viscoelastic Model

The *total* strain response $\varepsilon(t)$ of a SMP subject to arbitrary stress and time-varying temperature history can now be written as

$$\begin{aligned}\varepsilon(t) =& \sigma(0)J^{(0)}\left[\xi(t), T_g^0\right] + \int_0^t J^{(0)}\left[\xi(t) - \xi(s), T_g^0\right] \dot{\sigma}(s)ds \\ &+ \alpha_{\mathrm{g}}(T^* - T_0) + \begin{cases} \alpha_{\mathrm{r}}(T - T^*) & : T > T^* \\ \alpha_{\mathrm{g}}(T - T^*) & : T < T^* \end{cases}\end{aligned} \tag{5.22}$$

where, $\xi(t) = \displaystyle\int_0^t \frac{dx}{a_{\mathrm{T}}(T(x), T_g^0)}$.

Material properties T_{g}^0 and $a_{\mathrm{T}}(T, T_{\mathrm{g}}^0)$ have been calibrated, see Section 3.1. α_{g}, α_{r} and T^* have also been measured and is given in Section 3.2. The only material property in Eq. 5.22 not yet calibrated is $J^{(0)}(t, T_{\mathrm{g}}^0)$. The accuracy of this model depends up on the choice of the creep compliance function $J^{(0)}(t, T_{\mathrm{g}}^0)$ or the stress relaxation function $G^{(0)}(t, T_{\mathrm{g}}^0)$, which, for linear viscoelastic materials are related by the identity

$$1 = G^{(0)}(t, T_{\mathrm{g}}^0)J^{(0)}(0, T_{\mathrm{g}}^0) + \int_0^t G^{(0)}(t - s, T_{\mathrm{g}}^0)\dot{J}^{(0)}(s, T_{\mathrm{g}}^0)ds \tag{5.23}$$

This gives,

$$J^{(0)}(t, T_{\mathrm{g}}^0) = \mathcal{L}^{-1}\left\{\frac{1}{a^2}\left(\overline{G}^{(0)}(a, T_{\mathrm{g}}^0)\right)^{-1}\right\} \tag{5.24}$$

where, $\overline{G}^{(0)}(a, T_{\mathrm{g}}^0)$ is the Laplace transform of $G^{(0)}(t, T_{\mathrm{g}}^0)$. For simple forms of $G(t, T_{\mathrm{g}}^0)$ one can analytically solve Eq. 5.24 and obtain $J(t, T_{\mathrm{g}}^0)$. However, for more complicated forms, Eq. 5.23 has to be solved using numerical techniques for Volterra integral equations [32].

By assuming a relaxation modulus of form $G^{(0)}(t, T_{\mathrm{g}}^0) = G_\infty^{(0)} + \Delta G^{(0)}(t, T_{\mathrm{g}}^0)$, where $G_\infty^{(0)}$ is the equilibrium value of the relaxation modulus (i.e. $G_\infty^{(0)} = G^{(0)}(\infty, T_{\mathrm{g}}^0)$) and $\Delta G^{(0)}(t, T_{\mathrm{g}}^0)$ is the decaying transient term, the complex modulus is [32]

$$G^{*(0)}(\omega, T_{\mathrm{g}}^0) = G^{(0)}(\infty, T_{\mathrm{g}}^0) + i\omega \int_0^\infty \Delta G^{(0)}(s, T_{\mathrm{g}}^0) \exp\left(-i\omega s\right) ds \tag{5.25}$$

The real and imaginary parts of this complex modulus gives us the storage ($G'^{(0)}(\omega, T_{\mathrm{g}}^0)$) and loss moduli ($G''^{(0)}(\omega, T_{\mathrm{g}}^0)$) which can be fit to experimental data shown in Fig. 3.3. This calibrates the relaxation modulus for the undegraded SMP at the reference temperature ($G^{(0)}(t, T_{\mathrm{g}}^0)$). $J^{(0)}(t, T_{\mathrm{g}}^0)$ is then calculated using Eq. 5.23 or 5.24

5.2.1 12-Term Prony Series Model

In this work, a Prony series form is chosen for the relaxation function of the original undegraded SMP. That is,

$$G^{(0)}(t, T_{\mathrm{g}}^0) = G_\infty^{(0)} + \sum_{n=1}^{N_0} G_n^{(0)} \exp\left(-\frac{t}{\tau_{\mathrm{R}n}^{(0)}}\right) \tag{5.26}$$

where, $G_{\infty}^{(0)}$, $G_{n}^{(0)}$ and $\tau_{\mathrm{R}n}^{(0)}$ are material properties. Using 5.26 in Eq.5.25, the expressions for storage and loss moduli are obtained to be

$$G'^{(0)}(\omega, T_{\mathrm{g}}^{0}) = G_{\infty}^{(0)} + \sum_{n=1}^{N_0} G_{n}^{(0)} \frac{(\omega\tau_{\mathrm{R}n}^{(0)})^2}{1 + (\omega\tau_{\mathrm{R}n}^{(0)})^2} \tag{5.27}$$

$$G''^{(0)}(\omega, T_{\mathrm{g}}^{0}) = \sum_{n=1}^{N_0} G_{n}^{(0)} \frac{\omega\tau_{\mathrm{R}n}^{(0)}}{1 + (\omega\tau_{\mathrm{R}n}^{(0)})^2} \tag{5.28}$$

Equation 5.27 and 5.28 is used to fit the data shown in Fig. 3.3. Because Eq. 5.27 and 5.28 share some of the material parameters, they cannot be used independently to fit the G'-f and G''-f data. A least squares minimization routine is used to fit the storage modulus and loss modulus data and the objective function for this is defined as

$$f_{\mathrm{Obj}} = \sqrt{(G'_{\mathrm{Exp}} - G'_{\mathrm{Model}})^2 + (G''_{\mathrm{Exp}} - G''_{\mathrm{Model}})^2} \tag{5.29}$$

A 12-term Prony series expansion is used to fit the data ($N = 12$ in Eqs. 5.27 and 5.28). Figure 5.3 shows the fit to the experimental storage modulus-frequency and loss modulus-frequency data. A plot of $G_{n}^{(0)}$ vs $\tau_{\mathrm{R}n}^{(0)}$ is known as the discrete relaxation spectrum. The discrete relaxation spectrum indicates the concentration of relaxation processes in certain regions of the logarithmic time scale [31]. Figure 5.4 shows the discrete relaxation spectrum resulting at the reference temperature T_{g}^{0}.

From FTSP, the storage and loss modulus at a temperature T is given by

$$G'^{(0)}(\omega, T) = G_{\infty}^{(0)} + \sum_{n=1}^{N_0} G_{n}^{(0)} \frac{(\omega a_{\mathrm{T}}(T, T_{\mathrm{g}}^{0})\tau_{\mathrm{R}n}^{(0)})^2}{1 + (\omega a_{\mathrm{T}}(T, T_{\mathrm{g}}^{0})\tau_{\mathrm{R}n}^{(0)})^2} \tag{5.30}$$

$$G''^{(0)}(\omega, T) = \sum_{n=1}^{N_0} G_{n}^{(0)} \frac{\omega a_{\mathrm{T}}(T, T_{\mathrm{g}}^{0})\tau_{\mathrm{R}n}^{(0)}}{1 + (\omega a_{\mathrm{T}}(T, T_{\mathrm{g}}^{0})\tau_{\mathrm{R}n}^{(0)})^2} \tag{5.31}$$

where, $a_{\mathrm{T}}(T, T_{\mathrm{g}}^{0})$ is the temperature shift function. Observe that if $T = T_{\mathrm{g}}^{0}$, Eqs. 5.30 and 5.31 reduce to 5.27 and 5.28 since $a_{\mathrm{T}}(T_{\mathrm{g}}^{0}, T_{\mathrm{g}}^{0}) = 1$. Using Eqs. 5.30 and 5.31,

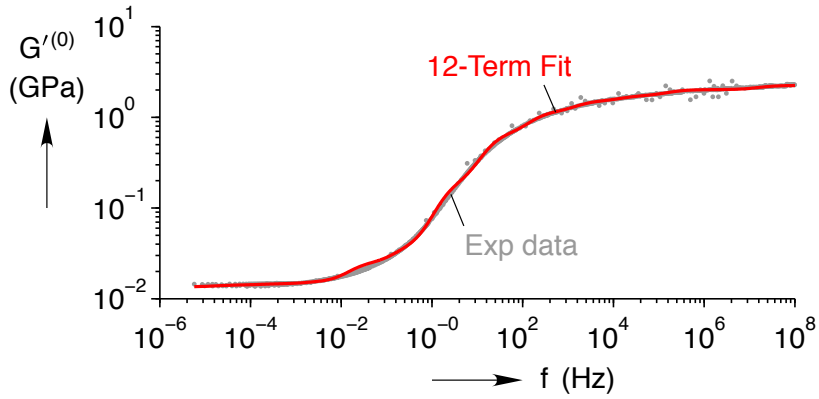

(a)

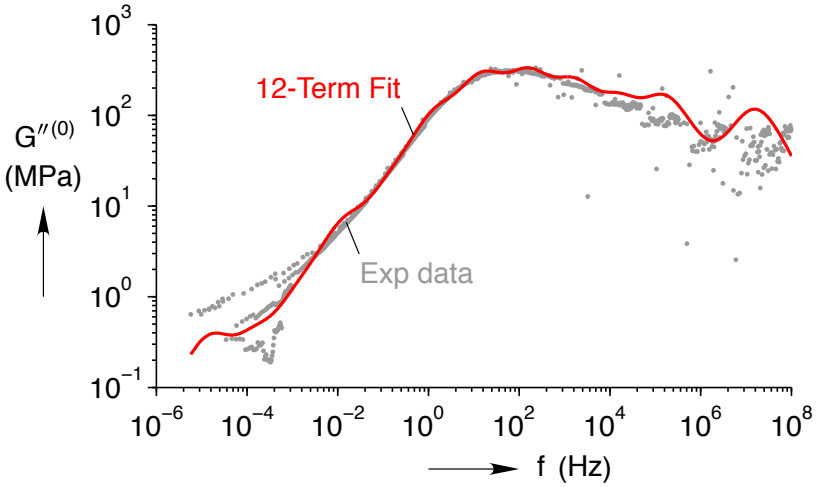

(b)

Figure 5.3: Fit to the (a) Storage modulus-frequency (b) Loss modulus-frequency curves at the reference temperature T_g^0 using a 12-term Prony Series

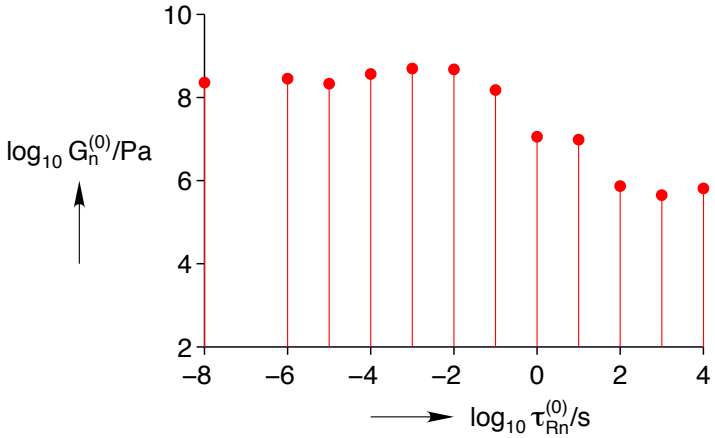

Figure 5.4: Discrete relaxation spectrum at the reference temperature T_g^0

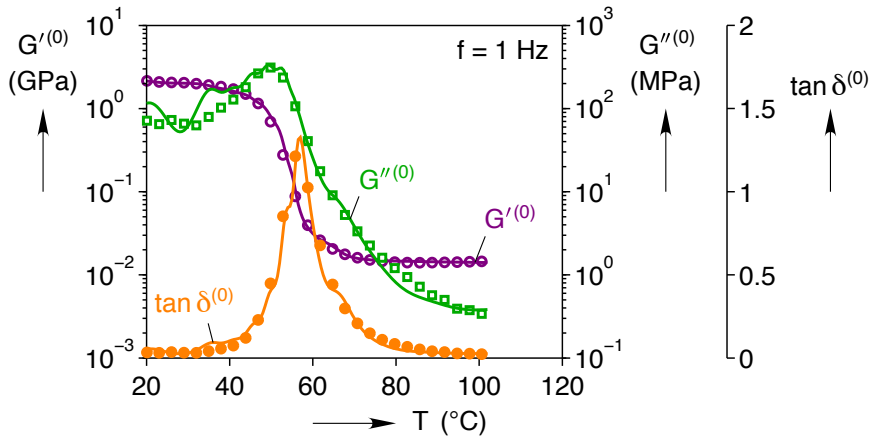

Figure 5.5: Variation of storage and loss moduli ($G'^{(0)}$, $G''^{(0)}$), $\tan\delta^{(0)}$ with temperature: Experimental data (markers) and Model simulation (solid line)

the variation of storage modulus $G'^{(0)}$, loss modulus $G''^{(0)}$ and $\tan\delta^{(0)}$ with T can be obtained at a constant frequency. This is shown in Figure 5.5 for a frequency of 1 Hz. Experimental data points from Fig. 3.2 are also shown for comparison.

With this, $G^{(0)}(t,T)$ is completely characterized. Therefore, from $G^{(0)}(t,T_g^0)$ and the identity in Eq. 5.24, $J^{(0)}(t,T_g^0)$ can be numerically obtained. The resulting form for $J^{(0)}(t,T_g^0)$ would be

$$J^{(0)}(t,T_g^0) = J_\infty^{(0)} + \sum_{n=1}^{N_0} J_n^{(0)} \exp\left(-\frac{t}{\tau_{Cn}^{(0)}}\right) \tag{5.32}$$

where, $J_\infty^{(0)}$, $J_n^{(0)}$ and $\tau_{Cn}^{(0)}$ are material properties and are related in some way to $G_\infty^{(0)}$, $G_n^{(0)}$ and $\tau_{Rn}^{(0)}$. A plot of $J_n^{(0)}$ vs $\tau_{Cn}^{(0)}$ is known as the discrete retardation spectrum. The interpretation of the discrete retardation spectrum is similar to that of the relaxation spectrum [31]. Figure 5.6 shows the discrete retardation spectrum at the reference temperature T_g^0.

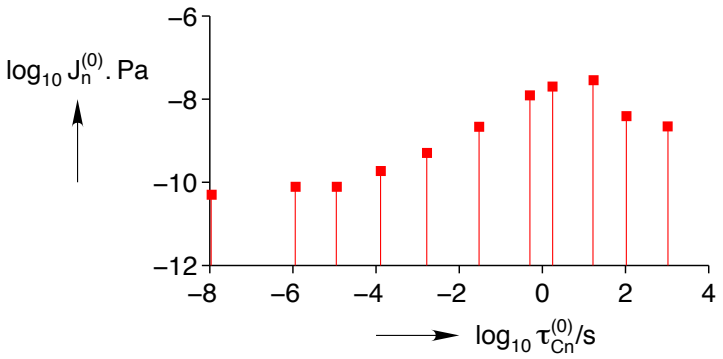

Figure 5.6: Discrete retardation spectrum at the reference temperature T_g^0

5.2.2 1-Term or a SLS Model

A 1-term Prony series ($N_0 = 1$) or a SLS model is calibrated for comparison purposes. Figure 5.7 shows the fit to the experimental storage modulus and loss modulus-frequency data. It is observed that this SLS model does not fit the data as accurately as the 12-term model however, it does capture the trends qualitatively. While the short and long frequency values of $G'^{(0)}$ are matched much better than the intermediate frequencies, the opposite is true for the $G''^{(0)}$ data fit. Using the temperature shift function $a_T(T, T_g^0)$, the variation of storage modulus $G'^{(0)}$, loss modulus $G''^{(0)}$ and $\tan\delta^{(0)}$ with T is obtained at a 1 Hz frequency. This is shown in Figure 5.8. Experimental data points from Fig. 3.2 are also shown for comparison. From Fig. 5.8 it is observed that the SLS model predicts the $G'^{(0)}$ data much better than the $G''^{(0)}$ data and it captures the location of the $\tan\delta$ peak, though not its magnitude. A summary of the 12-term and the SLS viscoelastic model parameters is provided in Table 5.1

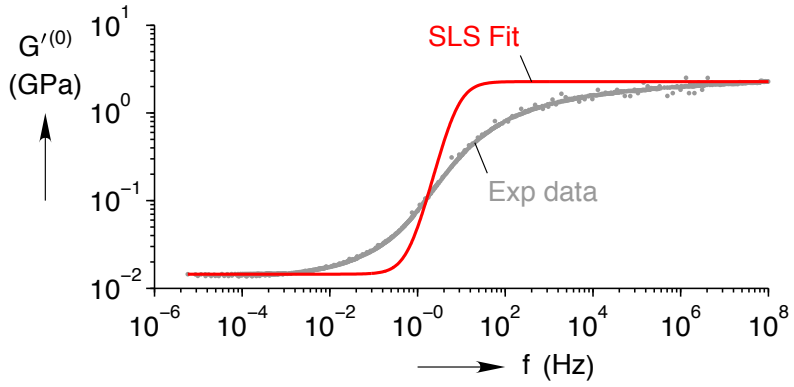

(a)

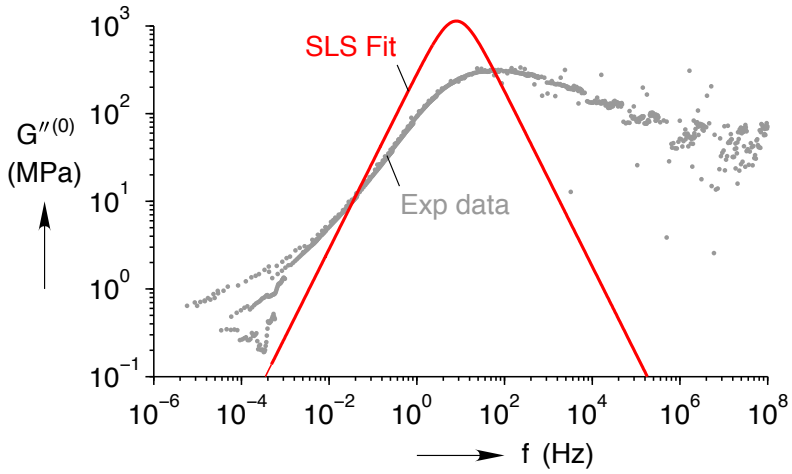

(b)

Figure 5.7: Fit to the (a) Storage modulus-frequency (b) Loss modulus-frequency curves at the reference temperature T_g^0 using a SLS model

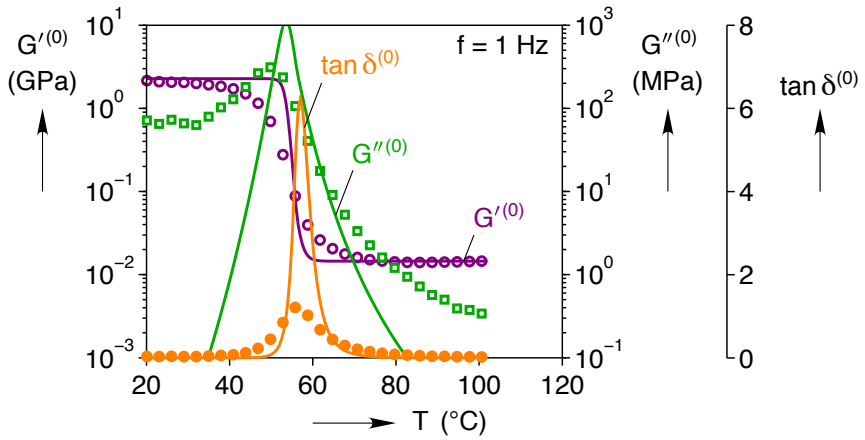

Figure 5.8: Variation of storage and loss moduli ($G'^{(0)}$, $G''^{(0)}$), $\tan\delta^{(0)}$ with temperature: Experimental data (markers) and SLS Model simulation (solid line)

Basic Material Properties	CTE and Transition Temperatures $\alpha_{\mathrm{g}} = 7.9 \times 10^{-5}$ /°C, $\alpha_{\mathrm{r}} = 20.5 \times 10^{-5}$ /°C $T^{*} = 52.9$ °C, $T_{\mathrm{g}}^{0} = 56.2$ °C Viscoelastic Shift Function $C_1 = 7.34$, $C_2 = 29.76$ °C $C_3 = 16.11$, $C_4 = 44.10$ °C
12-Term Prony Series Model	Stress Relaxation Function $G_{\infty}^{(0)} = 13.52$ MPa $G_n^{(0)} = \big(227.98,\ 282.52,\ 214.10,\ 367.26,$ $495.02,\ 473.33,\ 150.53,\ 11.35,$ $9.65,\ 0.74,\ 0.45,\ 0.65\big)$ MPa $\tau_{\mathrm{R}n}^{(0)} = \big(10^{-8},\ 10^{-6},\ 10^{-5},\ 10^{-4},\ 10^{-3},$ $0.01,\ 0.1,\ 1,\ 10,\ 100,\ 1000,\ 10^{4}\big)$ s Creep Compliance Function $J_{\infty}^{(0)} = 0.074$ /MPa $J_n^{(0)} = -\big(0.05,\ 0.078,\ 0.078,\ 0.187,\ 0.51$ $2.162,\ 12.32,\ 20.03,\ 28.60,$ $3.902,\ 2.2,\ 3.429\big) \times 10^{-3}$ /MPa $\tau_{\mathrm{C}n}^{(0)} = \big(1.113 \times 10^{-8},\ 1.16 \times 10^{-6},\ 1.138 \times 10^{-5},$ $1.302 \times 10^{-4}, 1.675 \times 10^{-3},\ 0.03,\ 0.5,$ $1.758,\ 17.087,\ 105.53,\ 1031.9,\ 10484\big)$ s
SLS Model	Stress Relaxation function $G_{\infty}^{(0)} = 14.50$ MPa, $G_1^{(0)} = 2262.0$ MPa $\tau_{\mathrm{R}1}^{(0)} = 0.02$ s Creep Compliance function $J_{\infty}^{(0)} = 0.069$ /MPa, $J_1^{(0)} = -0.0685$ /MPa $\tau_{\mathrm{C}1}^{(0)} = 3.14$ s

Table 5.1: Summary of the 12-term and the SLS viscoelastic model parameters

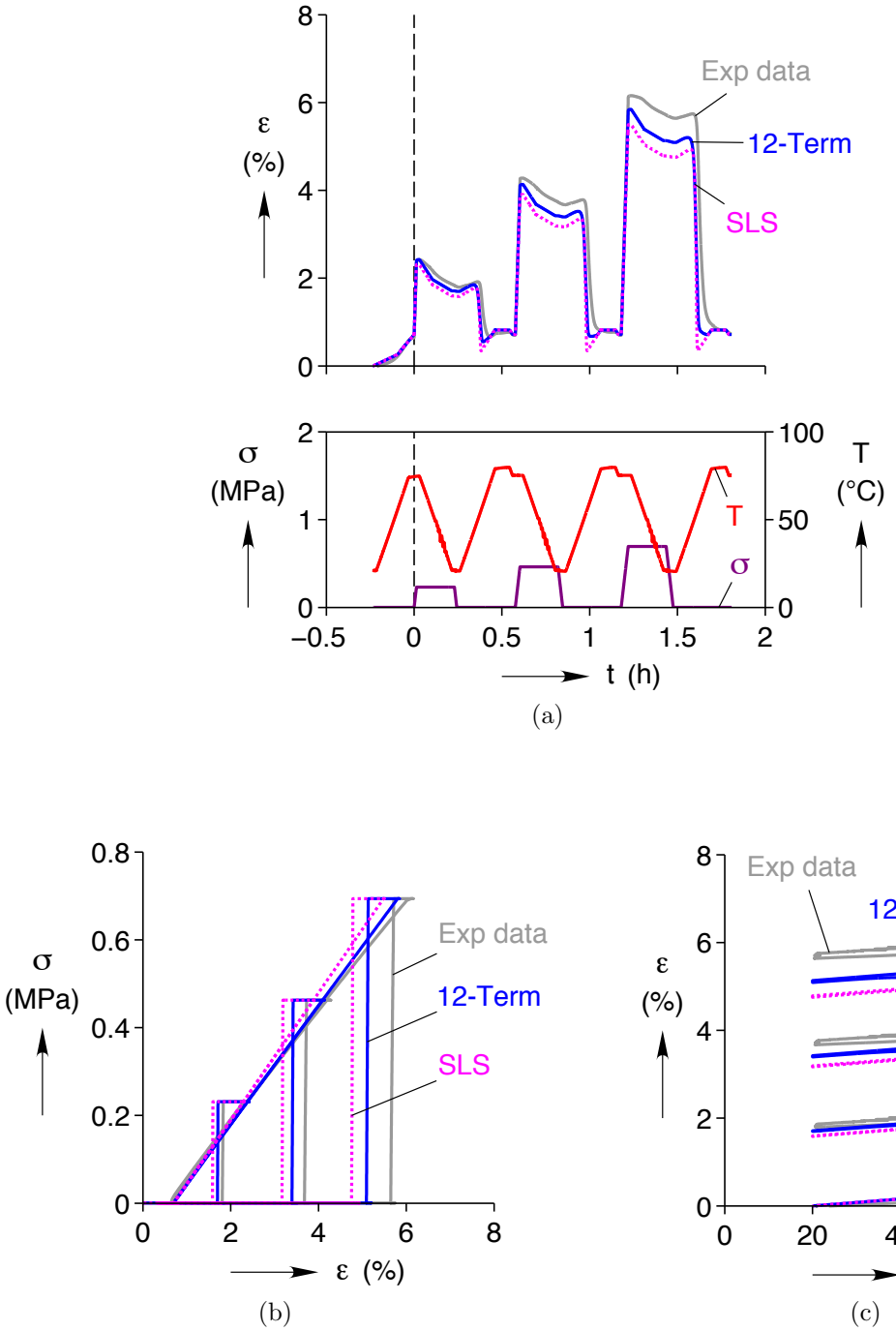

Figure 5.9: A comparison of model and experiment response to SMCs at $T_{\mathrm{d}} = 75$ °C with applied stress ranging from 0.23-0.69 MPa (a) stress (σ), temperature (T) and total strain (ε) history (b) Full data in $\sigma - \varepsilon$ space (c) Full data in $\varepsilon - T$ space

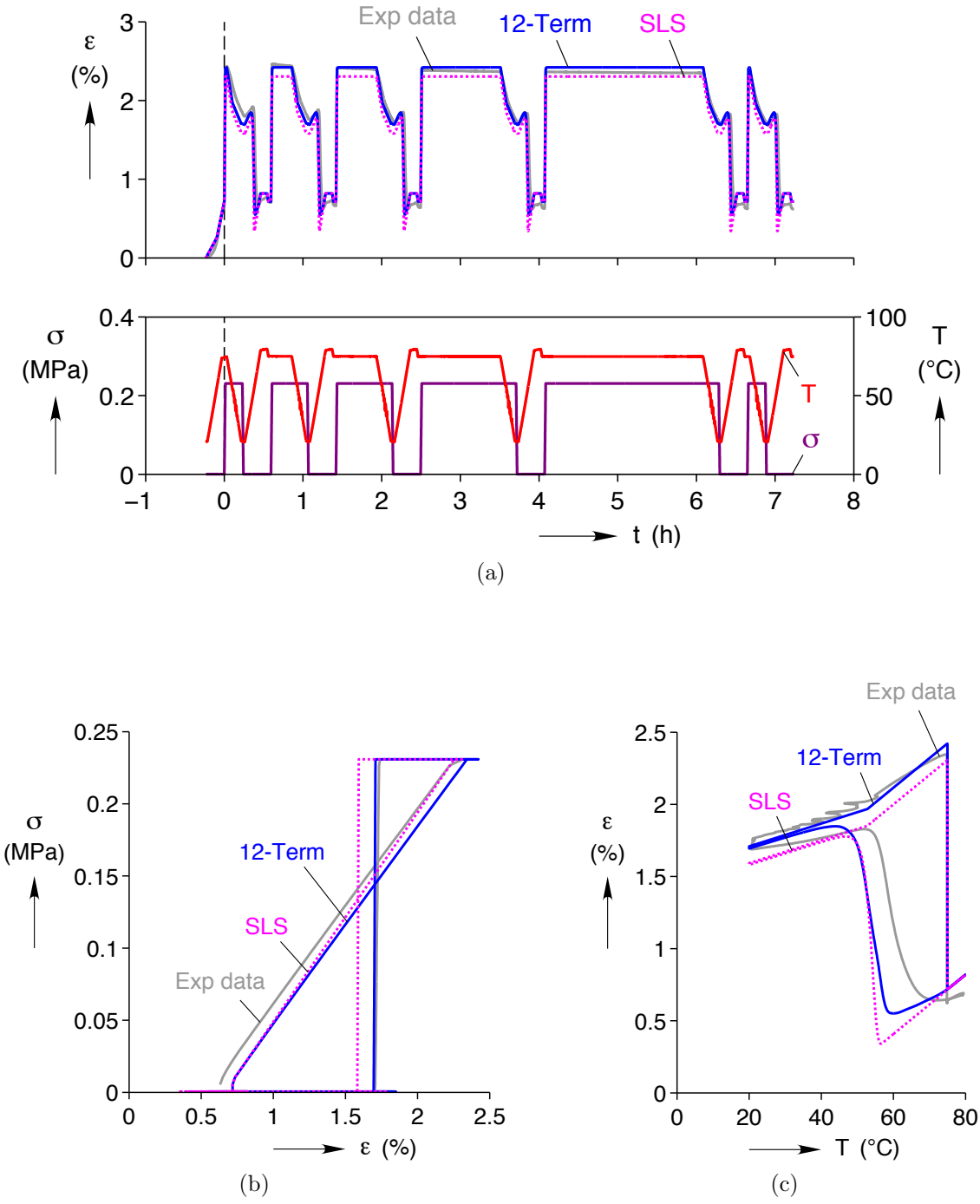

Figure 5.10: A comparison of model and experiment response to SMCs at $T_{\mathrm{d}} = 75$ °C with hold time ranging from 1-120 min (a) stress (σ), temperature (T) and total strain (ε) history (b) 6^{th} cycle data in $\sigma - \varepsilon$ space (c) 6^{th} cycle data in $\varepsilon - T$ space

5.3 Viscoelastic Model Evaluation

The 12-term viscoelastic model and the SLS model are evaluated by comparing their shape memory cycle responses with experimental data. Figure 5.9 shows a comparison of model and experiment response to SMCs at $T_{\mathrm{d}} = 75$ °C with applied stress ranging from 0.23-0.69 MPa. As expected, the 12-term Prony series model is much closer to the experimental response than the SLS model. Nevertheless, both the models capture all the trends observed in the experimental data. At small stress levels ($\sigma = 0.23$ MPa) the models capture the experimental response more accurately than at higher stress levels.

Figure 5.9 shows a comparison of model and experiment response to SMCs at $T_{\mathrm{d}} =$ 75 °C with hold time ranging from 1-120 min under a stress of $\sigma = 0.23$ MPa. The stress (σ), temperature (T) and total strain (ε) history are shown in Fig. 5.10a. The 6^{th} cycle data in $\sigma - \varepsilon$ space and in $\varepsilon - T$ space are shown in Figs. 5.10b and 5.10c. Again, both the models capture all the trends observed in the experimental data and the 12-term Prony series model better represents the experimental response. For the viscoelastic models, the fixity ratio is 99% and recovery ratio is 100% and they are independent of applied load, holding time and temperature.

5.4 A Chemo-Visco Model

According to multi-network theory, the macromolecular network structure of a virgin SMP consists entirely of an undegraded 1^{st} network and degradation results in a reduction of volume fraction of the 1^{st} network and formation of secondary networks with different material properties and reference configuration. In this section, a model for the thermo-mechanical behavior of SMP incorporating the degradation kinetics is presented.

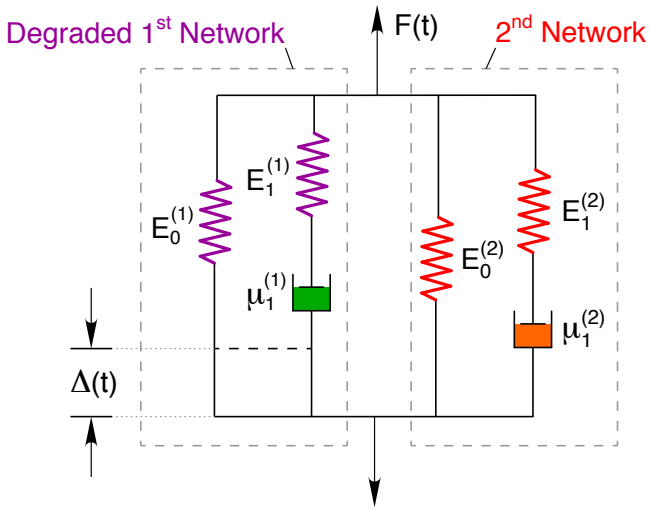

Figure 5.11: Mechanical analog model of a SMP undergoing chemical stress relaxation

5.4.1 Chemical Stress Relaxation

The stress relaxation behavior due to CR aging is referred to as *chemical stress relaxation*. The following simplifying assumptions are made for the derivation of this model: (1) the temperature ($T \geq T_{\text{cr}}$) is held constant during stress relaxation (2) just before the start of relaxation (at $t = 0$) the material is assumed to be undegraded. According to multi-network theory, chemical stress relaxation results in formation of only one secondary network. The reference length of the 2$^{\text{nd}}$ network is the same as the deformed length of the 1$^{\text{st}}$ network at the time of formation [6, 7]. Figure 5.11 shows a simple mechanical analog model of a SMP during chemical stress relaxation. The degraded 1$^{\text{st}}$ network and the newly formed 2$^{\text{nd}}$ network are represented by SLS elements.

The total force $F(t) = F^{(1)}(t) + F^{(2)}(t)$, where $F^{(1)}(t)$ is the force supported by the degraded 1$^{\text{st}}$ network and $F^{(2)}(t)$ is the force supported by the 2$^{\text{nd}}$ network. Since the reference length of the 2$^{\text{nd}}$ network is the same as the deformed length of the 1$^{\text{st}}$ network, the 2$^{\text{nd}}$ network does not undergo any elongation (unless Δ is changed). Therefore, $F^{(2)}(t) = 0$ and $F(t) = F^{(1)}(t)$. The force-elongation relation for the SMP

model is

$$\left(\frac{D}{E_1^{(1)}}+\frac{1}{\mu_1^{(1)}}\right)F(t)=\left[D\left(1+\frac{E_0^{(1)}}{E_1^{(1)}}\right)+\frac{E_0^{(1)}}{\mu_1^{(1)}}\right]\Delta(t) \tag{5.33}$$

where D is a differential operator. The resulting constitutive equation is

$$p_0^{(1)}\sigma+p_1^{(1)}\dot{\sigma}=q_0^{(1)}\varepsilon^{\mathrm{m}}+q_1^{(1)}\dot{\varepsilon}^{\mathrm{m}} \tag{5.34}$$

where, $p_0^{(1)}=\dfrac{1}{\mu_1^{(1)}}$, $p_1^{(1)}=\dfrac{1}{E_1^{(1)}}$, $q_0^{(1)}=\dfrac{E_0^{(1)}}{\mu_1^{(1)}}$, $q_1^{(1)}=1+\dfrac{E_0^{(1)}}{E_1^{(1)}}$, σ is the stress and ε^{m} is the mechanical strain. Similar to the viscoelastic case discussed in Section 5.1.1, the initial condition is obtained to be

$$q_1^{(1)}\varepsilon^{\mathrm{m}}(0+)=p_1^{(1)}\sigma(0+) \tag{5.35}$$

The stress relaxation response is obtained using the approach presented in Section 5.1.2. From the constitutive relation Eq. 5.34 and the initial condition 5.35, the stress relaxation response is given by

$$\sigma(t)=\widetilde{G}^{(1)}(t)\varepsilon_0^{\mathrm{m}} \tag{5.36}$$

where, $\widetilde{G}^{(1)}(t)$ is the relaxation function of the degrading SMP. Note that, so far in this derivation no assumptions have been made regarding the nature of relaxation. This is because the relaxation function $\widetilde{G}^{(1)}(t)$ could involve contributions from both viscoelastic and chemical stress relaxation.

To simplify things further, it is now assumed that the stress relaxation response in Eq. 5.36 is entirely due to CR aging. This is a valid assumption for crosslinked polymers whose viscoelastic relaxation is already completed at temperatures $T \geq T_{\mathrm{cr}}$. Evidence of this is seen as a plateau in G' vs T at $T \geq T_{\mathrm{cr}}$ (see Fig. 3.2). In other words, the stress relaxation at $T \geq T_{\mathrm{cr}}$ is entirely due to scission of the 1^{st} network.

Since at $t = 0$ the SMP is assumed to be undegraded, it is possible to define the volume fraction ($b^{(1)}$) of the 1$^{\text{st}}$ network as

$$b^{(1)}(t) = \frac{\sigma(t)}{\sigma(0)} \tag{5.37}$$

5.4.2 Chemical Creep

According to multi-network theory, chemical creep results in the formation of infinitely many secondary networks having different reference configurations [7]. Figure 5.12a shows a mechanical analog model of a SMP undergoing CR aging during creep. A representative chemical creep response is shown in Fig. 5.12b. $\hat{t}_i$ represents the time at which i^{th} network is formed and the elongation of the 1$^{\text{st}}$ network at that time instant is $\Delta(\hat{t}_i) = \Delta_0^{(i)}$. It is observed that at time t, the elongation of the n^{th} network $\Delta(t) - \Delta_0^{(n)} \approx 0$. Therefore, the force supported by the n^{th} network $F^{(n)} \approx 0$. Observe that while the elongation of the i^{th} network is much larger, the force supported by it depends on its stiffness and perhaps also on its volume fraction. Experimentally it is not possible to characterize the properties of infinitely many secondary networks. Therefore, to simplify the model, all the secondary networks are lumped into a single 2$^{\text{nd}}$ network with continuously evolving material properties and reference configuration.

Figure 5.13 shows a mechanical analog model of a SMP with a degrading 1$^{\text{st}}$ network and a continuously evolving 2$^{\text{nd}}$ network during chemical creep. $\Delta_0^{(2)}(t)$ is a measure of the reference configuration of the lumped 2$^{\text{nd}}$ network. The force elongation relations

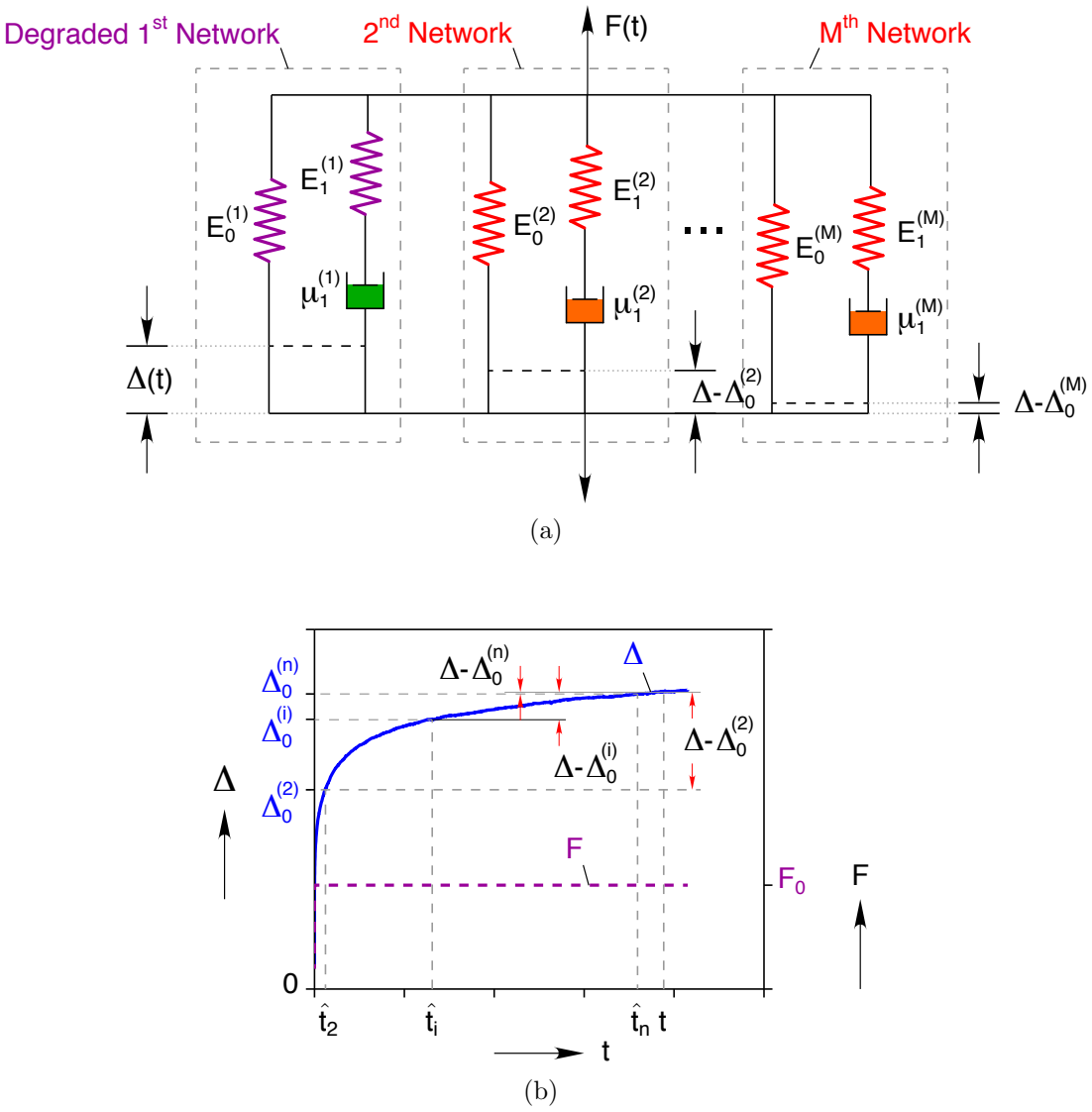

Figure 5.12: (a) Mechanical analog model of a SMP undergoing chemical creep (b) A representative chemical creep response

for this model are

$$\left(\frac{D}{E_1^{(1)}}+\frac{1}{\mu_1^{(1)}}\right)F^{(1)}(t)=\left[D\left(1+\frac{E_0^{(1)}}{E_1^{(1)}}\right)+\frac{E_0^{(1)}}{\mu_1^{(1)}}\right]\Delta(t) \tag{5.38}$$

$$\left(\frac{D}{E_1^{(2)}}+\frac{1}{\mu_1^{(2)}}\right)F^{(2)}(t)=\left[D\left(1+\frac{E_0^{(2)}}{E_1^{(2)}}\right)+\frac{E_0^{(2)}}{\mu_1^{(2)}}\right](\Delta(t)-\Delta_0^{(2)}(t)) \tag{5.39}$$

The total force $F(t)=F^{(1)}(t)+F^{(2)}(t)$. To eliminate $F^{(1)}(t)$ and $F^{(2)}(t)$ and introduce

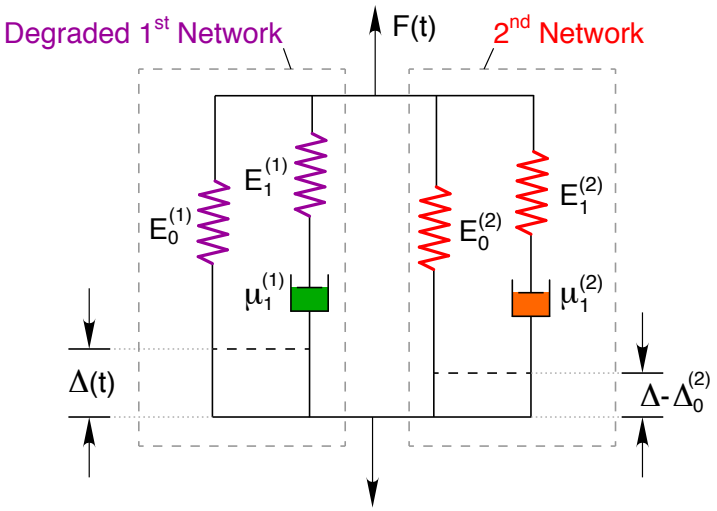

Figure 5.13: Mechanical analog model of a SMP with a degrading 1st network and a continuously evolving 2nd network during chemical creep

$F(t)$, Eq. 5.38 is operated with $\left(\frac{D}{E_1^{(2)}}+\frac{1}{\mu_1^{(2)}}\right)$ and Eq. 5.39 with $\left(\frac{D}{E_1^{(1)}}+\frac{1}{\mu_1^{(1)}}\right)$. The resulting force-elongation relation is

$$\left(\frac{D}{E_1^{(1)}}+\frac{1}{\mu_1^{(1)}}\right)\left(\frac{D}{E_1^{(2)}}+\frac{1}{\mu_1^{(2)}}\right)F(t)=\left(\frac{D}{E_1^{(2)}}+\frac{1}{\mu_1^{(2)}}\right)\left[D\left(1+\frac{E_0^{(1)}}{E_1^{(1)}}\right)+\frac{E_0^{(1)}}{\mu_1^{(1)}}\right]\Delta(t)$$
$$+\left(\frac{D}{E_1^{(1)}}+\frac{1}{\mu_1^{(1)}}\right)\left[D\left(1+\frac{E_0^{(2)}}{E_1^{(2)}}\right)+\frac{E_0^{(2)}}{\mu_1^{(2)}}\right]\left(\Delta(t)-\Delta_0^{(2)}(t)\right) \qquad (5.40)$$

This results in a constitutive equation of form

$$P(D)\sigma(t)=Q(D)\varepsilon^{\mathrm{m}}(t)-R(D)\varepsilon_0^{(2)}(t) \qquad (5.41)$$

where,

$$P(D) = \left(\frac{D}{E_1^{(1)}} + \frac{1}{\mu_1^{(1)}}\right)\left(\frac{D}{E_1^{(2)}} + \frac{1}{\mu_1^{(2)}}\right) = p_0 + p_1 D + p_2 D^2$$

$$Q(D) = \left(\frac{D}{E_1^{(2)}} + \frac{1}{\mu_1^{(2)}}\right)\left[D\left(1 + \frac{E_0^{(1)}}{E_1^{(1)}}\right) + \frac{E_0^{(1)}}{\mu_1^{(1)}}\right] + \left(\frac{D}{E_1^{(1)}} + \frac{1}{\mu_1^{(1)}}\right)\left[D\left(1 + \frac{E_0^{(2)}}{E_1^{(2)}}\right) + \frac{E_0^{(2)}}{\mu_1^{(2)}}\right] = q_0 + q_1 D + q_2 D^2$$

$$R(D) = \left(\frac{D}{E_1^{(1)}} + \frac{1}{\mu_1^{(1)}}\right)\left[D\left(1 + \frac{E_0^{(2)}}{E_1^{(2)}}\right) + \frac{E_0^{(2)}}{\mu_1^{(2)}}\right] = r_0 + r_1 D + r_2 D^2$$

The initial condition for this case can be derived similar to the viscoelastic case in Section 5.1.1 by repeated integration and application of the limit process. This results in compatibility conditions that relate $\sigma(0+)$, $D\sigma(0+)$, $\varepsilon^{\mathrm{m}}(0+)$, $D\varepsilon^{\mathrm{m}}(0+)$ and $\varepsilon_0^{(2)}(0+)$, $D\varepsilon_0^{(2)}(0+)$. Taking the Laplace transform of Eq. 5.41 and applying the initial conditions results in

$$P(a)\overline{\sigma} = Q(a)\overline{\varepsilon}^{\mathrm{m}} - R(a)\overline{\varepsilon}_0^{(2)} \tag{5.42}$$

where, $P(a) = p_0 + p_1 a + p_2 a^2$, $Q(a) = q_0 + q_1 a + q_2 a^2$ and $R(a) = r_0 + r_1 a + r_2 a^2$. For a creep test, $\sigma(t) = \sigma_0$ for $t \geq 0$, i.e. $\overline{\sigma} = \dfrac{1}{a}\sigma_0$. Equation 5.42 can be written as

$$\frac{\overline{\varepsilon}^{\mathrm{m}}}{\sigma_0} = \frac{P(a)}{aQ(a)} + \frac{R(a)}{aQ(a)}\frac{a\overline{\varepsilon}_0^{(2)}}{\sigma_0} \tag{5.43}$$

After factoring the denominator, Eq. 5.43 can be written in the form

$$\frac{\overline{\varepsilon}^{\mathrm{m}}}{\sigma_0} = \frac{\widetilde{J}_\infty}{a} + \frac{\widetilde{J}_1}{a + \frac{1}{\widetilde{\tau}_{C1}}} + \frac{\widetilde{J}_2}{a + \frac{1}{\widetilde{\tau}_{C2}}} + \left(\frac{\widetilde{S}_\infty}{a} + \frac{\widetilde{S}_1}{a + \frac{1}{\widetilde{\tau}_{C1}}} + \frac{\widetilde{S}_2}{a + \frac{1}{\widetilde{\tau}_{C2}}}\right)\frac{a\overline{\varepsilon}_0^{(2)}}{\sigma_0} \tag{5.44}$$

for some constants $\widetilde{J}_\infty$, $\widetilde{J}_1$, $\widetilde{J}_2$, $\widetilde{S}_\infty$, $\widetilde{S}_1$, $\widetilde{S}_2$, $\widetilde{\tau}_{C1}$ and $\widetilde{\tau}_{C2}$. Equation 5.44 can also be written as

$$\overline{\varepsilon}^{\mathrm{m}}(a) = \sigma_0\overline{\widetilde{J}}(a) + \varepsilon_0^{(2)}(0)\overline{\widetilde{S}}(a) + \overline{\widetilde{S}}(a)\left(a\overline{\varepsilon}_0^{(2)} - \varepsilon_0^{(2)}(0)\right) \tag{5.45}$$

It can be recognized that $\overline{\widetilde{J}}(a)$ is the Laplace transform of a creep compliance function $\widetilde{J}(t)$ and $\overline{\widetilde{S}}(a)$ is the Laplace transform of a dimensionless function $\widetilde{S}(t)$ that relates the reference configuration of the lumped 2$^{\text{nd}}$ network and the creep strain response. Taking the inverse Laplace transform of Eq. 5.45, the time domain strain response of the SMP during chemical creep is

$$\varepsilon^{\text{m}}(t) = \sigma_0 \widetilde{J}(t) + \varepsilon_0^{(2)}(0)\widetilde{S}(t) + \int_0^t \widetilde{S}(t-s)\dot{\varepsilon}_0^{(2)}(s)ds \tag{5.46}$$

Observe that in Eq. 5.46 $\widetilde{J}(t)$ is the *overall* creep compliance function and because this is a case of chemical creep, $\widetilde{J}(t)$ must depend on the amount of CR degradation or the volume fraction of the 1$^{\text{st}}$ network. From this derivation it is unclear what the specific form of $\widetilde{J}(t)$ is and it would be up to the experimentalist/modeler to come up with a suitable form based on the data.

Similarly, in Eq. 5.46 $\widetilde{S}(t)$ is a function that relates the reference configuration of the lumped 2$^{\text{nd}}$ network ($\varepsilon_0^{(2)}(t)$) and the creep strain response. Although Eq. 5.44 suggests that the retardation times of $\widetilde{J}(t)$ and $\widetilde{S}(t)$ are the same, the exact form of $\widetilde{S}(t)$ is unknown. To better understand the influence of $\widetilde{S}(t)$ and $\varepsilon_0^{(2)}(t)$, consider the following scenario. Let a virgin SMP sample ($\varepsilon_0^{(2)}(0) = 0$) be subject to chemical creep under a stress σ_0 for a duration t_1 and then instantaneously unloaded. For $t > t_1$, stress $\sigma_0 = 0$ and the strain from Eq. 5.46 at time t_1 is given by

$$\varepsilon^{\text{m}}(t_1) = \int_0^{t_1} \widetilde{S}(t-s)\dot{\varepsilon}_0^{(2)}(s)ds \tag{5.47}$$

This represents the residual strain at the end of a creep-unload test. Obviously, the residual strain must depend on the amount of thermo-mechanical aging, but it may also depend on the applied stress since the amount of deformation influences the reference configuration of the continuously evolving 2$^{\text{nd}}$ network. Furthermore, if

this hypothetical creep-unload test is conducted on an already degraded SMP sample ($\varepsilon_0^{(2)}(0) \neq 0$), but at a temperature below the CR temperature, then reference configuration of the lumped 2$^{\text{nd}}$ network must not evolve further, i.e. $\dot{\varepsilon}_0^2 = 0$ due to the absence of CR aging. With the knowledge of these constraints, a suitable form for $\widetilde{S}(t)$ and $\varepsilon_0^{(2)}(t)$ has to be chosen based on experiments to capture the evolution of residual strain. This is addressed later in Section 5.5.3.

5.4.3 Isothermal Response to Arbitrary Stress and Strain Histories

From Eq. 5.42,

$$\overline{\varepsilon}^{\text{m}} = \frac{P(a)}{aQ(a)}(a\overline{\sigma}) + \frac{R(a)}{aQ(a)}(a\overline{\varepsilon}_0^{(2)}) \tag{5.48}$$

Recognizing that $\dfrac{P(a)}{aQ(a)} = \overline{\widetilde{J}}(a)$ and $\dfrac{R(a)}{aQ(a)} = \overline{\widetilde{S}}(a)$, Eq. 5.48 can be written as

$$\overline{\varepsilon}^{\text{m}} = \overline{\widetilde{J}}(a)\left(a\overline{\sigma} - \sigma(0)\right) + \sigma(0)\overline{\widetilde{J}}(a) + \overline{\widetilde{S}}(a)\left(a\overline{\varepsilon}_0^{(2)} - \varepsilon_0^{(2)}(0)\right) + \varepsilon_0^{(2)}(0)\overline{\widetilde{S}}(a) \tag{5.49}$$

Taking the inverse Laplace transform, the mechanical strain response to arbitrary stress history is obtained as

$$\varepsilon^{\text{m}}(t) = \sigma(0)\widetilde{J}(t) + \int_0^t \widetilde{J}(t-s)\dot{\sigma}(s)ds + \varepsilon_0^{(2)}(0)\widetilde{S}(t) + \int_0^t \widetilde{S}(t-s)\dot{\varepsilon}_0^{(2)}ds \tag{5.50}$$

Likewise, the stress response to arbitrary mechanical strain history is given by

$$\sigma(t) = \varepsilon^{\text{m}}(0)\widetilde{G}(t) + \int_0^t \widetilde{G}(t-s)\dot{\varepsilon}^{\text{m}}(s)ds - \varepsilon_0^{(2)}(0)\widetilde{K}(t) - \int_0^t \widetilde{K}(t-s)\dot{\varepsilon}_0^{(2)}ds \tag{5.51}$$

where $\widetilde{K}(t)$ is a relaxation modulus like function that relates the reference configuration of the lumped 2$^{\text{nd}}$ network to the stress response.

As a consistency check, for a creep-test, in Eq 5.50 $\dot{\sigma}(s) = 0$ and we get back the

creep response Eq. 5.46. Likewise, for a stress relaxation test starting with a virgin SMP, in Eq. 5.51 $\dot{\varepsilon}^{\mathrm{m}} = 0$ and $\varepsilon^{(2)}(0) = 0$. Also, from multi-network theory, chemical stress relaxation results in the formation of a single 2^{nd} network with a reference configuration same as the deformed configuration of the 1^{st} network, i.e. $\varepsilon_0^{(2)}(t) = \varepsilon^{\mathrm{m}}(t)$ implying $\dot{\varepsilon}_0^{(2)} = 0$. The resulting form of Eq. 5.51 is the same as the stress relaxation response given in Eq. 5.36.

5.5 Calibration of the Chemo-Viscoelastic Model

Before generalizing the chemo-visco-model to time varying temperature histories, it is necessary to understand the influence of CR aging on the viscoelastic material properties. In the process, suitable forms of $b^{(1)}$, $\widetilde{G}$, $\widetilde{J}$, $\widetilde{S}$ and $\varepsilon_0^{(2)}$ are chosen and calibrated to represent the material behavior.

5.5.1 Kinetics of Scission - Volume fraction of 1^{st} network

The volume fraction of the 1^{st} network $b^{(1)}$ is used to represent the extent of CR aging. This can be measured using chemical stress relaxation tests as discussed in Section 5.4.1. Stress relaxation tests are conducted at deformation temperatures $T_{\mathrm{d}} =$ 150, 158, 166 and 175 °C. A mechanical strain of $\varepsilon^{\mathrm{m}} = 1.6\%$ is imposed and held for a duration of 4 h and the load response is measured. Figure 5.14 shows the mechanical strain ε^{m}, temperature T and stress history during the stress relaxation test at 175 °C. The volume fraction of the 1^{st} network is obtained by taking $b^{(1)}(t) = \dfrac{\sigma(t)}{\sigma(0)}$. The $b^{(1)}$ obtained from stress relaxation tests at different deformation temperatures is plotted in Fig 5.15a. $b^{(1)}$ represents a sequence of CR events involving scission of the 1^{st} network. Clearly, from Fig 5.15a an increase in temperature speeds up this process. By assuming that the sequence of micro-rheological events leading to CR aging does

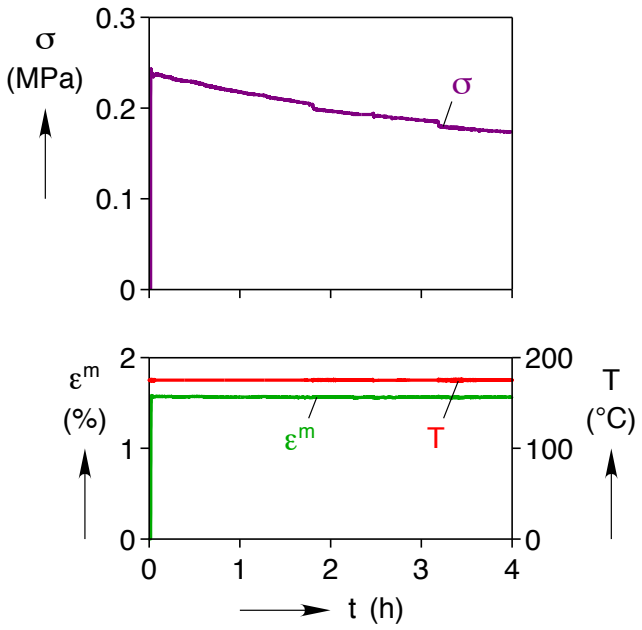

Figure 5.14: Stress relaxation response at $T_{\mathrm{d}} = 175$ °C (upper panel), corresponding mechanical strain and temperature history (lower panel)

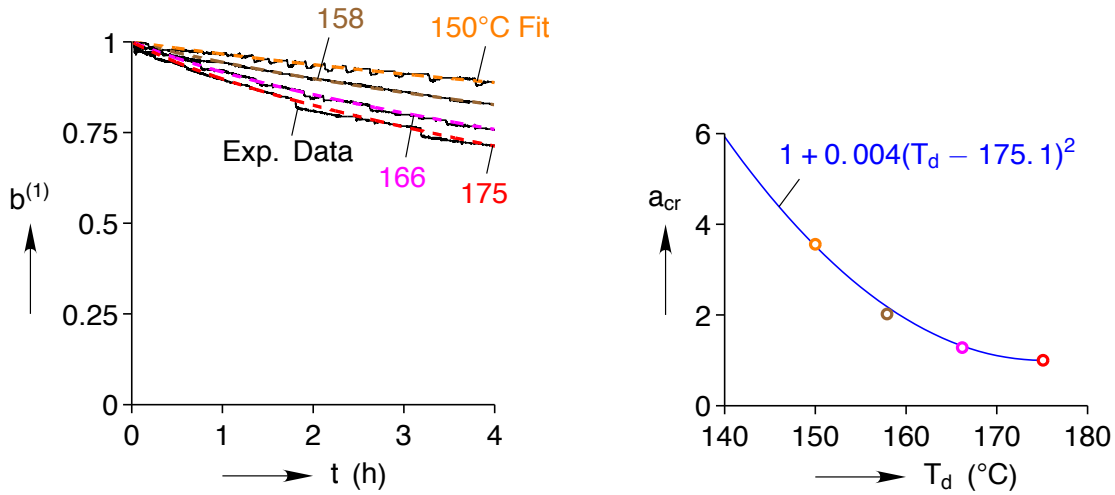

Figure 5.15: (a) Volume fraction of the 1st network at different deformation temperatures (b) Chemo-rheological shift function

not change and that temperature merely speeds up or slows down this process, $b^{(1)}$ can be fit using a function of form

$$b^{(1)}\left[t,T\right] = \psi_1 \exp\left(-\frac{t}{a_{\mathrm{cr}}\left[T,T^0_{\mathrm{cr}}\right]\tau_{\mathrm{cr1}}}\right) + \psi_2 \exp\left(-\frac{t}{a_{\mathrm{cr}}\left[T,T^0_{\mathrm{cr}}\right]\tau_{\mathrm{cr2}}}\right) \tag{5.52}$$

ψ_1	ψ_2	τ_{cr1} (s)	τ_{cr2} (s)	β	T^0_{cr} (°C)
0.94	0.06	51768	3420	1.30×10^{-7}	175.1

Table 5.2: Material constants for the volume fraction of 1st network $b^{(1)}$

where ψ_1, ψ_2, τ_{cr1}, τ_{cr2} are material constants and $a_{cr}\left[T, T^0_{cr}\right]$ is a CR shift function that represents the effect of temperature. a_{cr} takes a value of 1 at a CR reference temperature T^0_{cr}. The discrete values of a_{cr} obtained from a fit to the $b^{(1)}$ data at different deformation temperatures is shown in Fig. 5.15b. A fit to these discrete a_{cr} data points (also shown in Fig. 5.15b) gives the form of the CR shift function to be

$$a_{cr}\left[T, T^0_{cr}\right] = 1 + \beta\left(\frac{T}{T^0_{cr}} - 1\right)^2, \quad T < T^0_{cr} \tag{5.53}$$

A summary of the material constants is given in Table 5.2.

5.5.2 Creep compliance function of the degraded SMP

The stress relaxation function of the virgin SMP ($G^{(0)}(t,T)$) at a temperature is expressed using two material properties, the relaxation function at a reference temperature ($G^{(0)}(t,T^0_g)$) and a temperature shift function ($a_T(T,T^0_g)$). The influence of CR aging on on these material properties is required to determine the stress relaxation function of the degraded SMP ($\widetilde{G}(t,T)$).

As observed in Eqs. 5.50 and 5.51, the reference configuration of the second network influences the strain and stress response of the degraded SMP even when degradation ceases to occur. This complicates the measurement of relaxation modulus $\widetilde{G}$ and creep compliance $\widetilde{J}$. However, also observe that, if for a degraded SMP, the reference configuration of the lumped 2nd network is the same as that of the 1st network and

degradation process has ceased, Eqs. 5.50 and 5.51 take the form

$$\sigma(t) = \varepsilon^{\mathrm{m}}(0)\widetilde{G}(t) + \int_0^t \widetilde{G}(t-s)\dot{\varepsilon}^{\mathrm{m}}(s)ds \tag{5.54}$$

$$\varepsilon^{\mathrm{m}}(t) = \sigma(0)\widetilde{J}(t) + \int_0^t \widetilde{J}(t-s)\dot{\sigma}(s)ds \tag{5.55}$$

These forms are now similar to the viscoelastic case, see Eqs. 5.13 and 5.14 for comparison. This implies that such a degraded SMP can now be characterized just like a new viscoelastic SMP.

According to multi-network theory, when a polymer specimen undergoes CR aging under no-load, the reference configuration of the 2^{nd} network would correspond to the thermal strain of the 1^{st} network. If CR aging does not change the CTE appreciably, the residual strain would be approximately zero. Therefore, the reference configuration of the 2^{nd} network can be taken to be same as that of the 1^{st} network. With this assumption, SMP samples are aged under zero load at temperatures ranging from $150-175$ °C, for different lengths of time. Equation 5.52 is used to obtain the volume fraction of the 1^{st} network. The viscoelastic moduli of the degraded SMP samples are measured similar to that of the virgin material, see Section 3.1.

A mean force of 260 mN (144 kPa) with a sinusoidal dynamic amplitude of 200 mN (110 kPa) is applied over 0.1 to 10 Hz frequency range under isothermal conditions. Discrete temperatures are selected across the range 20-150 °C. From FTSP, storage modulus curves are constructed at the T_g^0.

Figure 5.16 shows the storage modulus-frequency curves of the aged epoxy SMP at T_g^0 for different levels of degradation. It is observed that the $G' - f$ curves shift towards lower frequencies due to degradation, which imply that the relaxation process takes longer. Since the $G' - f$ curves also represents the sequence of micro-rheological events that lead to viscoelastic relaxation, the change in shape of these curves is evidence

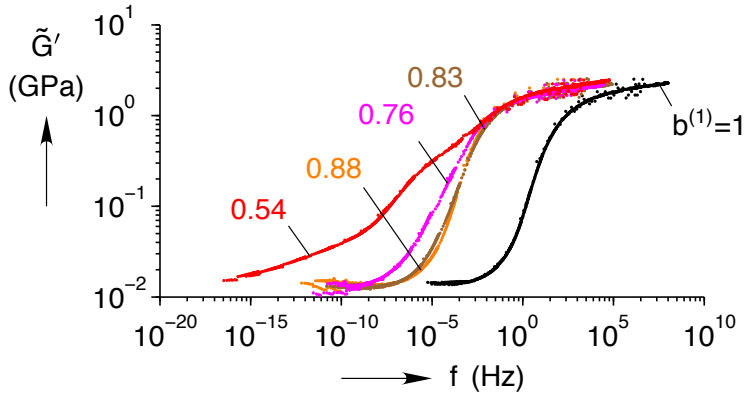

Figure 5.16: Storage modulus-frequency curves of the aged epoxy SMP at T_g^0 for different levels of degradation

that CR aging alters the sequence of events in a viscoelastic relaxation. This is to be expected because CR aging changes the macromolecular network structure of the SMP due to scission and crosslinking. However, it is interesting to observe that for $0.76 \leq b^{(1)} \leq 1$ the shape of $G' - f$ curves does not change appreciably, indicating CR aging does not drastically change the sequence of micro-rheological events, rather only slows it down. From this observation, it is possible to say that at a temperature $T_{\rm g}^0$ for a SMP with $\widetilde{b}^{(1)}$ volume fraction of 1$^{\rm st}$ network, the increment in $\widetilde{G}$ during a time interval (Δt) is the same as the increment in $\widetilde{G}$ of a virgin SMP at a temperature $T_{\rm g}^0$ during a time interval $\dfrac{\Delta t}{a_{\rm g}(\widetilde{b}^{(1)}, 1)}$, where $a_{\rm g}$ is a *glass-transition shift function.* The value of the glass-transition shift function $a_{\rm g} = 1$ for the virgin SMP material, i.e. if $\widetilde{b}^{(1)} = 1$.

The $G' - f$ curves of the aged epoxy SMP at the temperature T_g^0 shown in Fig 5.16 are constructed by assuming that TTSP holds for the degraded SMP. The resulting temperature shift function is shown in Fig. 5.17. Clearly, CR aging also influences the temperature shift function $\widetilde{a}_{\rm T}$. The experimental data points of the temperature shift function are fitted using the WLF equation above $T_{\rm g}^0$ and a reverse WLF equation

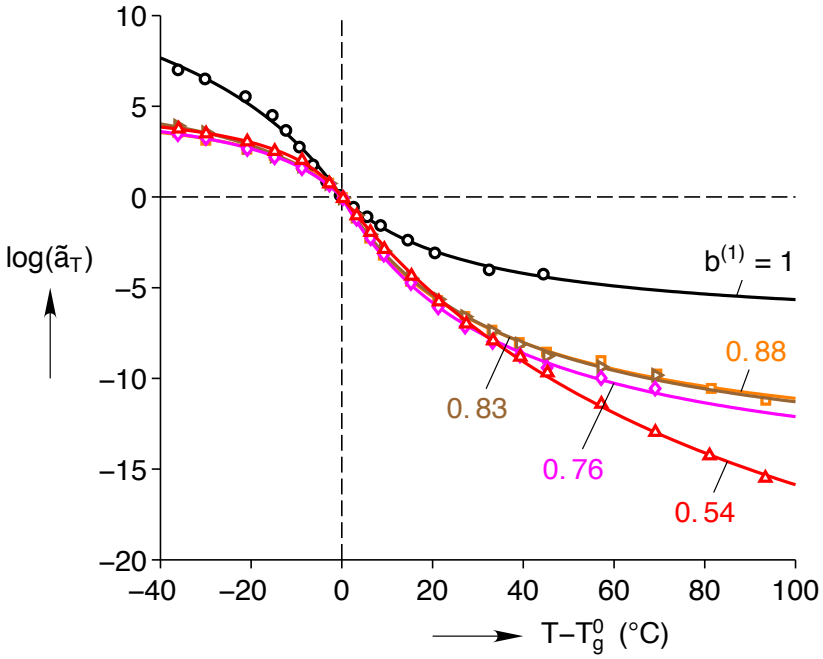

Figure 5.17: Temperature shift function of aged epoxy SMP for different levels of degradation

below T_g^0. The expressions for WLF and reverse WLF are given by

$$\log \widetilde{a}_T = \begin{cases} \dfrac{-\widetilde{C}_1(T - T_g^0)}{\widetilde{C}_2 + (T - T_g^0)} & : T > T_g^0 \\ \dfrac{-\widetilde{C}_3(T - T_g^0)}{\widetilde{C}_4 - (T - T_g^0)} & : T < T_g^0 \end{cases} \tag{5.56}$$

where, $\widetilde{C}_1$, $\widetilde{C}_2$, $\widetilde{C}_3$ and $\widetilde{C}_4$ are material properties which are now functions of $b^{(1)}$ as shown in Figs. 5.18 and summarized here

$$\begin{aligned} \widetilde{C}_1\left(b^{(1)}\right) &= -50.4b^{(1)} + 57.63 \\ \widetilde{C}_2\left(b^{(1)}\right) &= 448.1b^{(1)2} - 832.98b^{(1)} + 416.71 \\ \widetilde{C}_3\left(b^{(1)}\right) &= 113.41b^{(1)2} - 154b^{(1)} + 55.7 \\ \widetilde{C}_4\left(b^{(1)}\right) &= 165.8b^{(1)2} - 201.32b^{(1)} + 76.82 \end{aligned} \tag{5.57}$$

From TTSP, at a temperature T for a SMP with $\widetilde{b}^{(1)}$ volume fraction of 1st network,

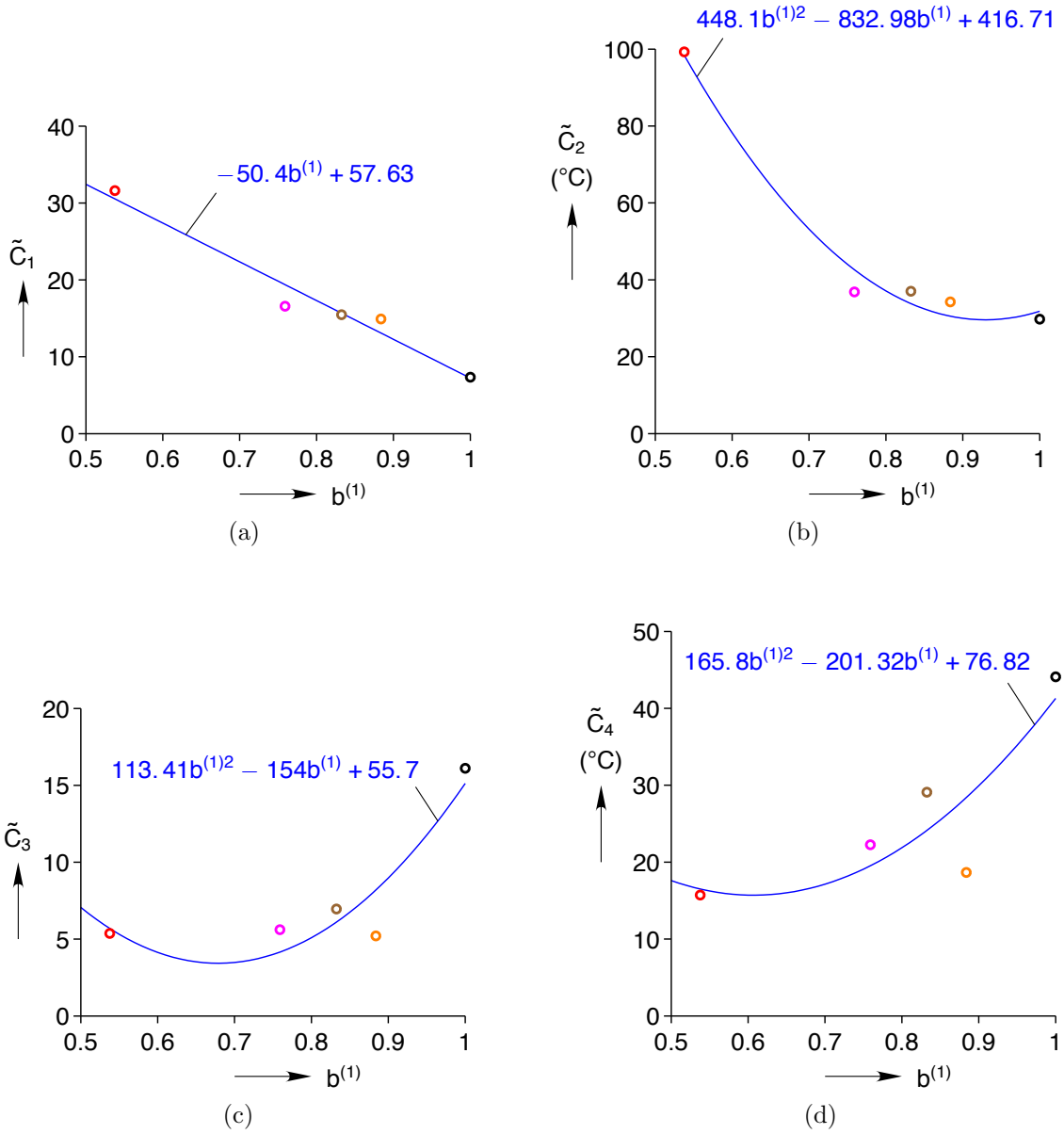

Figure 5.18: WLF and reverse WLF material properties as a function of volume fraction of the 1st network

the increment in $\widetilde{G}$ during a time interval (Δt) is the same as the increment in $\widetilde{G}$ of a virgin SMP at a temperature T_{g}^{0} during a time interval $\dfrac{\Delta t}{\widetilde{a}_{\mathrm{T}}\left(T, T_{\mathrm{g}}^{0}\right) a_{\mathrm{g}}(\widetilde{b}^{(1)}, 1)}$, where $\widetilde{a}_{\mathrm{T}}$ is the temperature shift function of the degraded SMP.

A SLS model is chosen to represent the viscoelastic behavior of the SMP. To further simplify the chemo-viscoelastic model, it is assumed that initial and long-time values

of the relaxation modulus does not change with CR aging, i.e. $\widetilde{G}(0) = G_0^{(0)}$ and $\widetilde{G}(\infty) = G_\infty^{(0)}$. The relaxation modulus of the SMP is now given by

$$\widetilde{G}\left(t,T\right) = G_0^{(0)} + G_1^{(0)} \exp\left(-\frac{t}{\widetilde{a}_{\mathrm{T}}\left(T,T_{\mathrm{g}}^0\right) a_{\mathrm{g}}(\widetilde{b}^{(1)},1)\tau_{\mathrm{R1}}^{(0)}}\right) \tag{5.58}$$

where $G_1^{(0)} = G_0^{(0)} - G_\infty^{(0)}$ and $\widetilde{b}^{(1)} = b^{(1)}\left(t,T\right)$ can be calculated using Eq. 5.52. Using Eq. 5.58 in Eq. 5.25, the storage and loss modulus at a temperature T is given by

$$\widetilde{G}'\left(\omega,T\right) = G_\infty^{(0)} + G_1^{(0)} \frac{\left(\omega\widetilde{a}_{\mathrm{T}}\left(T,T_{\mathrm{g}}^0\right) a_{\mathrm{g}}(\widetilde{b}^{(1)},1)\tau_{\mathrm{R1}}^{(0)}\right)^2}{1+\left(\omega\widetilde{a}_{\mathrm{T}}\left(T,T_{\mathrm{g}}^0\right) a_{\mathrm{g}}(\widetilde{b}^{(1)},1)\tau_{\mathrm{R1}}^{(0)}\right)^2} \tag{5.59}$$

$$\widetilde{G}''\left(\omega,T\right) = G_1^{(0)} \frac{\omega\widetilde{a}_{\mathrm{T}}\left(T,T_{\mathrm{g}}^0\right) a_{\mathrm{g}}(\widetilde{b}^{(1)},1)\tau_{\mathrm{R1}}^{(0)}}{1+\left(\omega\widetilde{a}_{\mathrm{T}}\left(T,T_{\mathrm{g}}^0\right) a_{\mathrm{g}}(\widetilde{b}^{(1)},1)\tau_{\mathrm{R1}}^{(0)}\right)^2} \tag{5.60}$$

Eq. 5.59 can now be used to fit the experimental data shown in Fig. 5.16 and obtain the value of the glass-transition shift function a_{g} for a set of discrete $b^{(1)}$ values. Figure 5.19a shows the $\widetilde{G}' - f$ model fit at the reference temperature T_{g}^0 for various levels of degradation (refer to Fig. 5.16 for the corresponding experimental data). The obtained discrete values of a_{g} and a fit to the glass-transition shift function are shown in Fig. 5.19b.

From this empirical fit, the glass-transition shift function is obtained to be

$$\ln a_{\mathrm{g}}\left(\widetilde{b}^{(1)},1\right) = -76.34\widetilde{b}^{(1)2} + 85.2\widetilde{b}^{(1)} - 8.86 \tag{5.61}$$

With this, the relaxation modulus of the degraded SMP is characterized. For the SLS, creep compliance $\widetilde{J}$ can be obtained by using Eq. 5.58 in the identity 5.23. The comparison of the experimental loss modulus-frequency data at T_{g}^0 for various levels of degradation and also the model response is shown in Fig. 5.20. While this simple model does not accurately represent the loss modulus response at a particular value of

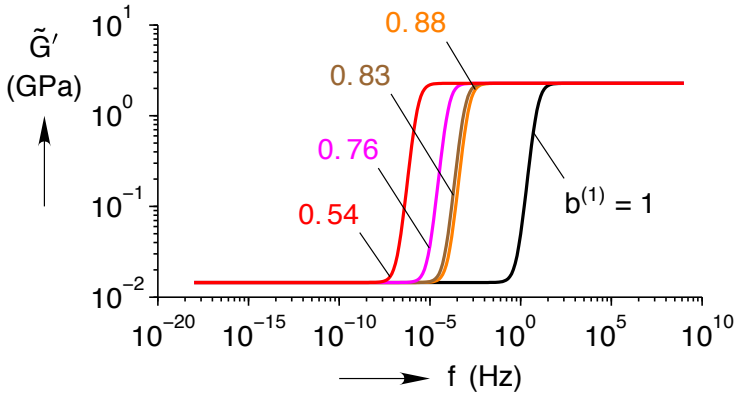

(a)

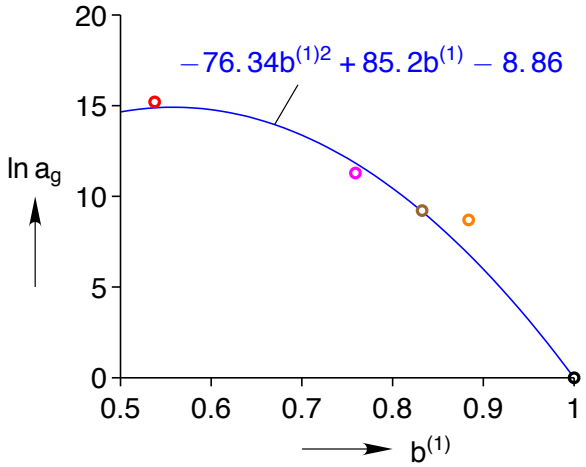

(b)

Figure 5.19: (a) A fit to the storage modulus-frequency curves of the aged epoxy SMP at T_g^0 for different levels of degradation (b) Variation of the glass-transition shift function with the volume fraction of the 1st network

$b^{(1)}$, it nevertheless captures the change in the response due to degradation. Similarly, Fig. 5.21 shows the experimental data and model response of storage modulus as a function of temperature for different levels of $b^{(1)}$. The corresponding loss modulus and $\tan\delta$ curves are shown in Figs. 5.22 and 5.23. Again, qualitatively this model captures all the trends observed in the experimental $\tan\delta - T$ plot in Fig. 5.23 for the case $b^{(1)} = 0.54$, two transition peaks are observed[2]. This can be attributed to the degraded 1st network

[2]Recall that the temperature corresponding to the $\tan\delta$ peak represents the T_g

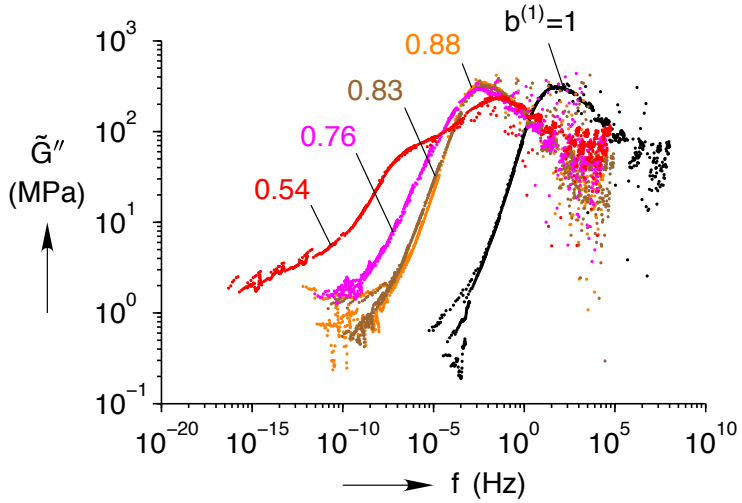

(a)

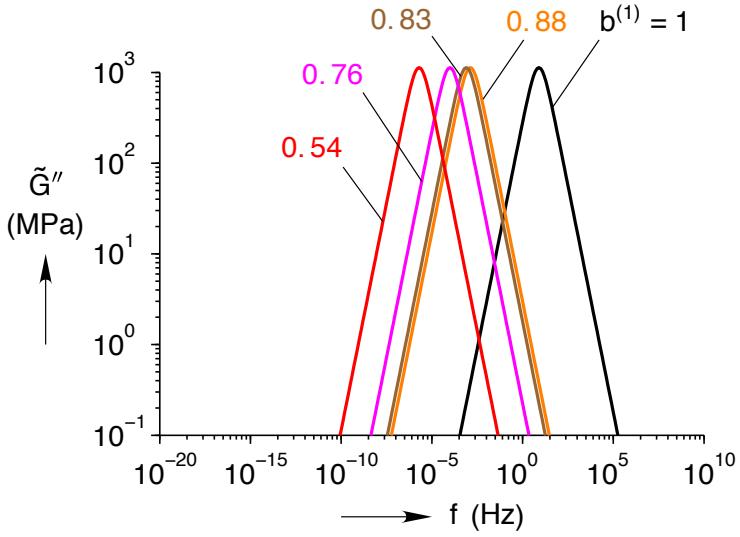

(b)

Figure 5.20: Loss modulus-frequency curves of the aged epoxy SMP at T_g^0 for different levels of degradation (a) Experimental data (b) Model response from Eq. 5.60

and the newly formed 2nd network, although, it is not possible to say exactly which is which. Clearly, the model is not adequate to capture the two transition temperatures. It is still interesting to see that even for the case of $b^{(1)} = 0.54$ the model captures the transition temperature corresponding to the significant $\tan\delta$ peak.

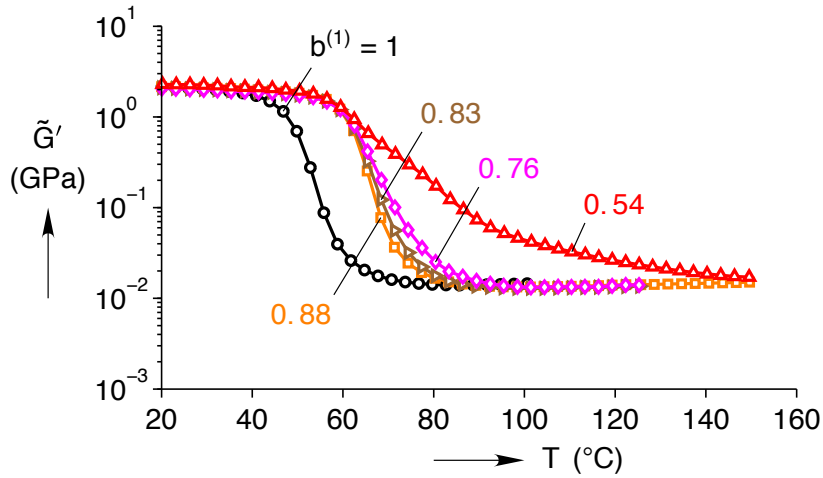

(a)

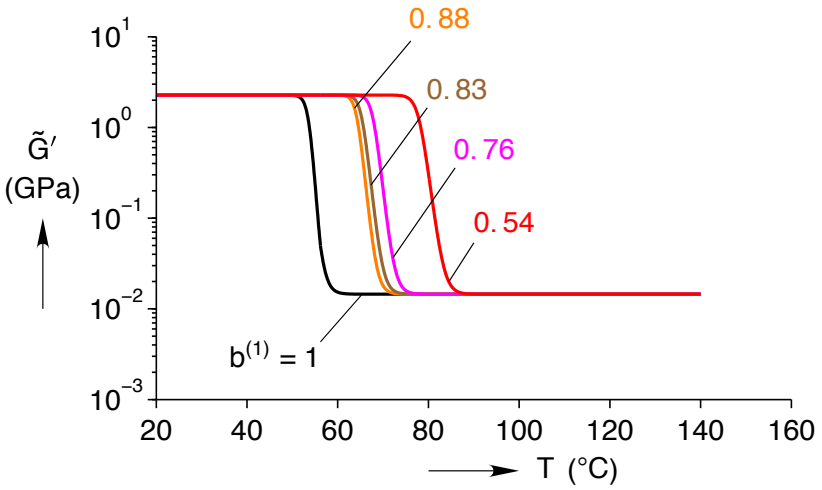

(b)

Figure 5.21: Storage modulus-Temperature curves of the aged epoxy SMP at a frequency of 1 Hz for different levels of degradation (a) Experimental data (b) Model response from Eq. 5.59

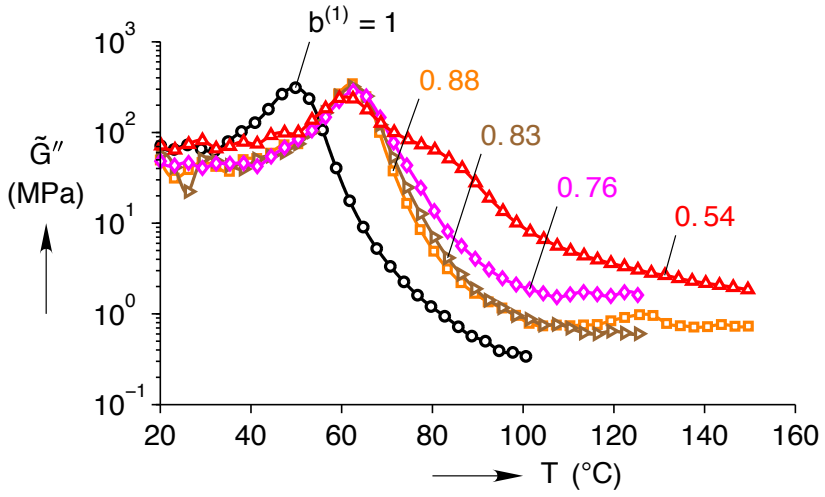

(a)

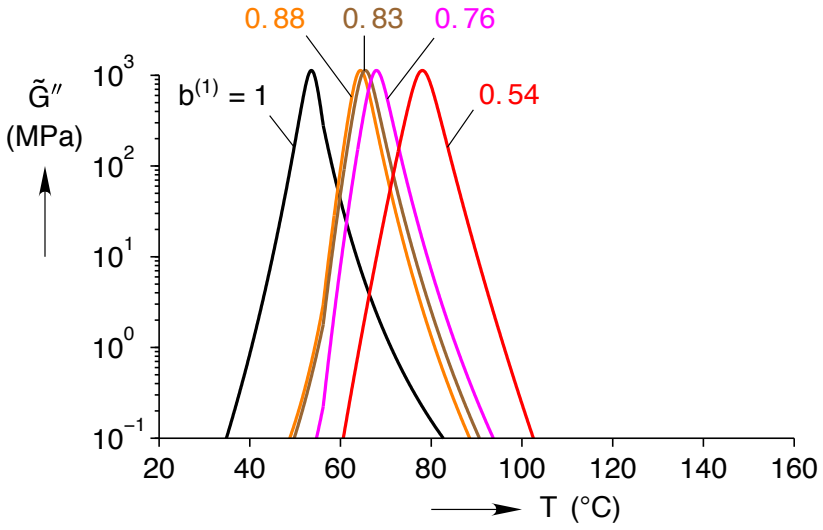

(b)

Figure 5.22: Loss modulus-Temperature curves of the aged epoxy SMP at a frequency of 1 Hz for different levels of degradation (a) Experimental data (b) Model response from Eq. 5.60

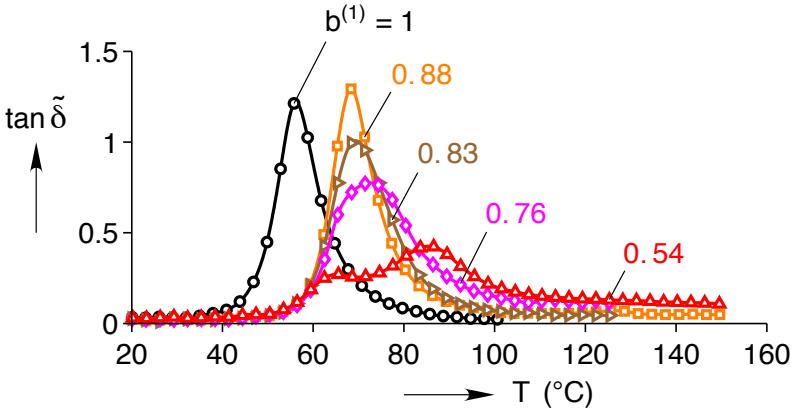

(a)

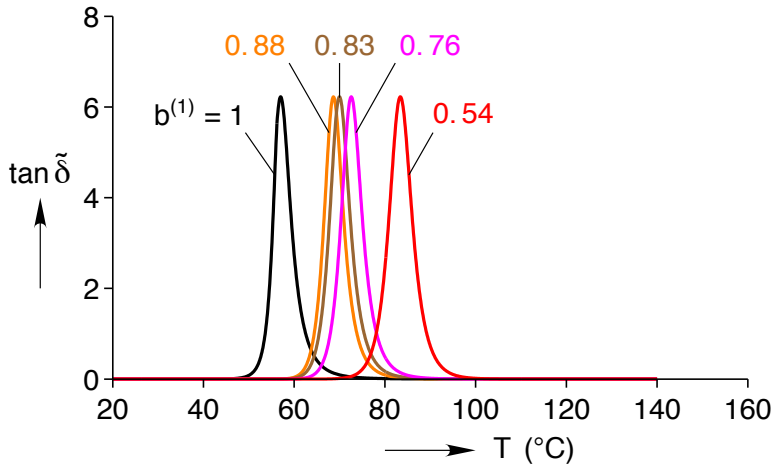

(b)

Figure 5.23: $\tan\delta$-Temperature curves of the aged epoxy SMP at a frequency of 1 Hz for different levels of degradation (a) Experimental data (b) Model response

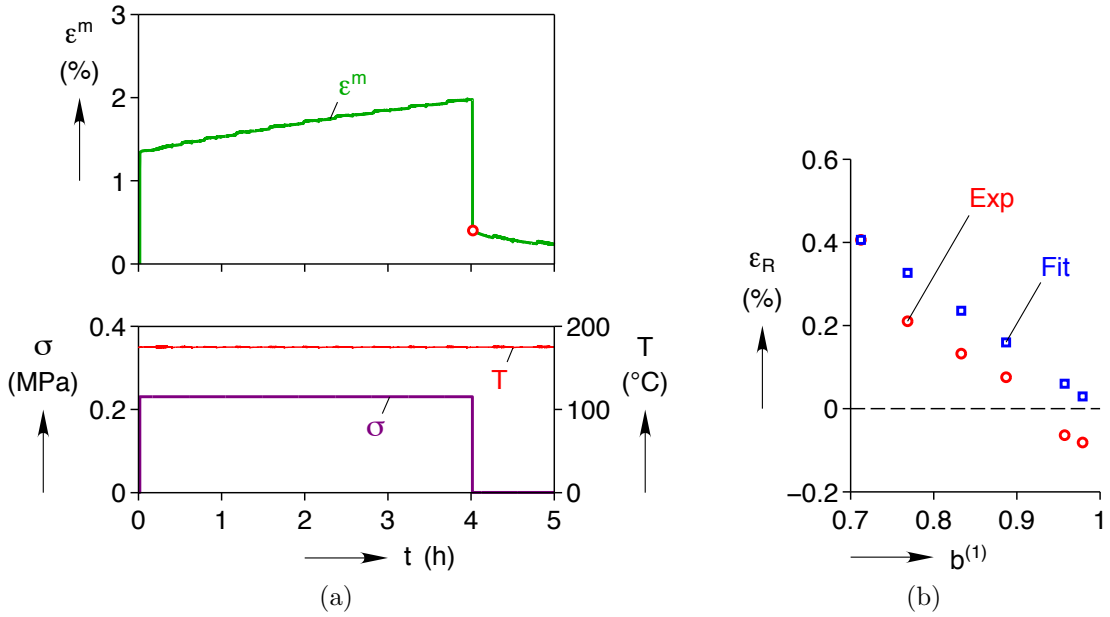

Figure 5.24: (a) Stress, Temperature and Mechanical strain history during a creep-recovery test at 175 °C (b) Residual strain from chemical creep-recovery tests (open circles) as a function of volume fraction of 1st network and model fit (open squares)

5.5.3 Residual Strain and Reference Configuration of the 2nd Network

The reference configuration of the lumped 2nd network is expressed by $\varepsilon_0^{(2)}$, and $\widetilde{S}(t)$ relates this reference configuration to the creep strain response. The form of $\varepsilon_0^{(2)}$ and $\widetilde{S}(t)$ can be picked based on creep-recovery test results as discussed in Section 5.4.2. Creep-recovery tests are conducted on a virgin specimen at temperatures 100, 125, 150, 158, 166 and 175 °C. At each temperature, the specimen is subject to 0.23 MPa of stress which is held for a duration of 4 h and then instantaneously unloaded and held for an hour under zero load. Figure 5.24a shows the stress, temperature and mechanical strain history. The mechanical strain here is measured as $\varepsilon(t) - \varepsilon(0)$, where $\varepsilon(t)$ is the total strain. In Fig. 5.24a, the mechanical strain increases under load due to chemical creep. Instantaneous unloading results in elastic recovery followed by *thermal aging* (CR aging under zero load). The mechanical strain after the elastic recovery is chosen as the residual strain ε_R and volume fraction of the 1st network

at this time instant is calculated from Eq. 5.52. Figure 5.24b shows the residual strain as a function of the volume fraction of the 1st network. The residual strains for $b^{(1)} > 0.95$ are negative because of the structural relaxation process. By defining the mechanical strain as $\varepsilon(t) - \varepsilon(0)$, it is implicitly assumed that the thermal strain at a temperature is a constant in time, given by $\varepsilon(0)$. The resulting error manifests as negative residual strain.

Mathematically, the residual strain for a virgin SMP sample subjected to a chemical creep and recovery test is given by Eq. 5.47. To model the experimental data shown in Fig. 5.24b, $\widetilde{S}(t) = E_1$ and $\varepsilon_0^{(2)}(t) = -b^{(1)}(t, T)$ are chosen, where E_1 is some constant. A fit to the experimental data gives $E_1 = 14.12 \times 10^{-3}$. The model response is also shown in Fig. 5.24b. At this point, the chemo-visco model for the strain response under arbitrary stress is completely characterized.

5.6 Extension to Time Varying Temperature Histories

It is assumed that the process of macromolecular reconfiguration for chemo-viscoelastic stress relaxation during a small interval of time depends on the volume fraction of the 1st network during this time interval. During stress relaxation, let $\hat{T}_1$ be the average temperature in $0 \leq s \leq t_1$. From TTSP and the empirically observed shift due to degradation, the increment in $\widetilde{G}$ at $\hat{T}_1$ during the interval $t_1 - 0$ is the same as the increment in $\widetilde{G}$ for a virgin SMP material at the reference temperature T_{g}^0 in the time interval $\dfrac{t_1 - 0}{\widetilde{a}_{\mathrm{T}}\left(\hat{T}_1, T_{\mathrm{g}}^0, \widetilde{b}_1^{(1)}\right) a_{\mathrm{g}}(\widetilde{b}_1^{(1)}, 1)}$, where $\widetilde{a}_{\mathrm{T}}$ is the temperature shift function, a_{g} is the glass-transition shift function and $\widetilde{b}_1^{(1)} = b^{(1)}\left[\dfrac{t_1 - 0}{a_{\mathrm{cr}}\left(\hat{T}_1, T_{\mathrm{cr}}^0\right)}, T_{\mathrm{cr}}^0\right]$. Thus,

$$\widetilde{G}\left[t_1, \mathrm{T}\substack{t_1 \\ (\mathrm{s}) \\ s=0}\right] = \widetilde{G}\left[\frac{t_1 - 0}{\widetilde{a}_{\mathrm{T}}\left(\hat{T}_1, T_{\mathrm{g}}^0, \widetilde{b}_1^{(1)}\right) a_{\mathrm{g}}(\widetilde{b}_1^{(1)}, 1)}, T_{\mathrm{g}}^0\right] \tag{5.62}$$

Similarly, during the interval $t_1 \leq s \leq t_2$, with an average temperature $\hat{T}_2$, the increment in $\widetilde{G}$ is

$$\widetilde{G}\left[t_1, \overset{t_2}{\underset{s=0}{\mathrm{T(s)}}}\right] = \widetilde{G}\left[\frac{t_1 - 0}{\widetilde{a}_{\mathrm{T}}\left(\hat{T}_1, T_{\mathrm{g}}^0, \widetilde{b}_1^{(1)}\right) a_{\mathrm{g}}(\widetilde{b}_1^{(1)}, 1)} + \frac{t_2 - t_1}{\widetilde{a}_{\mathrm{T}}\left(\hat{T}_2, T_{\mathrm{g}}^0, \widetilde{b}_2^{(1)}\right) a_{\mathrm{g}}(\widetilde{b}_2^{(1)}, 1)}, T_{\mathrm{g}}^0\right] \tag{5.63}$$

where,

$$\widetilde{b}_2^{(1)} = b^{(1)}\left[\frac{t_1 - 0}{a_{\mathrm{cr}}\left(\hat{T}_1, T_{\mathrm{cr}}^0\right)} + \frac{t_2 - t_1}{a_{\mathrm{cr}}\left(\hat{T}_2, T_{\mathrm{cr}}^0\right)}, T_{\mathrm{cr}}^0\right] \tag{5.64}$$

Continuing in this manner,

$$\widetilde{G}\left[t_n, \overset{t_n}{\underset{s=0}{\mathrm{T(s)}}}\right] = \widetilde{G}\left[\sum_{k=1}^{n} \frac{t_k - t_{k-1}}{\widetilde{a}_{\mathrm{T}}\left(\hat{T}_k, T_{\mathrm{g}}^0, \widetilde{b}_k^{(1)}\right) a_{\mathrm{g}}(\widetilde{b}_k^{(1)}, 1)}, T_{\mathrm{g}}^0\right] \tag{5.65}$$

where,

$$\widetilde{b}_k^{(1)} = b^{(1)}\left[\sum_{j=1}^{k} \frac{t_j - t_{j-1}}{a_{\mathrm{cr}}\left(\hat{T}_j, T_{\mathrm{cr}}^0\right)}, T_{\mathrm{cr}}^0\right] \tag{5.66}$$

where $\hat{T}_k$ is the average temperature during the interval $t_{k-1} \leq s \leq t_k$ and $\widetilde{b}_k^{(1)}$ is the volume fraction of the 1st network at time t_k. As the time intervals get smaller, in the limit, the relaxation function becomes,

$$\widetilde{G}\left[t, \overset{t}{\underset{s=0}{\mathrm{T(s)}}}\right] = \widetilde{G}\left[\int_0^t \frac{ds}{\widetilde{a}_{\mathrm{T}}\left(T(s), T_{\mathrm{g}}^0, \widetilde{b}^{(1)}(s)\right) a_{\mathrm{g}}(\widetilde{b}^{(1)}(s), 1)}, T_{\mathrm{g}}^0\right] \tag{5.67}$$

where,

$$\widetilde{b}^{(1)}(s) = b^{(1)}\left[\int_0^s \frac{dx}{a_{\mathrm{cr}}\left(T(x), T_{\mathrm{cr}}^0\right)}, T_{\mathrm{cr}}^0\right] \tag{5.68}$$

where, $\xi_{\mathrm{cr}}(s) = \displaystyle\int_0^s \frac{dx}{a_{\mathrm{cr}}\left(T(x), T_{\mathrm{cr}}^0\right)}$ can be called as a chemo-rheological intrinsic time and $\widetilde{\xi}(t) = \displaystyle\int_0^t \frac{ds}{\widetilde{a}_{\mathrm{T}}\left(T(s), T_{\mathrm{g}}^0, \widetilde{b}^{(1)}(s)\right) a_{\mathrm{g}}(\widetilde{b}^{(1)}(s), 1)}$ is a modified intrinsic time due to chemo-viscoelastic relaxation.

The applied stress is treated as a superposition of step stress increments. Assuming that scaling and superposition are still valid when the temperature varies and material undergoes CR degradation with time, the mechanical strain response at time t is given by the superposition of responses to step stress increments. For the stress increment $\sigma(t_k) - \sigma(t_{k-1})$ applied at time t_k, the strain response at time t is given by

$$\begin{aligned}
&[\sigma(t_k) - \sigma(t_{k-1})]\, \widetilde{J}\left[t, \mathrm{T}\overset{t}{\underset{s=t_k}{(\mathrm{s})}}\right] + \left[\varepsilon_0^{(2)}(t_k) - \varepsilon_0^{(2)}(t_{k-1})\right] \widetilde{S}\,(t - t_k) \\
&= [\sigma(t_k) - \sigma(t_{k-1})]\, \widetilde{J}\left[\widetilde{\xi}(t) - \widetilde{\xi}(t_k), T_{\mathrm{g}}^0\right] + \left[\varepsilon_0^{(2)}(t_k) - \varepsilon_0^{(2)}(t_{k-1})\right] \widetilde{S}\,(t - t_k)
\end{aligned}$$

From superposition of strain increments, the mechanical strain response at time t for arbitrary stress history and time varying temperature history is given by

$$\begin{aligned}
\varepsilon^{\mathrm{m}}(t) = \sigma(0)\widetilde{J}\left[\widetilde{\xi}(t), T_{\mathrm{g}}^0\right] + \int_0^t \widetilde{J}\left[\widetilde{\xi}(t) - \widetilde{\xi}(s), T_{\mathrm{g}}^0\right] \dot{\sigma}(s) ds \\
+ \varepsilon_0^{(2)}(0)\widetilde{S}(t) + \int_0^t \widetilde{S}\,[t - s]\, \dot{\varepsilon}_0^{(2)}(s) ds
\end{aligned} \tag{5.69}$$

where,

$$\widetilde{\xi}(t) = \int_0^t \frac{ds}{\widetilde{a}_{\mathrm{T}}\left(T(s), T_{\mathrm{g}}^0, \widetilde{b}^{(1)}(s)\right) a_{\mathrm{g}}(\widetilde{b}^{(1)}(s), 1)} \tag{5.70}$$

and $\widetilde{b}^{(1)}(s) = b^{(1)}\left[\xi_{\mathrm{cr}}(s), T_{\mathrm{cr}}^0\right]$, which is calculated using Eq. 5.52 and

$$\xi_{\mathrm{cr}}(s) = \int_0^s \frac{dx}{a_{\mathrm{cr}}\left(T(x), T_{\mathrm{cr}}^0\right)} \tag{5.71}$$

Similarly, the stress response at time t for arbitrary mechanical strain history and time varying temperature history is given by

$$\begin{aligned}
\sigma(t) = \varepsilon^{\mathrm{m}}(0)\widetilde{G}\left[\widetilde{\xi}(t), T_{\mathrm{g}}^0\right] + \int_0^t \widetilde{G}\left[\widetilde{\xi}(t) - \widetilde{\xi}(s), T_{\mathrm{g}}^0\right] \dot{\varepsilon}^{\mathrm{m}}(s) ds \\
- \varepsilon_0^{(2)}(0)\widetilde{K}(t) - \int_0^t \widetilde{K}\,[t - s]\, \dot{\varepsilon}_0^{(2)}(s) ds
\end{aligned} \tag{5.72}$$

5.7 Evaluation of the Chemo-Visco Model

The total strain response of the chemo-visco model is given by

$$\begin{aligned}\varepsilon(t) = \sigma(0)\widetilde{J}\left[\widetilde{\xi}(t), T_{\mathrm{g}}^{0}\right] &+ \int_{0}^{t} \widetilde{J}\left[\widetilde{\xi}(t) - \widetilde{\xi}(s), T_{\mathrm{g}}^{0}\right] \dot{\sigma}(s) ds \\ &+ \varepsilon_{0}^{(2)}(0)\widetilde{S}(t) + \int_{0}^{t} \widetilde{S}\left[t - s\right] \dot{\varepsilon}_{0}^{(2)}(s) ds \\ &+ \alpha_{\mathrm{g}}(T^{*} - T_{0}) + \begin{cases} \alpha_{\mathrm{r}}(T - T^{*}) & : T > T^{*} \\ \alpha_{\mathrm{g}}(T - T^{*}) & : T < T^{*} \end{cases} \end{aligned} \tag{5.73}$$

where, $\widetilde{\xi}$ is calculated from Eq. 5.70 , $\widetilde{b}^{(1)}(s) = b^{(1)}\left[\xi_{\mathrm{cr}}(s), T_{\mathrm{cr}}^{0}\right]$ is calculated using Eq. 5.52 and ξ_{cr} is calculated from Eq. 5.71. The effect of CR aging on the thermal strain response is not modeled.

Figures 5.25a and 5.25b show a comparison of the experimental total strain response and model prediction for SMCs at $T_{\mathrm{d}} = 150$ and 175 °C. The corresponding engineering stress (σ) and temperature (T) history are also shown. It can be seen that this simple chemo-visco model captures all the experimentally observed trends. For $T_{\mathrm{d}} = 150$ °C case, the minimum volume fraction of the 1st network is $b^{(1)} = 0.89$ at the end of SMCs. It is observed that the model predictions and the experimental data agree well for this case. For $T_{\mathrm{d}} = 175$ °C, the model and the experimental data are in close agreement during the initial cycles but deviate during the recovery path in later SMCs.

Figure 5.26a shows a comparison of the experimentally observed residual strain and the model predictions. While the model captures the trends, it under-predicts the residual strain in later cycles or at larger hold times. We believe this is because of the absence of structural relaxation and CR aging effects in the thermal strain modeling. Experimentally, structural relaxation causes the thermal strain to ratchet down and

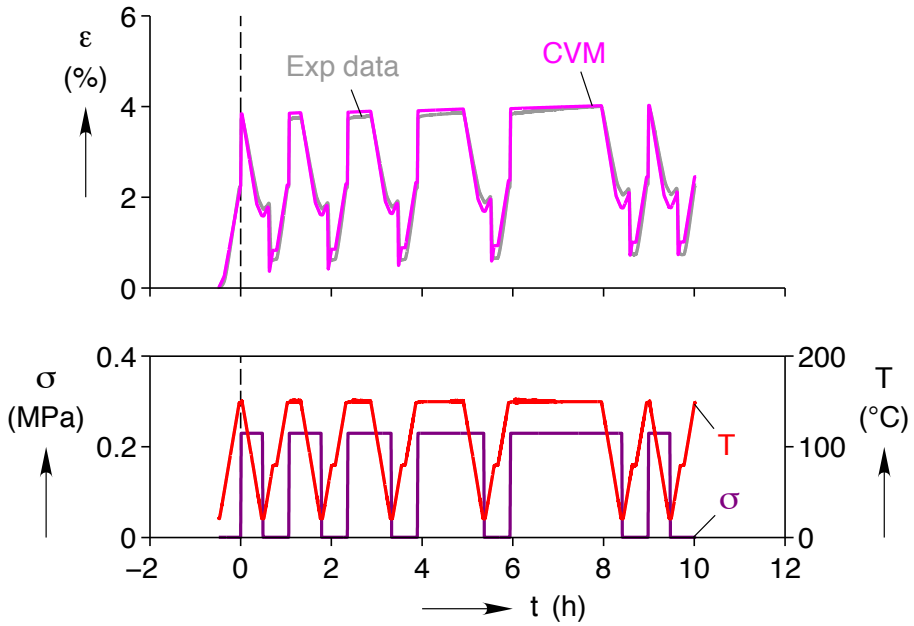

(a)

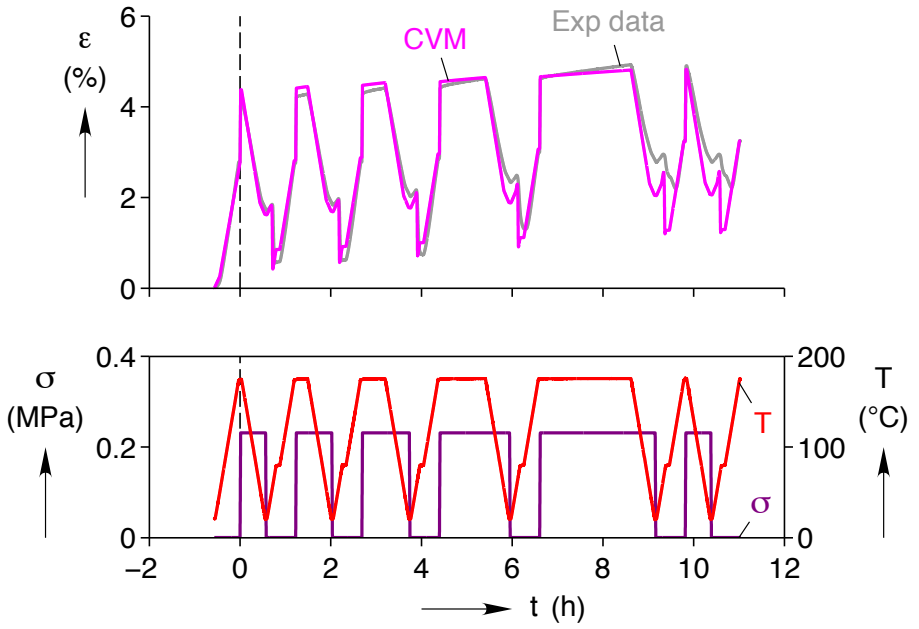

(b)

Figure 5.25: A comparison of the model and experiment response to SMCs at (a) $T_{\mathrm{d}} = 150$ °C (b) $T_{\mathrm{d}} = 175$ °C with an applied stress of 0.23 MPa and hold time ranging from 1-120 min

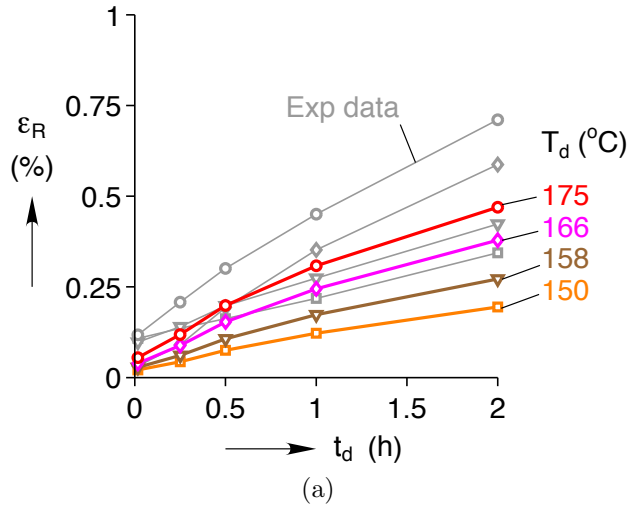

(a)

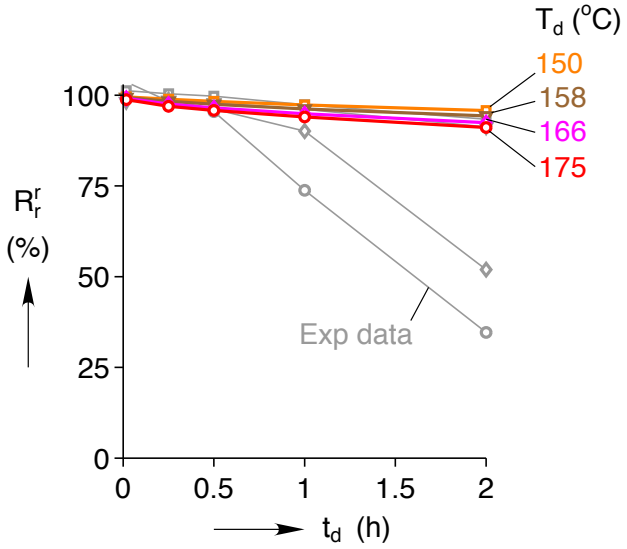

(b)

Figure 5.26: A comparison of the model and experimental (a) residual strains as a function of hold time (b) recovery ratio at a recovery temperature $T_{\mathrm{r}} = 80$ °C

CR aging decreases the thermal strain recovery and these effects contribute to increasing residual strain. The model on the other hand holds a steady thermal strain and predicts complete thermal strain recovery. These effects get progressively larger with cycles or at longer hold times. Naturally, under-prediction of residual strain also manifests as over-prediction of the recovery ratio at the deformation temperature ($R_{\mathrm{r}}^{\mathrm{d}}$), see definition in Section 4.1.2.

Similar to the viscoelastic model, the chemo-visco model predicts the shape fixity ratio to be 99%. The recovery ratio at the recovery temperature ($R_{\mathrm{r}}^{\mathrm{r}}$) is shown in Fig. 5.26b. Again, it is observed that the model and the experimental data agree closely at smaller levels of degradation ($b^{(1)} > 0.9$).

5.8 Summary

The purpose of this work was to develop a chemo-viscoelastic modeling framework to represent the CR aging behavior of SMPs. First, a viscoelastic modeling framework was presented. Two models, a 12-term Prony series and a basic SLS were calibrated and the model response was evaluated against SMC experiments. Both models captured all the trends in viscoelastic shape memory behavior. Understandably, the more accurate 12-term model captured the experimental data more closely than than the simple basic SLS model. Both models predicted 99% shape fixity and a 100% shape recovery.

Based on multi-network theory, a chemo-viscoelastic modeling framework was developed in three stages. First, the case of *chemical* stress relaxation was modeled to capture the kinetics of CR aging, i.e. scission and recrosslinking. Then, the case of *chemical* creep was modeled to study the effect of the disparity in the reference configurations of the 1$^{\mathrm{st}}$ and the 2$^{\mathrm{nd}}$ macromolecular network. Then, chemo-visco stress

relaxation and creep due to arbitrary mechanical strain and stress were modeled. The accuracy of the chemo-visco model strongly depends on the choice of the stress relaxation function. Based on the empirical data, kinetics of CR aging and a simple SLS based relaxation function were calibrated to capture the chemo-viscoelastic behavior. The chemo-visco model was then extended to the case of time-varying temperature histories. The effect of CR aging on the thermal strain response was not modeled. While the chemo-visco model captured all the trends observed in the experimental strain response, it under-predicted the residual strain accumulation due to CR aging at higher levels of degradation ($b^{(1)} < 0.9$). However, at smaller degradation levels ($b^{(1)} > 0.9$) this simple chemo-visco model was found to be more accurate.

CHAPTER VI

Conclusion

This thesis is a systematic investigation into the chemo-rheological (CR) aging response of shape memory polymers (SMPs). CR aging is different from physical aging as it results in permanent changes to the macromolecular network structure of the SMP due to scission and recrosslinking at high temperatures and loads. CR aging typically manifests as changed material properties and residual strains. On the other hand, physical aging is the result of structural relaxation (gradual sliding and untangling of the macromolecular chains) at temperatures below the rubber-glass transition temperature (T_{g}). While physical aging also changes the material properties, its timeframe is much longer than the CR aging process.

Due to the thermo-mechanical nature of the shape memory behavior, understanding the influence of CR aging is essential to establish a design envelope and determine the life cycle of SMP based devices. Existing studies focus on the thermo-mechanical response of SMPs in a narrow temperature zone surrounding the T_{g}. The current modeling attempts are also limited to the viscoelastic and structural relaxation behavior. In this concluding chapter, a brief summary of the dissertation and suggestions for future work are presented.

6.1 Summary

In the present work, the thermo-mechanical response of an epoxy SMP was studied at a wide range of temperatures extending well into the CR zone. Based on the shape memory cycling process, several experimental parameters such as deformation temperature, applied load, hold time, cooling rate, recovery temperature and recovery time were identified as potentially variables that influence the material response. A parametric study was conducted to investigate the effect of these variables. Prevalent performance metrics such as shape fixity ratio and recovery ratio were re-defined for consistency with the obtained data. Other metrics such as temperature at the start of recovery, residual strain and failure strain were defined to observe the effects of CR aging on the material properties.

At deformation temperatures close to T_g large failure strains were observed. At higher deformation temperatures, the failure strains dropped drastically. Shape fixity ratio increased with applied stress while the recovery ratios remained constant. The increased applied stress also resulted in an earlier start of recovery. The critical chemo-rheological temperature $T_{cr} = 100\ ^{o}C$ was identified based on color development in the SMP test specimens. Recovery time and cooling rate were found to be interdependent and have no effect on the material performance in the absence of CR aging. Also, in the absence of CR aging, shape fixity ratio marginally improved with hold times while the residual strains and recovery ratios were observed to be constant. The start of recovery temperature increased with hold times and reached a plateau. CR aging resulted is an increase in the residual strains and a drastic decrease in the recovery ratio at the recovery temperature (below T_{cr}). However, heating up to the deformation temperature (above T_{cr}) slightly improved the recovery ratio. The temperature at the start of recovery monotonically increased with hold times during CR aging.

Two viscoelasticity based models, a basic one (referred to as SLS model) with a total of 11 material parameters and the other (referred to as 12-term Prony series model) with 33 material parameters were first calibrated. Structural relaxation effects were not modeled and only the equilibrium thermal strain response was modeled. Both models captured all the trends observed in the shape memory response in the absence of CR aging. Understandably, the 12-term Prony series model was found to be more accurate than the SLS model.

Based on multi-network theory, a simple constitutive model for the shape memory behavior incorporating the kinetics of CR aging was developed and calibrated. This chemo-visco constitutive model was an extension of the SLS viscoelasticity based model. The effect of CR aging on the thermal strain response was not modeled. The magnitude of degradation was represented by the volume fraction of the original macromolecular network. Due to CR aging, almost all of the material parameters of the viscoelastic model were found to be nonlinearly dependent on the volume fraction of the original network. The predictions of this model was evaluated using shape memory cycle test data. Despite several simplifying assumptions, the chemo-visco model captured all the trends observed in strain response due to CR aging. While the model under-predicted the CR aging effects at large levels of degradation, for small levels of degradation (under 10%) the model was found to be accurate.

6.2 Future Work

This dissertation is one of the first steps towards understanding and modeling the CR aging of shape memory polymers. Some of the possible ideas for the future direction of this work is listed here.

In this work, structural relaxation effects were not modeled. A natural extension of

this work would be to also include the structural relaxation effects in the chemo-visco model. For single deployment SMP devices, physical aging resulting from structural relaxation would be critical to determining the life cycle.

A very simple choice of stress relaxation function was used in the chemo-visco model. Because of that, the drastic changes to the viscoelastic behavior at higher levels of degradation were not accurately represented. A more complicated relaxation function with similar number of material parameters can be implemented to improve the accuracy of the chemo-visco model.

The framework presented in this work for characterizing and modeling the CR aging of SMPs is general and applicable to other SMPs. Depending up on the material, other experimental variables such as humidity and concentration of other solvents might play an important role. It would be interesting to study and model the effect of these variables on the shape memory behavior of SMPs.

APPENDICES

APPENDIX A

Numerical Scheme for Viscoelastic Model

The viscoelastic model Eq. 5.22 involves integration to time t. Evaluating this integral at every time step is a computationally intensive task. To simplify the evaluation of this model, a numerical scheme involving a set of recursion relations is developed to march forward in time.

The reduced time at t_n is given by

$$\xi_n = \xi(t_n) = \int_0^{t_n} \frac{dx}{a_{\mathrm{T}}\left(T(x), T_{\mathrm{g}}^0\right)} \tag{A.1}$$

This can be updated by using $\xi_0 = 0$ and $\xi_{n+1} = \xi_n + \Delta\xi_n$. Where,

$$\Delta\xi_n = \frac{\Delta t_n}{a_{\mathrm{T}}\left(\hat{T}_n, T_{\mathrm{g}}^0\right)} \tag{A.2}$$

where, $\Delta t_n = t_{n+1} - t_n$ and $\hat{T}_n$ is the average temperature in the interval (t_n, t_{n+1}).

For a Prony series form of $J^{(0)}$, given by

$$J^{(0)}(t) = J_\infty^{(0)} + \sum_{i=1}^{N} J_i^{(0)} \exp\left(-\frac{t}{\tau_{\mathrm{C}i}}\right) \tag{A.3}$$

the integral term in Eq. 5.22 at time t_n becomes

$$\int_0^{t_n} J^{(0)}\left[\xi_n - \xi(s), T_{\mathrm{g}}^0\right]\dot{\sigma}(s)ds = J_\infty^{(0)}\left(\sigma_n - \sigma_0\right) + \sum_{i=1}^{N} J_i^{(0)} \int_0^{t_n} \exp\left(-\frac{\xi_n - \xi(s)}{\tau_{\mathrm{C}i}}\right)\dot{\sigma}(s)ds \tag{A.4}$$

The integral term

$$I_{i,n}^{(0)} = \int_0^{t_n} \exp\left(-\frac{\xi_n - \xi(s)}{\tau_{\mathrm{C}i}}\right)\dot{\sigma}(s)ds \tag{A.5}$$

can be updated by considering $I_{i,0}^{(0)} = 0$, and representing $\dot{\sigma}(s)$ by a linear ramp in the time interval (t_n, t_{n+1}). Then,

$$I_{i,n+1}^{(0)} = I_{i,n}^{(0)} \exp\left(-\frac{\Delta\xi_n}{\tau_{\mathrm{C}i}}\right) + \frac{1}{2}\Delta\sigma_n\left[1 + \exp\left(-\frac{\Delta\xi_n}{\tau_{\mathrm{C}i}}\right)\right] \tag{A.6}$$

where $\Delta\sigma_n = \sigma_{n+1} - \sigma_n$. Therefore, the strain response (Eq. 5.22) at time t_n becomes

$$\begin{aligned}\varepsilon_n =& \sigma_n J_\infty^{(0)} + \sigma_0 \sum_{i=1}^{N} J_i^{(0)} \exp\left(-\frac{\xi_n}{\tau_{\mathrm{C}i}}\right) + \sum_{i=1}^{N} J_i^{(0)} I_{i,n}^{(0)} \\ &+ \alpha_{\mathrm{g}}\left(T^* - T_0\right) + \begin{cases} \alpha_{\mathrm{r}}(T_n - T^*) & : T_n > T^* \\ \alpha_{\mathrm{g}}(T_n - T^*) & : T_n < T^* \end{cases}\end{aligned} \tag{A.7}$$

APPENDIX B

Numerical Scheme for the Chemo-Visco Model

A numerical scheme for the evaluation of the chemo-visco model Eq. 5.73 is presented here. The approach is similar to the viscoelastic model presented in Appendix A.

The chemo-rheological intrinsic time at t_n is given by

$$\xi_{\mathrm{cr}n} = \int_0^{t_n} \frac{d\hat{\tau}}{a_{\mathrm{cr}}\left(T(\hat{\tau}), T^0_{\mathrm{cr}}\right)} \tag{B.1}$$

This can be updated by using $\xi_{\mathrm{cr}0} = 0$ and $\xi_{\mathrm{cr}(n+1)} = \xi_{\mathrm{cr}n} + \Delta\xi_{\mathrm{cr}n}$. Where,

$$\Delta\xi_{\mathrm{cr}n} = \frac{\Delta t_n}{a_{\mathrm{cr}}\left(\hat{T}_n, T^0_{\mathrm{cr}}\right)} \tag{B.2}$$

where, $\Delta t_n = t_{n+1} - t_n$ and $\hat{T}_n$ is the average temperature in the interval (t_n, t_{n+1}) and a_{cr} is calculated from Eq. 5.53. The volume fraction of the 1^{st} network at time t_n is given by $\widetilde{b}^{(1)}_n = b^{(1)}\left[\xi_{\mathrm{cr}n}, T^0_{\mathrm{cr}}\right]$ and is calculated using Eq. 5.52.

The modified intrinsic time at t_n is given by

$$\widetilde{\xi}_n = \int_0^{t_n} \frac{ds}{\widetilde{a}_T\left(T(s), T^0_{\mathrm{g}}, \widetilde{b}^{(1)}(s)\right) a_{\mathrm{g}}(\widetilde{b}^{(1)}(s), 1)} \tag{B.3}$$

This can be updated by using $\widetilde{\xi}_n = 0$ and $\widetilde{\xi}_{n+1} = \widetilde{\xi}_n + \Delta\widetilde{\xi}_n$. Where,

$$\Delta\widetilde{\xi}_n = \frac{\Delta t_n}{\widetilde{a}_T\left(\hat{T}_n, T_{\mathrm{g}}^0, \widetilde{b}_{n+1}^{(1)}\right) a_{\mathrm{g}}(\widetilde{b}_{n+1}^{(1)}, 1)} \tag{B.4}$$

where, $\widetilde{a}_{\mathrm{T}}$ is calculated from Eqs. 5.56 and 5.57 and $a_t extg$ is calculated from Eq. 5.61

For a SLS form of $\widetilde{J}$, given by

$$\widetilde{J}(t) = \widetilde{J}_\infty + \left(\widetilde{J}_0 - \widetilde{J}_\infty\right) \exp\left(-\frac{t}{\widetilde{\tau}_{\mathrm{C}}}\right) \tag{B.5}$$

The creep compliance integral term in Eq. 5.73 given by

$$\int_0^{t_n} \widetilde{J}\left[\widetilde{\xi}_n - \widetilde{\xi}(s), T_{\mathrm{g}}^0\right] \dot{\sigma}(s) ds = \widetilde{J}_\infty\left(\sigma_n - \sigma_0\right) + \left(\widetilde{J}_0 - \widetilde{J}_\infty\right) \widetilde{I}_n \tag{B.6}$$

where,

$$\widetilde{I}_n = \int_0^{t_n} \exp\left(\frac{-\widetilde{\xi}_n + \widetilde{\xi}(s)}{\widetilde{\tau}_{\mathrm{C}}}\right) \dot{\sigma}(s) ds \tag{B.7}$$

This can be updated by considering $\widetilde{I}_0 = 0$ and by representing the $\dot{\sigma}(s)$ by a linear ramp in the time interval (t_n, t_{n+1}). Then,

$$\widetilde{I}_{n+1} = \widetilde{I}_n \exp\left(-\frac{\Delta\widetilde{\xi}_n}{\widetilde{\tau}_{\mathrm{C}}}\right) + \frac{1}{2}\Delta\sigma_n\left[1 + \exp\left(-\frac{\Delta\widetilde{\xi}_n}{\widetilde{\tau}_{\mathrm{C}}}\right)\right] \tag{B.8}$$

where, $\Delta\sigma_n = \sigma_{n+1} - \sigma_n$. Therefore the strain response at time t_n becomes

$$\begin{aligned}\varepsilon_n =& \sigma_0 \widetilde{J}\left[\widetilde{\xi}_n, T_{\mathrm{g}}^0\right] + \widetilde{J}_\infty\left(\sigma_n - \sigma_0\right) + \left(\widetilde{J}_0 - \widetilde{J}_\infty\right)\widetilde{I}_n + \varepsilon_0^{(2)} E_1 + E_1\left(1 - \widetilde{b}_n^{(1)}\right) \\ &+ \alpha_{\mathrm{g}}\left(T^* - T_0\right) + \begin{cases} \alpha_{\mathrm{r}}(T_n - T^*) & : T_n > T^* \\ \alpha_{\mathrm{g}}(T_n - T^*) & : T_n < T^* \end{cases}\end{aligned} \tag{B.9}$$

In this work, it is assumed that $\widetilde{J}_\infty = J_\infty^{(0)}$, $\widetilde{J}_0 = J_1^{(0)} + J_\infty^{(0)}$ and $\widetilde{\tau}_{\mathrm{C}} = \tau_{\mathrm{C1}}^{(0)}$

BIBLIOGRAPHY

BIBLIOGRAPHY

[1] Liu, C., Qin, H., and Mather, P. T., 2007. "Review of progress in shape-memory polymers". *J. Mater. Chem.,* ***17***, pp. 1543–1558.

[2] Otsuka, K., and Wayman, C. M., 1999. *Shape Memory Materials*. Cambridge University Press.

[3] Lendlein, A., and Kelch, S., 2002. "Shape-memory polymers". *Angewandte Chemie International Edition,* ***41***(12), pp. 2034–2057.

[4] Behl, M., Zotzmann, J., and Lendlein, A., 2010. *Shape-Memory Polymers and Shape-Changing Polymers*, Vol. 226 of *Advances in Polymer Science*. Springer-Verlag Berlin / Heidelberg.

[5] Lendlein, A., 2010. *Shape-Memory Polymers*. Advances in Polymer Science. Springer.

[6] Tobolsky, A., 1960. *Properties and structure of polymers*. Wiley series on the science and technology of materials. Wiley.

[7] Shaw, J. A., Jones, A. S., and Wineman, A. S., 2005. "Chemorheological response of elastomers at elevated temperatures: Experiments and simulations". *Journal of the Mechanics and Physics of Solids,* ***53***(12), pp. 2758 – 2793.

[8] May, C., 1988. *Epoxy Resins: Chemistry and Technology*. M. Dekker, ch. Physical, Mechanical Properties of Cured Resins.

[9] Struik, L., 1978. *Physical aging in amorphous polymers and other materials*, Vol. 106. Elsevier Amsterdam.

[10] Hutchinson, J. M., 1995. "Physical aging of polymers". *Progress in Polymer Science,* ***20***(4), pp. 703–760.

[11] Hutchinson, J., 1997. "Relaxation processes and physical aging". In *The physics of glassy polymers*. Springer, pp. 85–153.

[12] SPIE, 2005. Elastic Memory Composites (EMC) for deployable industrial and commercial applications, Vol. 5762.

[13] Di-Prima, M. A., Lesniewski, M., Gall, K., McDowell, D. L., Sanderson, T., and Campbell, D., 2007. "Thermo-mechanical behavior of epoxy shape memory polymer foams". *Smart Materials and Structures,* ***16***, pp. 2330–2340.

[14] Xie, T., and Rousseau, I. A., 2009. "Facile tailoring of thermal transition temperatures of epoxy shape memory polymers". *Polymer,* ***50***(8), 4, pp. 1852–1856.

[15] Rousseau, I. A., and Xie, T., 2009. "Shape memory epoxy: a systematic study of their performance". Z. Ounaies and J. Li, eds., Vol. 7289, SPIE, p. 72890X.

[16] Rousseau, I. A., and Xie, T., 2010. "Shape memory epoxy: Composition, structure, properties and shape memory performances". *J. Mater. Chem.,* ***20***, pp. 3431–3441.

[17] Feldkamp, D. M., and Rousseau, I. A., 2010. "Effect of the deformation temperature on the shape-memory behavior of epoxy networks". *Macromolecular Materials and Engineering,* ***295***(8), pp. 726–734.

[18] Castro, F., Westbrook, K. K., Hermiller, J., Ahn, D. U., Ding, Y., and Qi, H. J., 2011. "Time and temperature dependent recovery of epoxy-based shape memory polymers". *Journal of Engineering Materials and Technology,* ***133***(2), p. 021025.

[19] Leonardi, A. B., Fasce, L. A., Zucchi, I. A., Hoppe, C. E., Soulé, E. R., Pérez, C. J., and Williams, R. J. J., 2011. "Shape memory epoxies based on networks with chemical and physical crosslinks". *European Polymer Journal,* ***47***(3), 3, pp. 362–369.

[20] Biju, R., Gouri, C., and Nair, C. P. R., 2012. "Shape memory polymers based on cyanate ester-epoxy-poly (tetramethyleneoxide) co-reacted system". *European Polymer Journal,* ***48***(3), pp. 499–511.

[21] Fan, M., Yu, H., Li, X., Cheng, J., and Zhang, J., 2013. "Thermomechanical and shape-memory properties of epoxy-based shape-memory polymer using diglycidyl ether of ethoxylated bisphenol-a". *Smart Materials and Structures,* ***22***(5), p. 055034.

[22] Yu, K., McClung, A. J. W., Tandon, G. P., Baur, J. W., and Jerry Qi, H., 2014. "A thermomechanical constitutive model for an epoxy based shape memory polymer and its parameter identifications". *Mechanics of Time-Dependent Materials*, pp. 1–22.

[23] Fried, J., 2010. *Polymers in Aerospace Applications.* Rapra Review Reports, Report 192. Smithers Rapra Technology.

[24] Burton, B. L., 1993. "The thermooxidative stability of cured epoxy resins. 1". *Journal of Applied Polymer Science,* ***47***(10), pp. 1821–1837.

[25] Mailhot, B., Morlat-Thérias, S., Ouahioune, M., and Gardette, J.-L., 2005. "Study of the degradation of an epoxy/amine resin, 1". *Macromolecular Chemistry and Physics,* ***206***(5), pp. 575–584.

[26] Mailhot, B., Morlat-Thérias, S., Bussière, P.-O., and Gardette, J.-L., 2005. "Study of the degradation of an epoxy/amine resin, 2". *Macromolecular Chemistry and Physics,* ***206***(5), pp. 585–591.

[27] Rousseau, I. A., 2008. "Challenges of shape memory polymers: A review of the progress toward overcoming smp's limitations". *Polymer Engineering and Science,* ***48***(11), pp. 2075–2089.

[28] Hamerton, I., 1996. *Recent developments in epoxy resins*, Vol. 91. iSmithers Rapra Publishing.

[29] Pascault, J.-P., and Williams, R. J., 2009. *Epoxy polymers*. John Wiley & Sons.

[30] Reedlunn, B., Daly, S., Hector, L., Zavattieri, P., and Shaw, J., 2013. "Tips and tricks for characterizing shape memory wire part 5: Full-field strain measurement by digital image correlation". *Experimental Techniques,* ***37***(3), pp. 62–78.

[31] Ferry, J. D., 1980. *Viscoelastic properties of polymers*. John Wiley & Sons.

[32] Wineman, A., and Rajagopal, K., 2000. *Mechanical Response of Polymers: An Introduction*. Cambridge University Press.

[33] Knauss, W. G., Emri, I., and Lu, H., 2008. "Mechanics of polymers: Viscoelasticity". In *Springer Handbook of Experimental Solid Mechanics*, W. N. Sharpe, ed. Springer US, pp. 49–96.

[34] Liu, Y., Gall, K., Dunn, M. L., and McCluskey, P., 2003. "Thermomechanical recovery couplings of shape memory polymers in flexure". *Smart Materials and Structures,* ***12***(6), pp. 947–954.

[35] McClung, A. J. W., Tandon, G., and Baur, J., 2012. "Strain rate- and temperature-dependent tensile properties of an epoxy-based, thermosetting, shape memory polymer (veriflex-e)". *Mechanics of Time-Dependent Materials,* ***16***, pp. 205–221. 10.1007/s11043-011-9148-7.

[36] McClung, A., Tandon, G., and Baur, J., 2013. "Deformation rate-, hold time-, and cycle-dependent shape-memory performance of veriflex-e resin". *Mechanics of Time-Dependent Materials,* ***17***, pp. 39–52.

[37] Tobushi, H., Hayashi, S., Hoshio, K., and Miwa, N., 2006. "Influence of strain-holding conditions on shape recovery and secondary-shape forming in polyurethane-shape memory polymer". *Smart materials and structures,* ***15***(4), p. 1033.

[38] Tobushi, H., Hayashi, S., Hoshio, K., and Ejiri, Y., 2008. "Shape recovery and irrecoverable strain control in polyurethane shape-memory polymer". *Science and Technology of Advanced Materials,* ***9***(1), p. 015009.

[39] Wang, A., Li, G., and Meng, H., 2013. "Strain rate effect on the thermomechanical behavior of a thermoset shape memory polymer". *Smart Materials and Structures,* ***22***(8), p. 085033.

[40] Tobushi, H., Hashimoto, T., Hayashi, S., and Yamada, E., 1997. "Thermomechanical constitutive modeling in shape memory polymer of polyurethane series". *Journal of Intelligent Material Systems and Structures,* ***8***(8), pp. 711–718.

[41] Tobushi, H., Okumura, K., Hayashi, S., and Ito, N., 2001. "Thermomechanical constitutive model of shape memory polymer". *Mechanics of Materials,* ***33***(10), pp. 545 – 554.

[42] Abrahamson, E. R., Lake, M. S., Munshi, N. A., and Gall, K., 2003. "Shape memory mechanics of an elastic memory composite resin". *Journal of Intelligent Material Systems and Structures,* ***14***, October, pp. 623–632.

[43] Diani, J., Liu, Y., and Gall, K., 2006. "Finite strain 3d thermoviscoelastic constitutive model for shape memory polymers". *Polymer Engineering and Science,* ***46***(4), pp. 486–492.

[44] Liu, Y., Gall, K., Dunn, M. L., Greenberg, A. R., and Diani, J., 2006. "Thermomechanics of shape memory polymers: Uniaxial experiments and constitutive modeling". *International Journal of Plasticity,* ***22***(2), pp. 279–313.

[45] Kafka, V., 2008. "Shape memory polymers: A mesoscale model of the internal mechanism leading to the sm phenomena". *International Journal of Plasticity,* ***24***, pp. 1533–1548.

[46] Nguyen, T. D., Jerry Qi, H., Castro, F., and Long, K. N., 2008. "A thermoviscoelastic model for amorphous shape memory polymers: Incorporating structural and stress relaxation". *Journal of the Mechanics and Physics of Solids,* ***56***(9), pp. 2792–2814.

[47] Barot, G., Rao, I. J., and Rajagopal, K. R., 2008. "A thermodynamic framework for the modeling of crystallizable shape memory polymers". *International Journal of Engineering Science,* ***46***, pp. 325–351.

[48] Chen, Y.-C., and Lagoudas, D. C., 2008. "A constitutive theory for shape memory polymers. part i: Large deformations". *Journal of the Mechanics and Physics of Solids,* ***56***(5), pp. 1752–1765.

[49] Chen, Y.-C., and Lagoudas, D. C., 2008. "A constitutive theory for shape memory polymers. part ii: A linearized model for small deformations". *Journal of the Mechanics and Physics of Solids,* ***56***(5), pp. 1766–1778.

[50] Kim, J. H., Kang, T. J., and Yu, W.-R., 2010. "Thermo-mechanical constitutive modeling of shape memory polyurethanes using a phenomenological approach". *International Journal of Plasticity,* ***26***, pp. 204–218.

[51] Nguyen, T., Yakacki, C. M., Brahmbhatt, P. D., Chambers, M. L., et al., 2010. "Modeling the relaxation mechanisms of amorphous shape memory polymers". *Advanced Materials,* ***22***(31), pp. 3411–3423.

[52] Volk, B. L., Lagoudas, D. C., and Chen, Y.-C., 2010. "Analysis of the finite deformation response of shape memory polymers: Ii. 1d calibration and numerical implementation of a finite deformation, thermoelastic model". *Smart Materials and Structures,* ***19***(7), p. 075006.

[53] Volk, B. L., Lagoudas, D. C., and Maitland, D. J., 2011. "Characterizing and modeling the free recovery and constrained recovery behavior of a polyurethane shape memory polymer". *Smart Materials and Structures,* ***20***(9), p. 094004.

[54] Westbrook, K. K., Kao, P. H., Castro, F., Ding, Y., and Qi, H. J., 2011. "A 3d finite deformation constitutive model for amorphous shape memory polymers: a multi-branch modeling approach for nonequilibrium relaxation processes". *Mechanics of Materials,* ***43***(12), pp. 853–869.

[55] Zhang, Q., and Yang, Q.-S., 2012. "Recent advance on constitutive models of thermal-sensitive shape memory polymers". *Journal of applied polymer science,* ***123***(3), pp. 1502–1508.

[56] Reese, S., and Govindjee, S., 1998. "A theory of finite viscoelasticity and numerical aspects". *International journal of solids and structures,* ***35***(26), pp. 3455–3482.

[57] Arruda, E. M., and Boyce, M. C., 1993. "A three-dimensional constitutive model for the large stretch behavior of rubber elastic materials". *Journal of the Mechanics and Physics of Solids,* ***41***(2), pp. 389–412.